

# **Online Loss Minimization Based Direct Torque and Flux Control of IPMSM Drive**

HongBin Zou

SUBMITTED IN PARTIAL FULFILLMENT OF THE  
REQUIREMENTS FOR THE DEGREE OF MASTER  
OF SCIENCE  
AT LAKEHEAD  
UNIVERSITY THUNDER  
BAY, ONTARIO April, 2014

© Copyright by HongBin Zou, 2014

# Abstract

With the advent of high energy rare earth magnetic material such as, third generation neodymium-iron-boron (NdFeB), permanent magnet synchronous motor (PMSM) is becoming more and more popular in high power industrial applications (e.g., high-speed railway) due to its advantageous features such as high energy density, stable parameters, high power factor, low noise and high efficiency as compared to the conventional ac motors. Over the years, vector control and direct torque and flux control (DTFC) techniques have been used for high performance motor drives. But, the DTFC is faster than that of conventional vector control as the DTFC scheme doesn't need any coordinate transformation, pulse width modulation (PWM) and current regulators. The DTFC utilizes hysteresis band comparators for both flux and torque controls. Most of the past researches on DTFC based motor drives mainly concentrated on the development of the inverter control algorithm with less torque ripple as it is the major drawback of DTFC. The torque reference value is obtained online based on motor speed error between actual and reference values through a speed controller. Traditionally, researchers chose a constant value of air-gap flux reference based on trial and error method which may not be acceptable for high performance drives as the air-gap flux changes with operating conditions and system disturbance. Efficient high performance drives require fast and accurate speed response to cope with disturbances and algorithm to minimize motor losses. However, if the reference air-gap flux is maintained constant it is not possible to control the motor losses.

Therefore, this thesis presents a novel loss minimization based DTFC scheme for interior type PMSM drive so that the drive system can maintain both high efficiency and high dynamic performance. An online model based loss minimization algorithm (LMA) is developed to estimate the air-gap flux so that the motor operates at minimum loss condition while taking the general advantages of DTFC over conventional vector control. The performance the proposed LMA based DTFC for PMSM drive is tested in both simulation and real-time implementation at different operating conditions. The results verify the effectiveness of the proposed flux observer based DTFC scheme for PMSM drive.

# Acknowledgement

First, I would like to thank my creator who provided me this opportunity to study in Lakehead University and blessed me with the most precious gift of physical and mental health during the whole study period. Then, my supervisor Dr. M.N. Uddin who played the vital role by giving valuable guidelines and technical support. I am thankful to Dr. X.P. Liu for his valuable suggestions and help in my graduate study period. Then, I am also indebted to Q. Xin, Felipe and Garin, my lab mates to share the ideas and make the healthy and friendly working environment.

Last but not least, I like to thank my parents for their supplications and moral encouragement to do this job well in time.

# Contents

<b>Abstract</b> .....	I
<b>Acknowledgement</b> .....	II
<b>Contents</b> .....	III
<b>List of Symbols</b> .....	V
<b>List of Figures</b> .....	VI
<b>1. Introduction</b> .....	1
1.1 Why Permanent Magnet Synchronous Motor? .....	1
1.2 Application Example.....	4
1.3 Literature Review .....	6
1.4 Thesis Motivation.....	9
1.5 Overview of Loss Minimization Algorithm.....	10
1.5.1 Search Controller (SC) Based LMA .....	10
1.5.2 Loss Model Based Control (LMC) .....	11
1.5.3 Conclusion.....	13
1.6 Thesis Organization.....	13
<b>2. Modeling of IPMSM</b> .....	14
2.1 Introduction.....	14
2.2 Mathematical Model Development.....	14
2.3 Typical Direct Torque and Flux Control (DTFC).....	19
2.3.1 Introduction.....	19
2.3.2 DTFC Flux, Power and Torque Calculation.....	20
2.3.3 Flux and Torque Comparator.....	27
2.3.4 Three-Phase IGBT Inverter.....	28
<b>3. DTFC Based IPMSM Drive</b> .....	32
3.1 Introduction.....	32
3.2 Loss Minimization Based Reference Flux Estimation.....	32

3.3 Simulation Results.....	40
3.4 Comparison of DTFC and Vector Control Techniques for PMSM Drive with Loss Minimization Approach.....	51
3.5 Conclusion.....	57
<b>4. Experiment Verification of the Proposed DTFC Based IPMSM Drive.....</b>	<b>58</b>
4.1 Introduction.....	58
4.2 Hardware Implementation of the Drive.....	58
4.3 Hardware Setup.....	61
4.4 Software Implementation of the Drive.....	62
4.5 Experiment Results.....	65
4.6 Conclusion.....	71
<b>5. Conclusion.....</b>	<b>72</b>
5.1 Achievements of the Thesis.....	72
5.2 Future Scope of this Work.....	73
<b>References.....</b>	<b>74</b>
<b>Appendix-A IPMSM Parameters.....</b>	<b>82</b>
<b>Appendix-B MatLab/SimuLink Models.....</b>	<b>83</b>
<b>Appendix-C Real-time Implementation of DTFC/VC.....</b>	<b>89</b>
<b>Appendix-D Drive and Interface Circuit .....</b>	<b>90</b>

# List of Symbols

- , , a, b and c phase voltages.
  - , , a, b and c phase currents.
  - , d-q axis stator currents in synchronous rotating frame.
  - , d-q axis stator self-inductances.
  - , stator copper-loss and iron-loss resistances in synchronous rotating frame.
- P Number of pole pairs.
- Rotor magnetic-flux linkage.
- Motor air gap magnetic-flux linkage.
- Motor rotor mechanical speed.
- Motor actual electrical rotor speed.
- , d-q axis core-loss armature currents in synchronous rotating frame.
  - d-axis demagnetizing armature current in synchronous rotating frame.
  - q-axis torque-generating armature current in synchronous rotating frame.
- Electrical output torque.
- Motor rotor position.
- , Copper loss and iron loss of interior permanent magnet synchronous motor (IPMSM).
- Total electrical loss of IPMSM .

# List of Figures

Fig. 1.1: Cross section of (a) surface mounted (b) inset type (c) interior type PMSM motor..	3
Fig. 1.2: 350km/h high-speed railway.....	4
Fig. 1.3: TQ-600 PMSM for 350km/h high-speed railway.....	5
Fig. 1.4: 500km/hr high-speed railway.....	5
Fig. 2.1: Relative position of stationary d-q axis to the synchronously rotating $\omega$ - axis..	17
Fig. 2.2: d-q axis equivalent circuit model of IPMSM.....	19
Fig. 2.3: Typical direct torque and flux control (DTFC) strategy.....	20
Fig. 2.4: Relations of current vectors and magnet flux vectors .....	21
Fig. 2.5: (a) General vectors diagrams. (b) Vectors diagrams with .....	23
Fig. 2.6: Motor 3-phase current and stator windings .....	24
Fig. 2.7: Torque and flux hysteresis bands .....	27
Fig. 2.8(a): 3-phase IGBT inverter connected to a 3-phase motor.....	29
Fig. 2.8(b): Motor air gap sectors (1~6) and 6 voltage vectors .....	29
Fig. 2.9: Motor air gap flux zigzag path.....	31
Fig. 3.1: Reference flux and torque estimator for DTFC based PMSM drive.....	33
Fig. 3.2(a): d-axis model of IPMSM incorporating iron loss .....	34
Fig. 3.2(b): q-axis model of IPMSM incorporating iron loss .....	34
Fig. 3.3: Simulated starting responses of the proposed LMA based DTFC scheme for IPMSM drive at rated load ( ) and rated speed ( / ) conditions: (a) speed & efficiency, (b) speed and torque.....	42
Fig. 3.3: Simulated starting responses of the proposed LMA based DTFC scheme for IPMSM drive at rated load ( ) and rated speed ( / ) conditions: (c) single phase current (d) 3-phase stator current.....	43
Fig. 3.4: Responses of the proposed LMA based DTFC scheme for IPMSM drive at / for different load conditions: (a) , (b) .....	44
Fig. 3.5: Responses of the proposed LMA based DTFC scheme for IPMSM drive at low speed / : (a) , (b) .....	45

Fig. 3.6: Responses of the proposed LMA based DTFC scheme for IPMSM drive for step changes in command speeds from                    /    at full load: (a) speed & efficiency, (b) estimated flux.....	46
Fig. 3.6: Responses of the proposed LMA based DTFC scheme for IPMSM drive for step changes in command speeds from                    /    at full load: (c) current .....	47
Fig. 3.7: Motor speed and efficiency responses for step changes in command speed at full load with: (a) constant high flux command value, (b) constant low flux command value.....	48
Fig. 3.8: Motor efficiency for step changes in load at a speed of                    /    : (a) proposed LMA based DTFC, (b) constant low flux based DTFC scheme.....	50
Fig. 3.9: Typical Vector Control based IPMSM Drive.....	52
Fig. 3.10: Comparison of speed & efficiency responses for DTFC and VC based IPMSM drive at rated load and rated speed .....	54
Fig. 3.11: Stator 'a' phase current comparison between DTFC and VC schemes.....	54
Fig. 3.12: Speed and efficiency responses of PMSM drives using DTFC and VC schemes for step changes in command speed .....	55
Fig. 3.13: Speed and efficiency responses of PMSM drives using DTFC and VC schemes for step changes in load.....	55
Fig. 3.14(a): Voltage vectors of DTFC during sector 2 ( $30^0\sim90^0$ ) .....	56
Fig. 3.14(b): Selected voltage vectors of VC during sector-2 ( $30^0\sim90^0$ ) .....	56
Fig. 4.1: Block diagram of hardware schematic of VSI fed IPMSM drive.....	59
Fig. 4.2: Block diagram of DS1104 board .....	60
Fig. 4.3: Experimental setup of the proposed controller of IPMSM drive.....	62
Fig. 4.4: Flow chart of the software for real-time implementation of the proposed LMA based DTFC scheme of IPMSM drive.....	64
Fig. 4.5: Experimental starting responses of the proposed LMA based DTFC scheme for IPMSM drive at a speed of                    /    and load of                    : (a) speed & efficiency, (b) speed and torque.....	66
Fig. 4.6: Experimental current response of the proposed LMA based DTFC scheme for IPMSM drive: (a) 'a' phase currents, (b) 3-phase currents.....	67
Fig. 4.7: Experimental speed and efficiency responses of IPMSM drive at rated speed and	

25% of rated load condition: (a) DTFC (b)VC.....	68
Fig. 4.8: Experimental steady-state current responses of IPMSM drive at rated speed and 25% of rated load condition: (a) DTFC—‘a’ phase (b) VC—‘3-phase’.....	69
Fig. 4.9: Experimental speed and torque responses of IPMSM drive at 65 rad/s and 25% of rated load condition: (a) DTFC (b)VC.....	70
Fig. 4.10: Experimental speed response of the proposed LMA based DTFC scheme for IPMSM drive for a step increase in command speed from        /        / at 25% rated load.....	71

# Chapter 1

## Introduction

### 1.1 Why Choose IPMSM?

Direct current (DC) motor has dominated the drive system for almost one hundred years since it was invented in late 1870s due to its advantages such as being able to run at wide range of speed, high starting torque for heavy load, high speed response performance, free from harmonics and simple control system. However, the DC motor has many disadvantages such as, it requires increasing maintenance cost due to the sparking brushes and commutators. And it can't run under hazard work conditions [2]. Hence, alternating current (AC) motors such as induction motors and synchronous motors were developed due to their high reliability and maintenance free operation.

An AC motor is an electric motor driven by an alternating current and converting electric energy to mechanical energy such as induction motor (IM) and synchronous motor [3,4]. The rotor of induction motor is just winding of wire or a cage. Thus, the induction motor has no commutator and brush. Current is induced on the rotor due to the transformer reaction, therefore, the induction motor can self start and its operation and maintenance are much simpler than DC motors [5]. Although induction motors have many important advantages such as simple, reliability, low maintenance, directly connected to power source [6,7], induction motors have several disadvantages as well. The main disadvantage of induction motors is that its power factor is poor and it runs slower than the synchronous speed which will cause power loss and make speed control complex. Due to the IM complex variable parameter, complex modeling and estimation of motor parameters have to be applied for high performance drive system [7].

Compared to induction motors, synchronous motors can run at synchronous speed without the slip power loss. On the other hand, synchronous motors require extra power supply and brush for dc field excitation of the rotor. Thus, the synchronous motors need increasing maintenance support and have similar disadvantages to dc motors. The rotor winding will cause

extra power consumption and will significantly drag down the motor efficiency [8]. Due to these disadvantages, the permanent synchronous motor has been developed. In a permanent magnet synchronous motor, permanent magnets produce the flux and hence, the loss due to rotor winding is avoided [6].

Over the last two decades, the permanent magnet synchronous motor (PMSM) is becoming more and more popular since it has both advantages of induction motor and synchronous motor such as high reliability, high power factor and high efficiency. There are three types of PMSMs. Among them the interior permanent magnet synchronous motor (IPMSM) has the advantages of other PMSM motors such as it can produce more torque and can run at very high speed. The IPMSM can be found in hybrid electric vehicles and high speed railways. Therefore, the IPMSM is considered as a test motor in this thesis [9, 10, 11].

The classification for PMSM mostly is based on magnet configuration of motor rotor, it can be classified into three divisions.

- (1) Surface mounted PM motor: In this type of PM motor, the PMs are typically glued or banded with a non-conducting material to the surface of the rotor core as shown in Fig.1.1 (a). This type of motor is not suitable for high speed.
- (2) Inset type PM motor: In this type of PM motor, the PMs are typically glued directly or banded with a non-conducting material inside the rotor core as shown in Fig.1.1 (b). This type of motor is not suitable for high speed.
- (3) Interior type PM motor: In this type of PM motor, the PMs are imbedded in the interior of the rotor core as shown in Fig.1.1 (c). This is the most recently developed method of mounting the magnet. Interior magnet designs offer q-axis inductance larger than the d-axis inductance. The saliency makes possible a degree of flux weakening, enabling operation above nominal speed at constant voltage and should also help reduce the harmonic losses in the motor. This kind of PM motor has the same advantages of inset PM motor as well as the advantages of mechanical robustness and a smaller magnetic air gap. Therefore the interior magnet design is better suited to applications where operation in the voltage limited high speed region is desired.

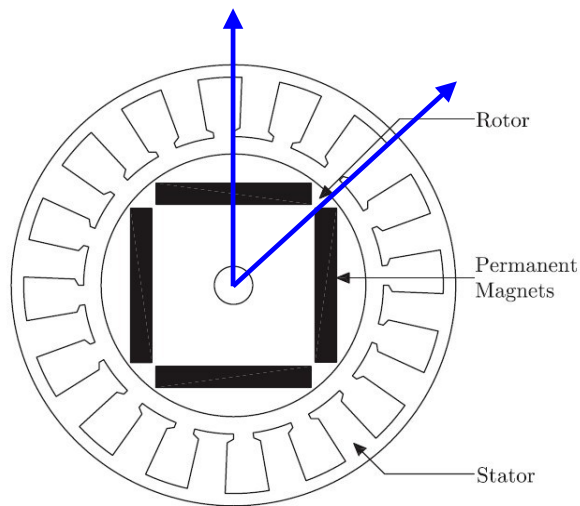
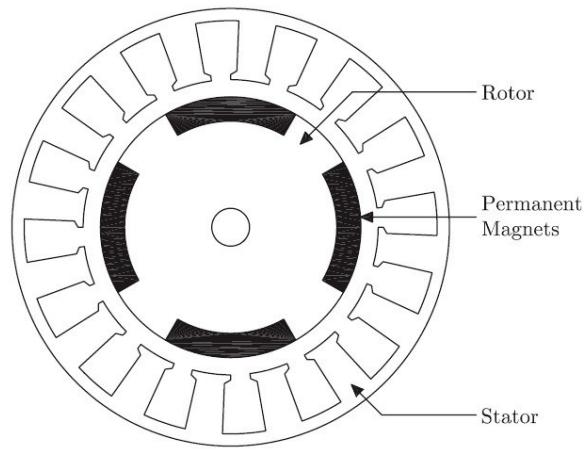
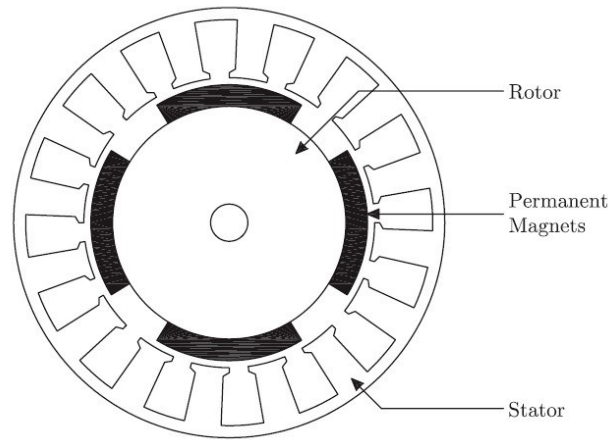


Fig.1.1: Cross section of (a) surface mounted (b) inset type (c) interior type PMSM motor.

## 1.2 Application of IPMSM

The continuous need for an increased power density in industry area is increasing. Rare earth magnetic material has excellent magnetic characteristic and it can keep a strong magnetic flux for a very longtime after magnetized. With rare earth magnetic material, motor can be made simple, reliable, small volume and high power density. In May 2013 a Chinese motor company developed a new kind of permanent magnet synchronous motor (TQ-600) which is successfully applied for high speed railway. The high speed railway and the newly developed PMSM are shown in Fig.1.3-1.5. These new motors replaced motors commonly used for 350km/h high speed rail way. The earlier motors used in Chinese high speed railway are 365kW AC motor. Comparing to the previous AC motor, each new PMSM power is increased by 65 percent; power density is increased by 31.5 percent and weight is decreased by 1/3. Thus, the total weight of the train is decreased by 3165kg.



Fig. 1.2: 350km/h high-speed railway.



Fig. 1.3: TQ-600 PMSM for 350km/h high-speed railway.



Fig. 1.4: 500km/hr high-speed railway.

## 1.3 Literature Review

Researchers have been using both vector control and direct torque control techniques for high performance AC motor drives [2, 7, 8, 10]. In vector control, an AC motor is decomposed into d-axis and q-axis components. The d-axis controls the magnetic flux and q-axis control the torque. Thus, the ac motor behaves like a separately excited DC motor while maintaining its general advantages over DC motor. Direct torque control (DTC) technique was initially developed for induction motor drives and was proposed in 1980s [12, 13]. DTC have been used due to some of its advantages such as simplicity, fast torque and flux control response for high performance ac motor drive applications. DTC is a strategy similar to vector control using variable frequency drive to control the AC motor output torque. This includes calculating the motor's output torque and motor's air gap magnetic flux based on the three phase currents of the AC motor system sensor [12,13]. The difference between the direct torque control and vector control is that DTC directly manipulate the motor stator magnetic flux linkage vector and output torque as control variables instead of the motor stator three phase currents as control variables in vector control. The research on direct torque and flux control (DTFC) includes several important topics such as flux control, rotor initial position estimation, torque ripple minimization and magnetic flux estimation, which are discussed below.

The flux for the DTFC can be controlled by using either maximum torque per ampere (MTPA) control below the rated speed and flux weakening (FW) above the rated speed [14-17]. In [14], mathematical functions for computing stator flux reference with d-q axis stator flux components are derived based on MTPA for DTFC based PMSM drive. Therefore, MTPA operation can be achieved for a DTC based IPMSM drive with the optimized stator flux reference estimation.

In [15], a varying reference flux through a MTPA. A reference flux calculating method with approximate equation is applied so that the reference flux is obtained from the torque. In [16], an online automatic search algorithm of the MTPA operating region is proposed. The search algorithm is based on a signal injection method. Only the motor stator resistance is required to perform the automatic search of MTPA region. In [17], a control algorithm based on DTC with flux weakening control is applied. The control algorithm only requires armature resistance instead of many other parameters for flux-weakening control. The authors emphasised

the applied control algorithm in the d-q axis model has several advantages such as, insensitivity to parameter variation and less calculation. However, the efficiency optimization issue wasn't considered in these works [14-16].

A viewpoint of DTFC field research insists that for a practical DTFC based PMSM drive system, the information of the initial rotor position is essential for motor starting. In[18], an initial rotor position estimation algorithm is applied to estimate the PMSM rotor initial position so that the mechanical position sensor can be removed. This initial rotor position estimation algorithm is proposed to a DTC based PMSM drive with a nonlinear model of PMSM.

Although DTC significantly improves the dynamic performance of the drive, DTC also presents notable disadvantages such as hysteresis controllers used in the DTC, generate a variable switching frequency causing electromagnetic torque oscillations. To overcome the disadvantages of torque ripples, several methods have been proposed.

In [19], a DTC based induction motor drive with the minimum torque ripple control is presented under constant switching frequency. A RMS torque ripple equation is derived using on-line torque equations and then an optimal voltage vector minimizing the torque ripple is selected based on the ripple equation. Authors claimed that the proposed algorithm improves the performance of the DTC by combining a low-torque-ripple characteristic in steady state with the fast torque dynamics.

One of the very popular approaches is space vector modulation (SVM) in DTC. In [20], a direct torque and flux controlled interior permanent magnet synchronous motor (IPMSM) drive using an adaptive back-stepping technique is presented. A space vector modulation (SVM) unit generates the reference voltage vectors so that the look-up table in the conventional DTC is replaced. Compared to the conventional DTC, the proposed back-stepping controller reduced torque and flux ripples. This research shows that SVM can reduce the ripples of the electromagnetic torque significantly and also have several advantages such as lower torque ripples, lower harmonics in motor currents, and simple calculation. However, in order to make smaller voltage vector to modulate new vector, the SVM require higher IGBT switching frequency which will cause power loss and affects the life of IGBT. Since conventional two-level DTC algorithms such as SVM to reduce torque ripples are proposed with high switching frequency (over 3 kHz), a three-level inverter based torque ripple reduction technique for DTC is applied so that the IGBT can work at low switching frequency (0.5~1 kHz) [21]. This algorithm

based on low switching frequency inverter system has demonstrated torque ripple reduction all over the operating speed region.

Another method is use fuzzy logic control to minimize the torque ripple. In [22], a fuzzy logic hysteresis comparator based DTC of an induction motor is proposed. The fuzzy logic controller (FLC) is used to adjust the bandwidth of the torque hysteresis bandwidth in order to reduce the torque and flux ripples. The FLC derives the optimum the torque hysteresis bandwidth with the slopes of stator current. In [23], the duty cycle control is also proposed to reduce the torque ripple. The author proposes a unified switching table to select three vectors rather than two vectors. The switching sequence of the three vectors is arranged so that the IGBT switching frequency can be significantly reduced. In [24], a sensorless hybrid DTC drive scheme has been developed using the TMS329F243 digital signal processor controller. The stator voltage vector is generated according to the stator flux components and the algorithm is simple and does not require any filter. In each digital signal processor cycle, the optimized voltage is applied to reduce torque ripple. However, in all of the works related to torque ripple minimization the reference flux was assumed constant, which is not capable to minimize the losses. In [25], the authors claimed that since DTC torque ripples is due to the use of lookup table, a control algorithm of stator flux and torque in DTC based IPMSM drive system is developed. A voltage vector selection algorithm is developed by using stator flux position and torque angle information to select the voltage vector and uses SVM to generate the applying voltage vector.

Magnetic flux estimation is one of the main requirements in DTC drive system. In [26], a stator flux estimation algorithm for DTC based surface mounted PMSM drive is proposed in order to achieve good low speed performance. The stator flux estimation is derived from stator currents and rotor position. With the developed algorithm, the torque ripple and current distortion keeps low in full speed region. In [27], a new technique based on the field reconstruction for the estimation of the magnetic flux in PMSM is presented. The distribution of the magnetic field in the air gap is applied to estimate flux linkages. Since this estimation is independent from stator resistance value, the corresponding errors are removed. On the other hand, there is no integration with respect to time. This removes the accumulation of errors and magnetic flux can be computed accurately over the entire speed range. In [28], a discrete time flux linkage observer is developed which contains two different flux estimation methods based on current and voltage models for flux linkage. This observer produces correctly estimated flux

linkages. In order to eliminate the sampling delay due to a characteristic of digital control computation, a complex vector model-based rotor reference frame current observer is also developed. In [29], a stator flux estimation algorithm based on a voltage model with low pass filtering is presented. In voltage based model, a low pass filter is applied instead of a pure integrator to avoid integration drift problem. In [30], a new torque control technique for IPMSM without d-q axis current controllers and coordinate transformation is proposed. A sensorless DTC based IPMSM with a speed estimator from the stator flux linkage vector and the torque angle is presented. In [31], an application of neural networks to DTC based IPMSM drive system is presented. The neural network is applied to determine the state selector of the DTC. The inputs of switching table are converted to digital signals so that the raining pattern is reduced.

## **1.4 Thesis Motivation**

The DTFC techniques to control PMSM attract increasing attention due to their advantages in eliminating the current controllers and quicker dynamic response, as compared to other motor control algorithms. However, high torque and stator flux ripples remain as one of the major drawbacks for DTFC technology. That is why most of the past research on DTFC based motor drives mainly concentrated on the development of the inverter control algorithms with less torque ripple as it is the major drawback of DTFC [32-45]. In DTFC scheme the motor actual torque and air gap flux linkage values are compared with their corresponding reference values. The torque and flux hysteresis comparators take the corresponding error signals and generate the logic signals of the voltage vector lookup table. Therefore, for proper speed control of DTFC based motor drive system a flux reference estimator is mandatory. The torque reference value is obtained online based on motor speed error between actual and reference values through a speed controller. Traditionally, researchers choose a constant value of air-gap flux reference based on trial and error method which may not be acceptable for high performance drives as the air-gap flux changes with operating conditions and system disturbances. The high performance efficient motor drives require fast and accurate speed response coping with systems disturbances and high efficiency of the drive system. However, if the reference air-gap flux is maintained constant it is not possible to control the motor losses and hence, the efficiency of the drive system cannot be optimized.

Recently, the IPMSM becomes popular due to some of its advantages over other ac motors such as high torque to current ratio, high power to weight ratio, high efficiency, high power factor [46, 47]. Researchers have been applying DTFC for PMSM drive. However, the air-gap flux is assumed constant at the rated value. But in PMSM due to magnetic saturation the air-gap flux changes with operating conditions. Thus, the reported works on DTFC based PMSM drive fail to optimize the efficiency of the drive.

Therefore, this thesis makes an attempt to estimate the reference flux for the DTFC based on a model based loss minimization algorithm (LMA). The purpose of LMA is to minimize the losses and hence optimize the efficiency while the DTFC maintains high dynamic performance. Another objective is to implement the proposed LMA based flux observer for DTFC based IPMSM drive in real-time using DSP based DS1104.

## **1.5 Overview of Loss Minimization Algorithm**

More than 50% of the total electrical energy produced in the world is consumed by motors [48]. Hence, the efficiency improvement of adjustable speed drive system is important not only from the viewpoints of energy saving and cooling system operation, but also from the broad perspective of environmental pollution [49]. The motor power loss includes mechanical loss and electrical loss. The motor mechanical loss includes the motor rotor inertia loss and motor bearing friction loss which can't be avoided and it is assumed constant. The motor electrical loss includes the copper loss of motor stator winding and core loss of the stator and rotor which can be reduced by several methods. The first method is optimizing the motor structure design in order to improve the motor electro-magnetic characteristics [50]. Instead of changing the motor physical structure, second method is applying loss minimization algorithms (LMA) to minimize the input power of the motor for a certain speed and load torque conditions. Therefore, the efficiency of motor is maximized [51-61]. The LMA includes two main groups such as search based LMA and loss model based LMA.

### **1.5.1 Search Controller (SC) Based LMA**

For SC based LMA, the motor drive system command variable such as current or flux value is discrete in steps, the SC algorithm approaches the minimum losses by searching with

these small steps until the minimum input power point is detected for certain load and speed conditions. In this way, the SC algorithm operates with a black box which means the system parameters are unnecessary. The SC algorithm is simple and flexible. Since the control variable has to be changed in small steps to search the minimum input power, sometimes it will create torque ripples. At the same time, the SC algorithm is kind of slow since it takes times to search in small steps and as the system operation conditions change such as speed and load torque, the SC algorithm has to search again to find the minimum power operation point [49,51].

In [52], the author presented a permanent magnet synchronous motor (PMSM) drive system with an adaptive control to find the maximum efficiency operating point. The efficiency control measures the current on the dc link and adjusting the voltage output of the inverter to minimize input power to the motor. The system optimizes the both motor and inverter efficiency. In [8], the author also showed that as the load condition changes, the PM rotor will start oscillating. In [53], a vector controlled PM drive with SC efficiency optimization is presented. Since the vector control is operating with current, so the SC algorithm is manipulating with the stator current d-axis component so that minimizes power losses. Although loss model of the PM is unnecessary, an experimental procedure is applied to test PMSM parameters and the loss model of the PM motor is used as a basis for deriving loss minimization conditions. In [54], authors emphasize the weakness of SC algorithm as the minimum of the input power is not distinct for large efficiency motor. This may cause the approximation of minimum input power not being successful. Meanwhile, the oscillation of the air-gap flux around its optimal value will create torque ripples. Authors also emphasized that instead of the input power minimum value, the motor stator current minimum value can be easily detected. Finally authors concluded that the loss minimization through the stator current is much better than the loss minimization through the input power, especially for high efficiency motors.

### **1.5.2 Loss Model Based Control (LMC)**

The loss model based control (LMC) technique is the algorithm that calculates the control variable such as motor stator current or motor air gap magnetic flux with the loss model of the motor to minimize the power loss. In this technique the response of the motor is fast and does not have torque ripple, so it can be used for high performance drives. The knowledge about

the motor model is mandatory and the accuracy of the motor loss model parameters is important for LMC performance.

In [55], a loss model based controller to achieve the maximum efficiency of induction motor drive is presented. Authors presented a LMC to determine the flux level for the efficiency optimization of the vector-controlled induction motor drive. In order to build a simple loss model, the induction motor model is referenced to the rotor magnetizing current so no leakage inductance on the rotor side. Hence, the proposed LMC based LMA is simple, but leakage inductances are not omitted. In [56], authors presented an optimal control method of armature current vector in order to minimize the controllable losses. The reluctance torque and the d-axis armature reaction are effectively utilized to minimize the losses in the proposed control algorithm. In order to simplify the control algorithm, an approximated control algorithm is also proposed. The proposed control algorithm is applied to the experimental PM motor drive system, in which one digital signal processor is employed to execute the control algorithms.

In [57], an off line efficiency optimization controller for permanent magnet synchronous machines is applied under direct torque and flux control. The flux command is obtained based on an optimization procedure to yield a maximum efficiency. In [58], an online adaptive loss minimization controller for interior permanent magnet motor drives is presented. The LMC controller provides a novel pattern of change in d-axis stator current to achieve a minimum drive input power at any operating condition. In [59], an efficiency optimization control algorithm for IPMSM drives with online estimation of motor parameters is presented. The control method ensures the minimization of the motor losses with an optimal control of the armature current minimizing the electrical loss. In [60], an LMC for IPMSM drives is presented, in which a speed controller is integrated with the loss minimization control. The MTPA based LMC minimized the motor input power by regulating the command flux current at its optimal point to minimize motor electrical losses. In order to reduce the iron loss caused by torque ripples, a denoising technique is applied.

Meanwhile, the LMC and SC also can be combined together to control the motor drive system. In [61], an efficiency optimization control method using both SC and LMC algorithm is presented. The approximate optimal d-axis current is calculated by using LMC so that the search interval of SC is reduced. Hence, the convergence time of the SC algorithm is shortened and the adverse effect caused by motor parameters variation is avoided.

However, to simplify the algorithm in this thesis only LMC based loss minimization is considered to estimate the reference flux of DTFC based IPMSM drive.

### **1.5.3 Conclusion**

A literature search on both SC and LMC based loss minimization approach of motor drives is presented. The advantages and disadvantages of SC and LMC algorithms are also discussed. Finally the LMC based loss minimization algorithm is recommended to estimate the reference flux of DTFC scheme so that the IPMSM drive can achieve both high efficiency and high dynamic performance.

## **1.6 Thesis Organization**

The remaining part of this thesis is organized in the following sequence. The Chapter-1 introduced the advantages of IPMSM, reviewed the DTFC research topics and also provides an overview of the loss minimization algorithms.

Chapter-2 is the mathematic modeling of an IPMSM motor and analyses the basic DTFC scheme.

Chapter-3 discusses the loss minimization algorithm used in this thesis. It also provides simulation results of the proposed LMA based flux observer for DTFC based IPMSM drive using Matlab/SimuLink.

Chapter-4 introduces the real time implementation system and also show some experimental results.

Chapter-5 concludes about the achievement of the thesis and provides some suggestions for future scope of the work.

# Chapter 2

## Modeling of IPMSM Drive

### 2.1 Introduction

Analytically, the IPMSM is same as the conventional wire-wound excited synchronous motor with the exception that the excitation is provided by the permanent magnets instead of wire wound dc rotor field. Therefore, the standard d-q axes model for synchronous machines can be used for the d-q axis model of the IPMSM by removing the equation related to field current and associated dynamics.

### 2.2 IPMSM Mathematical Model Development

If  $\lambda_p$  is the constant flux linkage provided by the permanent magnets, then the flux linkages in the three phase stator winding due to PM of the rotor can be given as[7,8],

$$\begin{bmatrix} \lambda_{p1} \\ \lambda_{p2} \\ \lambda_{p3} \end{bmatrix} = \lambda_p \begin{bmatrix} \cos(\theta_r) \\ \cos(\theta_r - 120^\circ) \\ \cos(\theta_r + 120^\circ) \end{bmatrix} \quad (2.1)$$

where  $\lambda_{p1}$ ,  $\lambda_{p2}$ ,  $\lambda_{p3}$  are the flux linkages in the three phase stator winding due to PM of the rotor and  $\theta_r$  is the rotor position. So total air gap flux linkage for three phases are the summation of the flux linkage for the corresponding phase current, mutual flux linkage for the currents in other phases and the flux linkages in the three phase stator winding due to PM of the rotor. The equations for the air gap flux linkage for three phases are given as,

$$\begin{bmatrix} v_a \\ v_b \\ v_c \end{bmatrix} = \begin{bmatrix} L_{aa} & L_{ab} & L_{ac} \\ L_{ba} & L_{bb} & L_{bc} \\ L_{ca} & L_{cb} & L_{cc} \end{bmatrix} \begin{bmatrix} i_a \\ i_b \\ i_c \end{bmatrix} + \begin{bmatrix} \frac{d\lambda_a}{dt} \\ \frac{d\lambda_b}{dt} \\ \frac{d\lambda_c}{dt} \end{bmatrix} \quad (2.2)$$

where  $\lambda_a, \lambda_b, \lambda_c$  are the air gap flux linkage for the phase a, b, c, respectively;  $L_{aa}, L_{bb}, L_{cc}$  are the self inductances and  $L_{ab}, L_{bc}, L_{ca}$  are the mutual inductances, respectively. The phase voltage is the voltage drop in each phase plus the voltage drop due to the rate of change of flux linkage. The voltage equations of the three phases of the IPMSM can be defined as:

$$\begin{aligned} v_a &= R_a i_a + \frac{d\lambda_a}{dt} \\ v_b &= R_b i_b + \frac{d\lambda_b}{dt} \\ v_c &= R_c i_c + \frac{d\lambda_c}{dt} \end{aligned}$$

where  $v_a, v_b, v_c$  are the three phase voltages,  $i_a, i_b, i_c$  are the three phase currents and  $R_a, R_b, R_c$  are the three phase stator resistances. These equations can be written in matrix form as,

$$\begin{bmatrix} v_a \\ v_b \\ v_c \end{bmatrix} = \begin{bmatrix} R_a & 0 & 0 \\ 0 & R_b & 0 \\ 0 & 0 & R_c \end{bmatrix} \begin{bmatrix} i_a \\ i_b \\ i_c \end{bmatrix} + \begin{bmatrix} \frac{d\lambda_a}{dt} \\ \frac{d\lambda_b}{dt} \\ \frac{d\lambda_c}{dt} \end{bmatrix} \quad (2.6)$$

These voltage equations depend on the flux linkage components which are function of rotor position  $\theta$ . In order to keep away from the difficulty of calculations, all the equations have to be changed to the synchronously revolving rotor reference frame where the machine equations are no longer dependent on the rotor position. These transformations can be accomplished in two steps using Park's & Clark's transformation equations [9]. In the first step, the machine equations are changed from the stationary a-b-c frame into the stationary d-q frame and in second step, from the stationary d-q frame to the synchronously rotating d-q-0 frame. The phase variables in terms of d-q-0 variables can be written in matrix form as

$$\begin{bmatrix} i_a \\ i_b \\ i_c \end{bmatrix} = \begin{bmatrix} \cos(\theta) & -\sin(\theta) & 0 \\ \sin(\theta) & \cos(\theta) & 0 \\ 0 & 0 & 1 \end{bmatrix} \begin{bmatrix} i_d \\ i_q \\ i_0 \end{bmatrix} \quad (2.7)$$

The corresponding inverse relation can be written as,

$$\begin{bmatrix} \vdots \\ \vdots \\ \vdots \end{bmatrix} = \begin{pmatrix} \cos & -\sin \\ \sin & \cos \end{pmatrix} \begin{bmatrix} \vdots \\ \vdots \\ \vdots \end{bmatrix} \quad (2.8)$$

where, the variable could be the voltage or current .

The rotor location or rotor position angle is defined as,

$$\theta = \int \omega_r dt + \theta_0 \quad (2.9)$$

where, the variable is motor rotor speed and variable is the rotor initial position.

For balanced three phases, '0' sequence component ( ) does not exist, and it is convenient to set initial rotor position so that the q axis coincides with a-phase. Under these conditions the above equation can be written as,

$$\begin{bmatrix} \vdots \\ \vdots \end{bmatrix} = \begin{bmatrix} \frac{\sqrt{2}}{2} & -\frac{\sqrt{2}}{2} \\ \frac{\sqrt{2}}{2} & \frac{\sqrt{2}}{2} \end{bmatrix} \begin{bmatrix} \vdots \\ \vdots \end{bmatrix} \quad (2.10)$$

And

$$\begin{bmatrix} \vdots \\ \vdots \end{bmatrix} = \begin{bmatrix} \frac{1}{\sqrt{2}} & -\frac{1}{\sqrt{2}} \\ \frac{1}{\sqrt{2}} & \frac{1}{\sqrt{2}} \end{bmatrix} \begin{bmatrix} \vdots \\ \vdots \end{bmatrix} \quad (2.11)$$

The quantities in the stationary d-q frame can be converted to synchronously rotating - frame as shown as Fig.2.1,

$$\begin{bmatrix} \vdots \\ \vdots \end{bmatrix} = \begin{bmatrix} \cos & -\sin \\ \sin & \cos \end{bmatrix} \begin{bmatrix} \vdots \\ \vdots \end{bmatrix} \quad (2.12)$$

and inverse relation is given by,

$$[ ] [ ] [ ] [ ] \quad (2.13)$$

If the eddy current and hysteresis losses are negligible, the induced electro-magnetic force is sinusoidal, the stator resistance of the three phases are balanced, neglecting the saturation and using equations (2.6), (2.8), (2.12),

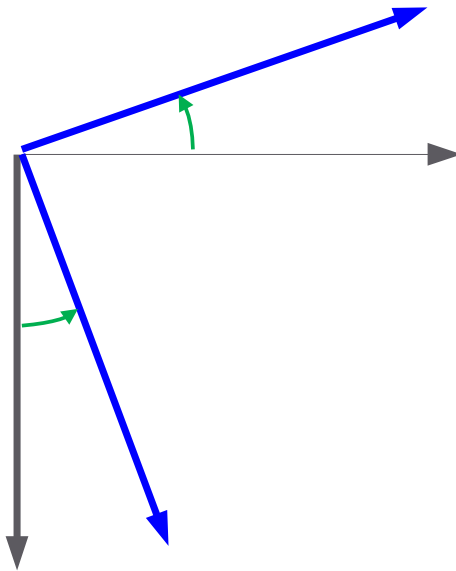


Fig. 2.1: Relative position of stationary d-q axis to the synchronously rotating  $\theta$  - axis.

The  $\theta$  - axis model of IPMSM can be derived as follows,

$$\begin{aligned} & \text{---} \\ & \text{---} \end{aligned}$$

where,  $v_d, v_q$  are d-q axis voltages and  $i_d, i_q$  are d-q axis currents,  $\lambda_d, \lambda_q$  are d-q axis flux linkages and  $R_s$  is the stator resistance per phase and  $\omega_s$  is the stator frequency. The d-q axis flux linkage,  $\lambda_d$  and  $\lambda_q$  can be written as,

where,  $\omega_r$  ;

$L_d$  and  $L_q$  are d-q axis inductances,  $L_{md}$ ,  $L_{mq}$  are d-q axis magnetizing inductances and  $L_{ls}$  is the leakage inductance per phase. The stator frequency is related to rotor frequency as,

Using equations (2.14)-(2.17), the motor equations can be written as,

In these equations all the stator voltages and currents are in rotor reference frame. The total average energy coming from the source which is also the developed power per phase is given by,

$$- \left( \frac{d}{dt} \left[ \frac{1}{2} (L_d i_d^2 + L_q i_q^2) + L_{ls} i_s^2 \right] \right)$$

The total power developed by the machine is given by,

$$- \left[ \frac{d}{dt} \left( \frac{1}{2} (L_d i_d^2 + L_q i_q^2) + L_{ls} i_s^2 \right) \right] \quad (2.21)$$

According to (2.16)-(2.19), the d-q axis equivalent circuit diagram can be drawn as shown in Fig. 2.2.

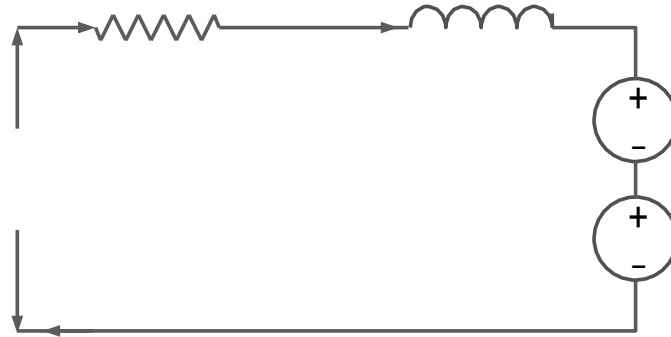
So the developed torque is given by,

$$T = \frac{3}{2} p \left[ L_q i_d i_q - L_d i_q i_d \right] \quad (2.22)$$

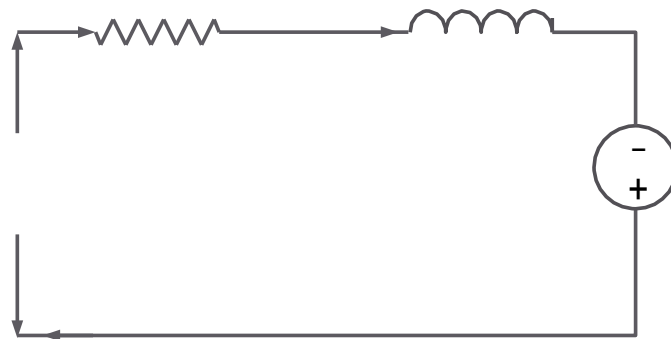
The motor dynamic can be represented by the following equation:

$$\frac{d}{dt} \left[ \frac{1}{2} (L_d i_d^2 + L_q i_q^2) + L_{ls} i_s^2 \right] = \dots \quad (2.23)$$

where,  $T_L$  is the load torque in  $\text{Nm}$ ,  $B$  is the friction damping coefficient in  $\text{Ns/rad}$  and  $J$  is rotor inertia constant in  $\text{kg}\cdot\text{m}^2$ .



(a) q-axis equivalent circuit.



(b) d-axis equivalent circuit.

Fig. 2.2: d-q axis equivalent circuit model of IPMSM.

## 2.3 Typical Direct Torque and Flux Control (DTFC)

### 2.3.1 Introduction

In 1980s, the direct torque and flux control (DTFC) was introduced for voltage fed PWM inverter drives. The basic concept of DTFC technology is explained later on. Fig. 2.3 shows the typical DTFC based motor drives where the voltage vector for the inverter is selected through a look-up table.

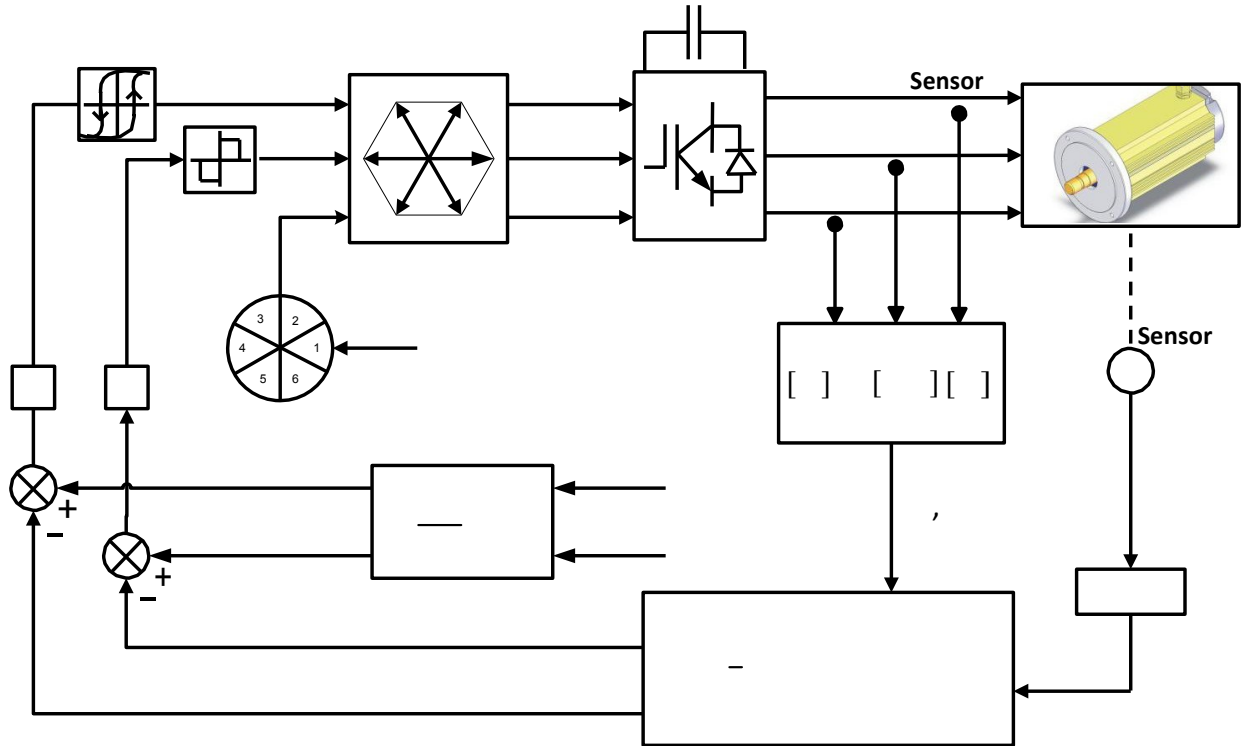


Fig. 2.3: Typical direct torque and flux control (DTFC) strategy.

### 2.3.2 DTFC Flux, Power and Torque Calculation

The flux and torque observers calculate the motor air gap flux value ( ) and motor output torque ( ) with the motor current ( ) obtained from current sensor and motor angle speed ( ) and rotor position angle ( ) obtained from position encoder. Before explaining the control principle, a torque expression as a function of the stator and rotor fluxes will be developed at first. The relations of IPMSM current vectors and magnet flux vectors are shown in Fig. 2.4.

The air-gap flux linkage is defined as,

$$\lambda = \int v dt = \int \left( \frac{d\psi}{dt} + R i \right) dt = \psi + \int R i dt$$

$$\lambda = \int v dt = \int \left( \frac{d\psi}{dt} + R i \right) dt = \psi + \int R i dt$$

$$\lambda = \int v dt = \int \left( \frac{d\psi}{dt} + R i \right) dt = \psi + \int R i dt \quad ( )$$

The motor torque is produced by the electro-magnetic force, which is given by,

where,  $i_s$  is the stator current and  $\lambda_{ag}$  is the air gap flux linkage.

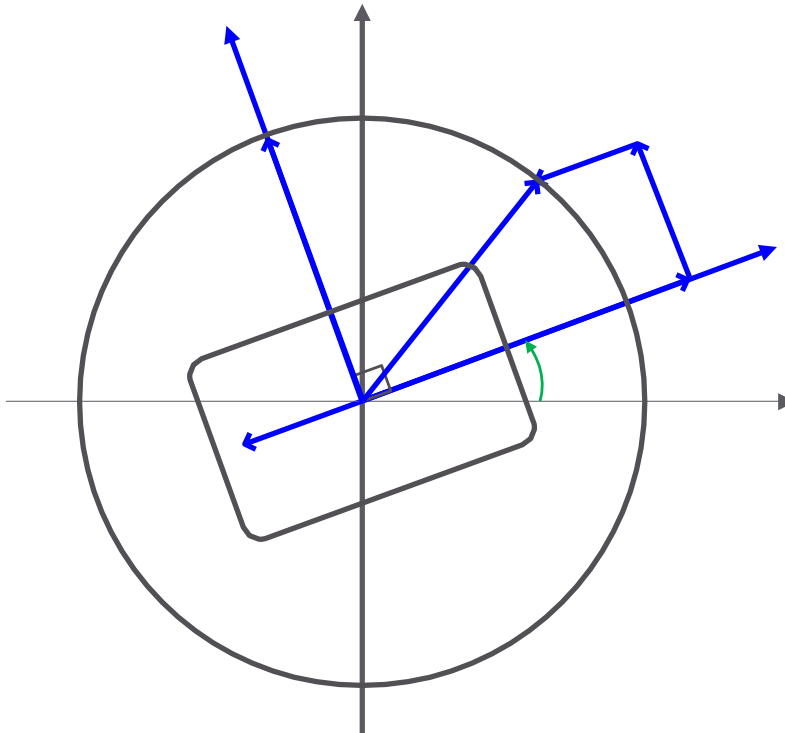


Fig. 2.4: Relations of current vectors and magnet flux vectors.

In previous analysis, the IPMSM model equations can be transformed from 3-phase frame to the synchronously rotating d-q frame so that sinusoidal voltage becomes constant like a dc voltage. In case of dc motor, the developed torque is,

where,  $i_a$  is the armature current,  $i_f$  is the field current and  $K$  is a constant. Both  $i_d$  and  $i_q$  are orthogonal and decoupled vectors. So the control becomes easier for separately excited dc motor. In torque equation (2.21), the first term represents the reluctance torque produced by the interaction of d-q axis inductances and currents; the second term represents the magnet torque

produced by the permanent magnet flux and q axis current. As d-axis current,  $i_d$ , the torque equation becomes linear with  $i_q$  and torque control becomes simple.

—

However with the assumption of  $i_d = 0$ , as per equation (2.17), the flux cannot be controlled in an IPMSM. Without a proper flux control, motor cannot be operated above the rated speed while maintaining voltage and current within the rated capacity of the motor/inverter. In the proposed work, the flux will be properly controlled so that the motor can be controlled efficiently below and above the rated speed. Thus, the IPMSM can be controlled like a separately excited DC motor where  $i_d$  controls torque and  $i_q$  controls flux.

The steady state phase voltage  $v_a$  can be derived from  $v_d$  axis voltage at steady state with equation (2.18) and (2.19) as,

$$\begin{aligned} v_a &= v_d \cos(\theta) - v_q \sin(\theta) \\ &= (R_s i_d \cos(\theta) + \omega \lambda_m \sin(\theta) - R_s i_q \sin(\theta) - \omega L_d i_d \cos(\theta) - \omega L_q i_q \sin(\theta)) \cos(\theta) \\ &\quad - (R_s i_d \sin(\theta) + \omega L_d i_d \sin(\theta) - R_s i_q \cos(\theta) - \omega L_q i_q \cos(\theta)) \sin(\theta) \end{aligned}$$

At steady state conditions,  $\frac{di_d}{dt} = 0$  and  $\frac{di_q}{dt} = 0$ ,

The phase current

So the finally equation of  $v_a$  as,

$$v_a = (R_s i_d \cos(\theta) + \omega \lambda_m \sin(\theta) - R_s i_q \sin(\theta) - \omega L_d i_d \cos(\theta) - \omega L_q i_q \sin(\theta)) \cos(\theta) - (R_s i_d \sin(\theta) + \omega L_d i_d \sin(\theta) - R_s i_q \cos(\theta) - \omega L_q i_q \cos(\theta)) \sin(\theta)$$

In the case of IPMSM motor, the  $i_d$  axis current is negative and it demagnetizes the main flux provided by the permanent magnets. Thus in order to take the absolute value of  $i_d$ , rewrite the equation as,

$$v_a = (R_s i_d \cos(\theta) + \omega \lambda_m \sin(\theta) - R_s i_q \sin(\theta) - \omega L_d i_d \cos(\theta) - \omega L_q i_q \sin(\theta)) \cos(\theta) - (R_s i_d \sin(\theta) + \omega L_d i_d \sin(\theta) - R_s i_q \cos(\theta) - \omega L_q i_q \cos(\theta)) \sin(\theta)$$

Based on equation (2.28), the basic vector diagram of the IPMSM is shown in Fig.2.5(a). The stator current vector can be controlled by controlling the individual d-q current components. As

$i_d < 0$ , all the flux linkages are oriented in the  $-d$  axis as shown in Fig. 2.5(b). The torque then

is a function of only the  $i_d$ -axis current component; hence the torque can be controlled by adjusting  $i_q$ . Constant torque can be achieved by ensuring that  $i_d$  is kept constant. If the flux control is needed the  $i_d$  can be calculated as a function of  $i_q$  and speed based on algorithms such as LMA.

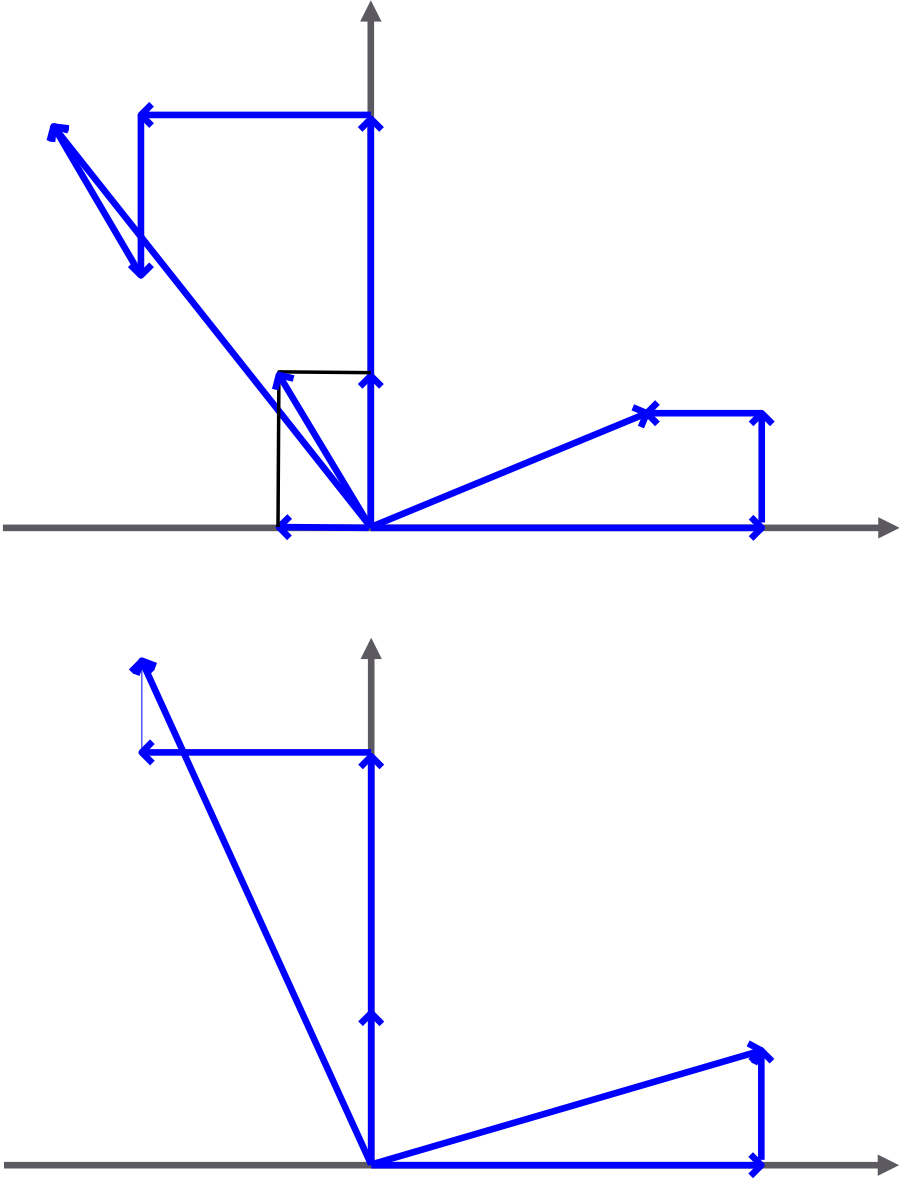


Fig. 2.5: (a) General vectors diagrams, (b) Vectors diagrams with  $i_d$  constant.

When 3-phase balanced currents are applied to stator windings, they create a rotating magnetic field which causes the rotor to get the torque and rotate. This phenomenon is illustrated

below. Fig. 2.6 shows the balanced 3-phase currents along with stator windings assuming there are two poles in the machine.

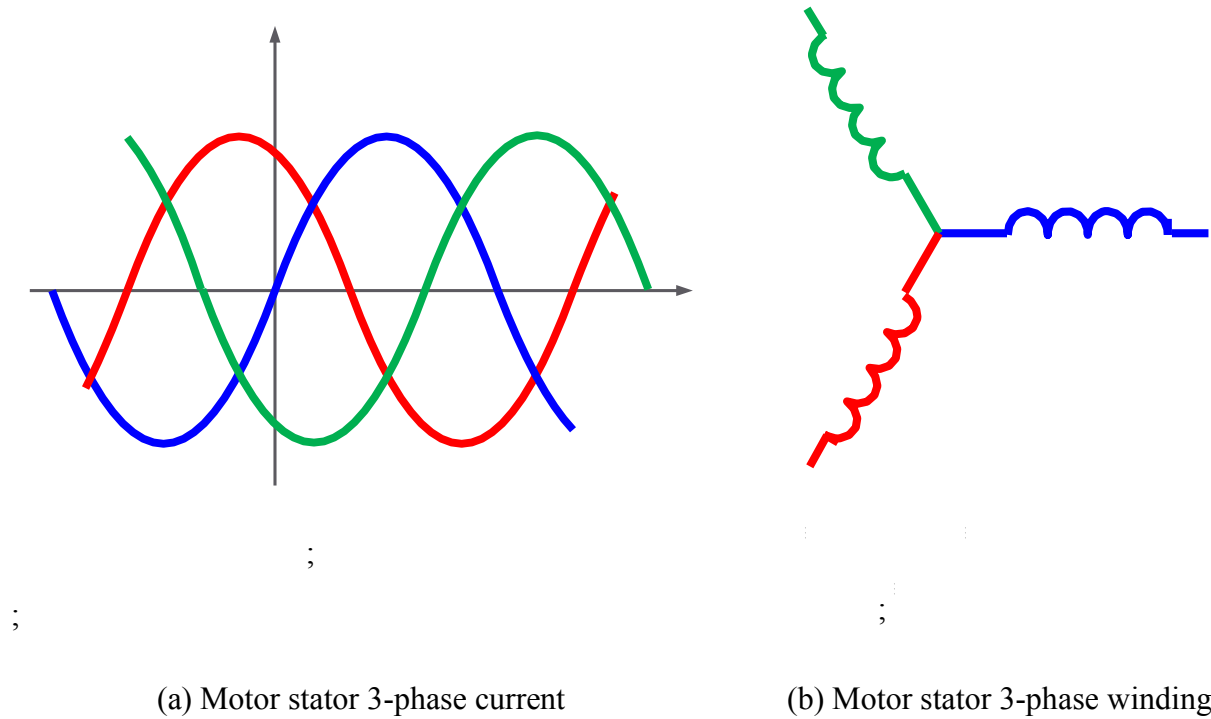


Fig. 2.6: Motor 3-phase current and stator windings.

As 3-phase currents are passing through three phase stator windings, so total instantaneous electromagnetic torque can be obtained as,

$$\begin{aligned}
 & \left( \frac{2}{3} \right) \\
 & \left( \frac{2}{3} \right) \\
 & \left( \frac{2}{3} \right) \\
 & \left( \frac{2}{3} \right)
 \end{aligned}$$

The real part of the above equation can be separated as follows,

$$\begin{aligned}
& \left( \frac{\sqrt{-1}}{2} \right) \left( \frac{\sqrt{-1}}{2} \right) \\
& \left[ \left( \frac{\sqrt{-1}}{2} \right) \left( \frac{\sqrt{-1}}{2} \right) \right] \left( \frac{\sqrt{-1}}{2} \right) \\
& \left[ \left( \frac{\sqrt{-1}}{2} \right) \left( \frac{\sqrt{-1}}{2} \right) \right] \left( \frac{\sqrt{-1}}{2} \right) \\
& \left[ \left( \frac{\sqrt{-1}}{2} \right) \left( \frac{\sqrt{-1}}{2} \right) \right] \left( \frac{\sqrt{-1}}{2} \right) \\
& \left( \frac{\sqrt{-1}}{2} \right) \left( \frac{\sqrt{-1}}{2} \right) \left( \frac{\sqrt{-1}}{2} \right) \left( \frac{\sqrt{-1}}{2} \right) \\
& - \left( \frac{\sqrt{-1}}{2} \right) \left( \frac{\sqrt{-1}}{2} \right) \\
& - \left( \frac{\sqrt{-1}}{2} \right) \left( \frac{\sqrt{-1}}{2} \right) \\
& - \left( \frac{\sqrt{-1}}{2} \right) \left( \frac{\sqrt{-1}}{2} \right)
\end{aligned}$$

Similarly, the imaginary part can be calculated as,

$$\begin{aligned}
& \left( \frac{\sqrt{-1}}{2} \right) \left( \frac{\sqrt{-1}}{2} \right) \\
& \left[ \left( \frac{\sqrt{-1}}{2} \right) \left( \frac{\sqrt{-1}}{2} \right) \right] \left( \frac{\sqrt{-1}}{2} \right) \\
& \left[ \left( \frac{\sqrt{-1}}{2} \right) \left( \frac{\sqrt{-1}}{2} \right) \right] \left( \frac{\sqrt{-1}}{2} \right) \\
& \left[ \left( \frac{\sqrt{-1}}{2} \right) \left( \frac{\sqrt{-1}}{2} \right) \right] \left( \frac{\sqrt{-1}}{2} \right)
\end{aligned}$$

$$\begin{aligned}
 & \left[ \begin{array}{c} \sqrt{2} \\ \sqrt{2} \end{array} \right] \left( \begin{array}{c} \sqrt{2} \\ \sqrt{2} \end{array} \right) \\
 & \left[ \begin{array}{c} \sqrt{2} \\ \sqrt{2} \end{array} \right] \left( \begin{array}{c} \sqrt{2} \\ \sqrt{2} \end{array} \right) \\
 & - \left( \begin{array}{c} \sqrt{2} \\ \sqrt{2} \end{array} \right) \left( \begin{array}{c} \sqrt{2} \\ \sqrt{2} \end{array} \right)
 \end{aligned}$$

Therefore, the total torque can be expressed in the vector form as follows:

$$-$$

Substituting (2.29) and (2.30) into (2.31),

$$\begin{aligned}
 & - \left( \begin{array}{c} \sqrt{2} \\ \sqrt{2} \end{array} \right) \left( \begin{array}{c} \sqrt{2} \\ \sqrt{2} \end{array} \right) \\
 & - \left( \begin{array}{c} \sqrt{2} \\ \sqrt{2} \end{array} \right) \left( \begin{array}{c} \sqrt{2} \\ \sqrt{2} \end{array} \right)
 \end{aligned}$$

Therefore we can have:

$$\begin{aligned}
 & - \left( \begin{array}{c} \sqrt{2} \\ \sqrt{2} \end{array} \right) \\
 & - \left( \begin{array}{c} \sqrt{2} \\ \sqrt{2} \end{array} \right) \\
 & - \left( \begin{array}{c} \sqrt{2} \\ \sqrt{2} \end{array} \right)
 \end{aligned}$$

Substituting the equation into torque expression, so the final torque expression as follows:

$$\begin{aligned}
 & - \left[ \begin{array}{c} \sqrt{2} \\ \sqrt{2} \end{array} \right] \left( \begin{array}{c} \sqrt{2} \\ \sqrt{2} \end{array} \right) \\
 & - \left[ \begin{array}{c} \sqrt{2} \\ \sqrt{2} \end{array} \right] \left( \begin{array}{c} \sqrt{2} \\ \sqrt{2} \end{array} \right) \\
 & - \left[ \begin{array}{c} \sqrt{2} \\ \sqrt{2} \end{array} \right] \left( \begin{array}{c} \sqrt{2} \\ \sqrt{2} \end{array} \right)
 \end{aligned}$$

### 2.3.3 Flux and Torque Comparator

The calculated motor air gap flux ( ) and output torque ( ) will be compared with the desired air gap torque ( ) and desired output torque ( ), respectively. Both of these value are calculated based on the command speed ( ) and motor nominal parameters. For the flux comparator, the error between actual air gap flux ( ) and the reference flux ( ) can be defined as, . The flux comparator logic is given below,

For the torque comparator, the error between the reference and actual torque ( ) is defined as:

The torque and flux hysteresis band controls are also shown in Fig. 2.7.

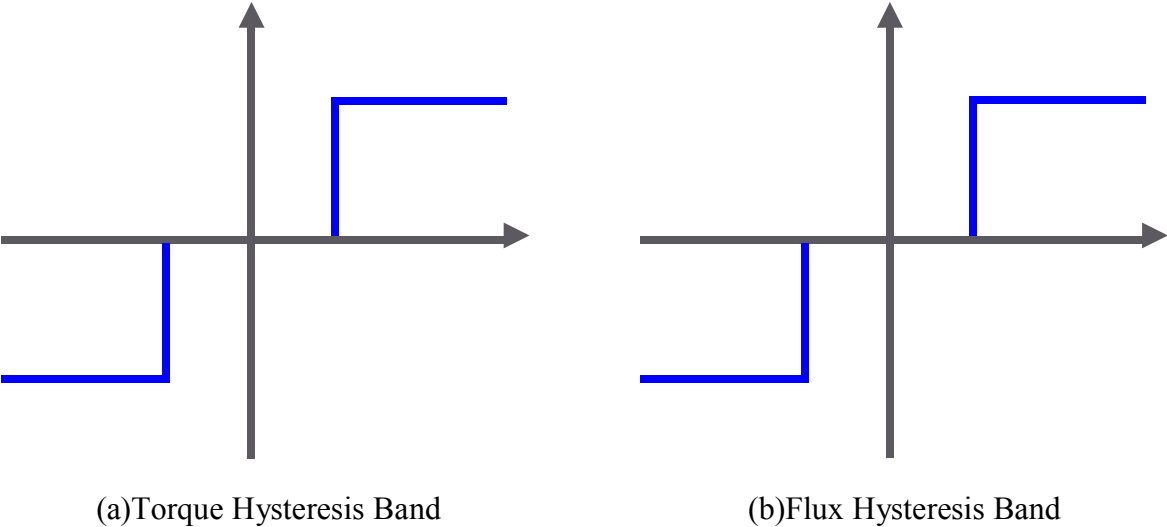


Fig. 2.7: Torque and flux hysteresis bands.

### 2.3.4 Three-Phase IGBT Inverter

The power electronics is the interface of computer digital technology and high power device such as PMSM. The development of power electronics and DSP technology prompt the permanent magnet synchronous motor for high performance drive applications. A variable speed drive (VSD) is used in electro-mechanical drive systems to control AC motor speed and torque by varying motor input voltage and frequency. Fig. 2.8(a) shows the connection of a 3-phase IGBT inverter to the stator circuit of an ac motor.  $V_{H1}, V_{H2}, V_{H3}$  indicate the high side and  $V_{L1}, V_{L2}, V_{L3}$  indicate the low side of three legs of the inverter. Each stator phase can form two direction voltage vectors (One is pointed outside the phase and the other is pointed to the connection center of the three phases) as shown in Fig. 2.8(b). Therefore, the motor stator air gap can be divided into six sectors, which is also shown in Fig. 2.8(b).

Based on the output of the torque and flux comparators and sector numbers the switching logic and voltage vectors are shown in Table 2.1 and Table 2.2 respectively.

Table 2.1: IGBT Inverter Switching Logic.

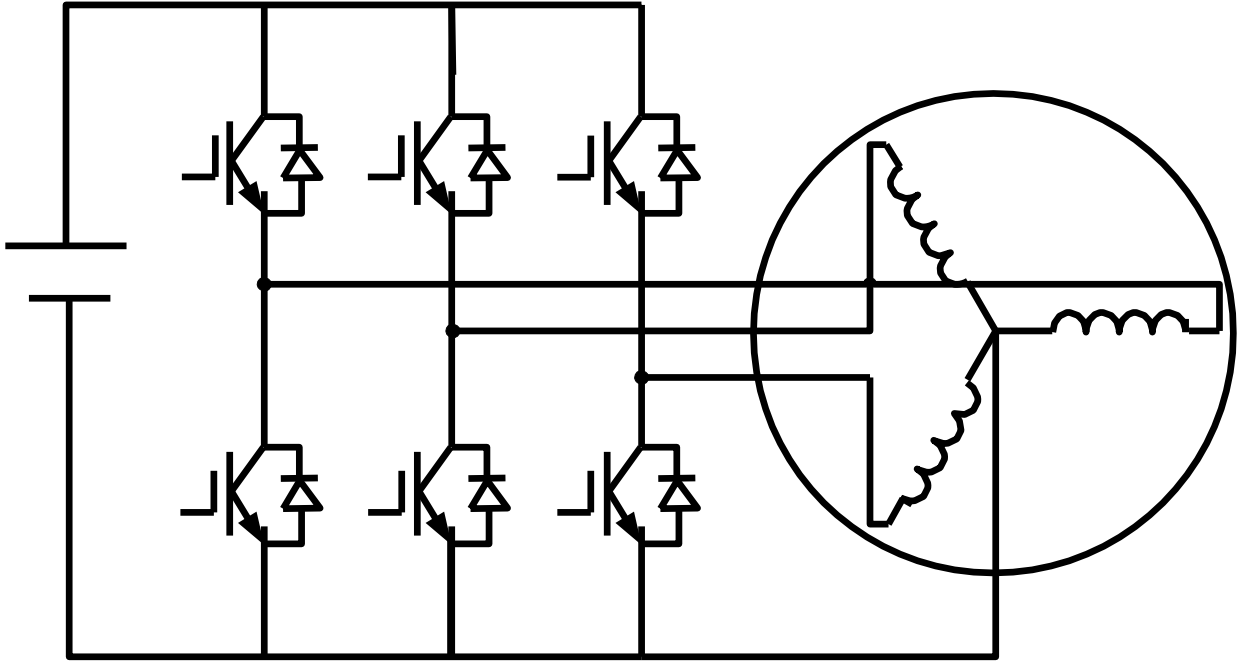
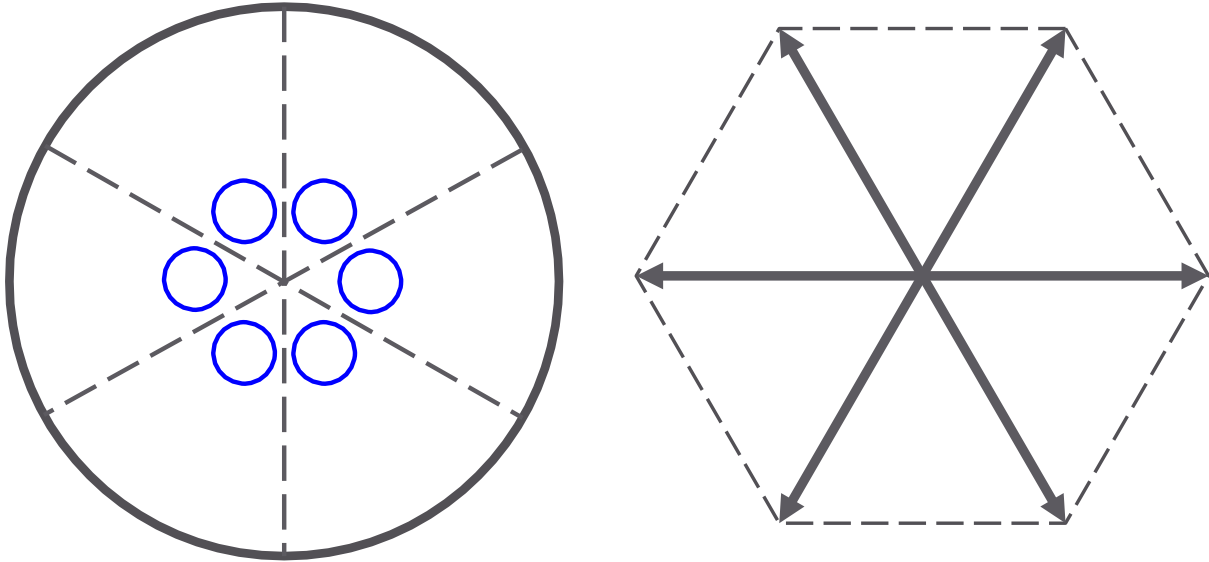



Fig. 2.8(a): 3-phase IGBT inverter connected to a 3-phase motor.



6 sectors of motor air gap

8 voltage vectors of inverter

Fig. 2.8(b): Motor air gap sectors (1~6) and 6 voltage vectors

With the input value which is the output of the flux and torque comparators, the voltage vector lookup table will output the IGBT inverter control signal. The lookup table is shown as following:

Table 2.2: DTFC Look-up Table for Inverter.


For example, at sector 1(                    ), if the flux is too high (                    and the torque (                    is too high, the voltage vector v2(110) is applied to the IGBT inverter. The voltage vector follows the zigzag path within the flux hysteresis band                    |                    | as vector shown in fig. 2.8. Thus, the actual flux, follows the reference flux vector. As the motor stator flux rotates in the air gap, the DTC system will select the right voltage vector from the lookup table. The selected voltage vector will make the air gap flux track the flux reference                    which is provided by the flux reference controller (discussed in next chapter). In this control strategy, the flux reference value                    and                    will satisfy the following relation:

$$\lambda_{ref} = \lambda_{*} + \Delta\lambda$$

The stator air gap flux is constrained within the hysteresis band therefore it tracks the reference flux in a zigzag trajectory, as shown in the Fig. 2.9.

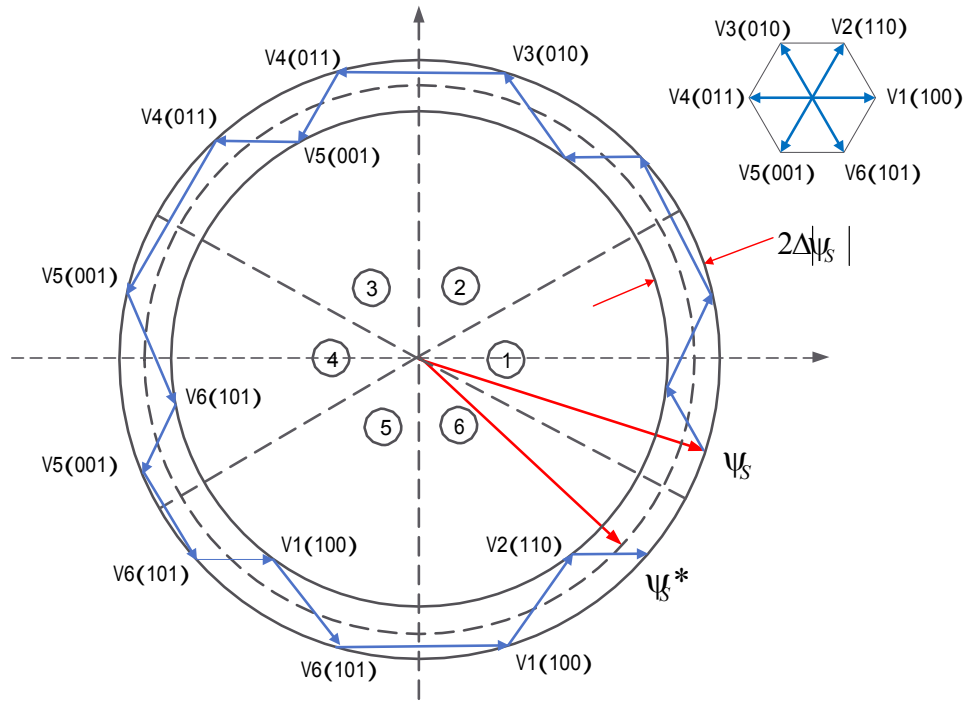


Fig. 2.9: Motor air gap flux zigzag path.

# Chapter 3

## Flux Controller Based DTFC for IPMSM Drive

### 3.1 Introduction

The advantages of direct torque and flux control (DTFC) over field vector control are that the DTFC scheme does not need any coordinate transformation, pulse width modulation (PWM) and current regulators. The DTFC utilizes hysteresis band comparators for both flux and torque controls. The PWM modulator stage takes almost 10 times longer processing time than the DTFC to respond to the actual change [32-33]. The DTFC uses flux and torque as primary control variables, which are directly obtained from the motor itself. Thus, the DTFC is simpler and much faster to respond as compared to the conventional vector control.

Most of the reported works on DTFC based IPMSM drive considered the reference flux constant corresponding to rated condition [32-45]. Thus, it is not possible to optimize the efficiency of IPMSM drive as the flux is not controlled.

Therefore, this chapter presents a novel loss minimization based adaptive flux observer for DTFC control of PMSM drive so that the drive system can maintain both high efficiency and high dynamic performance. Several loss minimization algorithms (LMAs) for PMSM drives have been reported in the literature [62-66]. Among different LMAs the model based LMA has the advantage of fast convergence and less torque ripple as compared to the search based LMA [67]. Thus, in this work a model based LMA for interior type PMSM is developed to estimate the reference air-gap flux for DTFC scheme. The motor efficiency is optimized by minimizing the electrical losses through LMA.

### 3.2 Loss Minimization Based Reference Flux Estimation

Fig. 3.1 shows the proposed LMA based DTFC scheme for IPMSM drive. The basic principle of DTFC was discussed in Chapter 2. The voltage and air-gap flux vectors in different sectors for DTFC scheme were shown in Fig. 2.8. The command air gap flux reference ( ) and

motor reference torque ( ) magnitudes are compared with their respective actual values obtained from observers and the errors are processed through hysteresis band controllers. As the motor stator flux rotates in the air gap, the DTFC scheme will select the right voltage vector from the lookup table. The selected voltage vector will make the air gap flux ( ) to track the flux reference ( ). In this control strategy, actual air gap flux follows the reference flux within hysteresis band ( $=2 | |$ ) as follows:  $| |$   $| |$

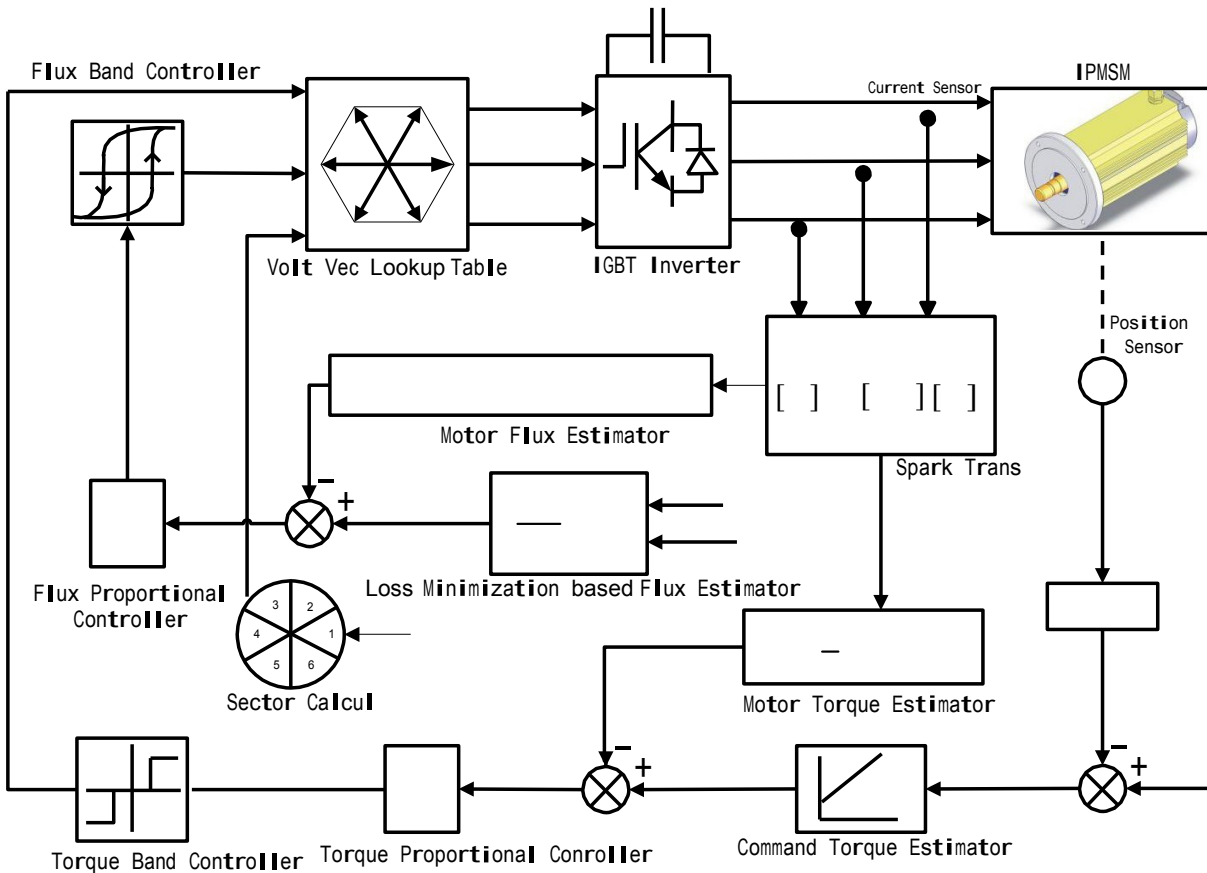


Fig. 3.1: Reference flux and torque estimator for DTFC based IPMSM drive.

A model based LMA is developed to obtain the optimal flux value, which will act as command flux for the DTFC based IPMSM drive. In PMSM the flux cannot be controlled directly as the main flux is supplied by the permanent magnet. In an IPMSM the d-axis armature reaction current,  $i_d$  is utilized to control the flux. The optimum value of  $i_d$  is calculated through LMA so that it minimizes the electric power losses of the motor. The d-q axis mathematical model of

PMSM incorporating the iron loss is shown in Fig. 3.2. From this figure the d-q axis currents are obtained as:

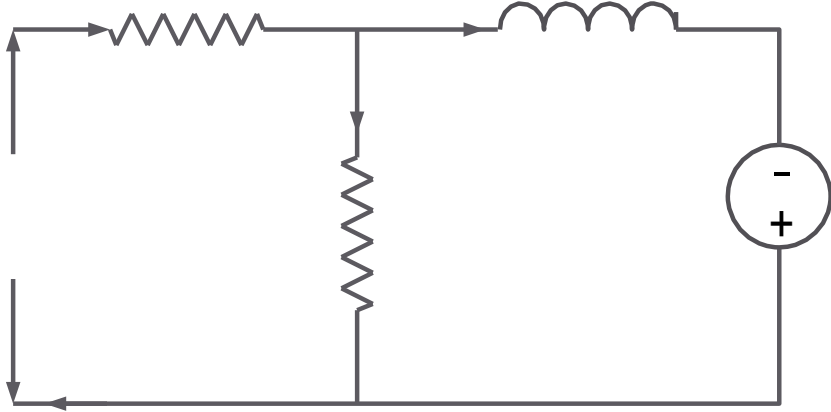


Fig. 3.2(a): d-axis model of IPMSM incorporating iron loss

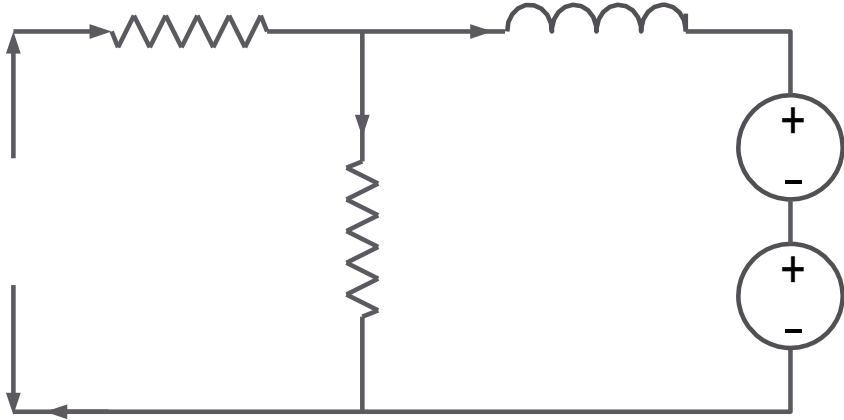


Fig. 3.2(b): q-axis model of IPMSM incorporating iron loss

From the Fig. 3.2 the d-q axis voltage and current are obtained as following,  
 The d-axis voltage,  $v_d$  can be written as,

where,  $v_{d,core}$  is the d-axis core loss component and  $v_{d,mag}$  is the magnetizing component of  $v_d$ .

Substituting the  $\frac{1}{2} \frac{d\psi}{dt}$  into  $v = R i + \frac{d\psi}{dt}$ ,

Again,

Substituting the  $\frac{1}{2} \frac{d\psi}{dt}$  into  $v = R i + \frac{d\psi}{dt}$ ,

$$v = R i + \frac{d\psi}{dt} = R i + \frac{d}{dt} \left( \frac{1}{2} L i^2 + \psi_m \right)$$

$$= R i + L i \frac{di}{dt} + \frac{d\psi_m}{dt}$$

$$= R i + \frac{d}{dt} \left( \frac{1}{2} L i^2 \right) + \frac{d\psi_m}{dt}$$

$$= R i + \frac{d}{dt} \left( \frac{1}{2} L i^2 + \psi_m \right)$$

The q-axis voltage,  $v_q$  can be written as,

where  $R_q$  is the q-axis core loss component and  $\frac{d\psi_m}{dt}$  is the magnetizing component of  $v_q$ .

Substituting the  $\frac{1}{2} \frac{d\psi}{dt}$  into  $v = R i + \frac{d\psi}{dt}$ ,



Total electric power loss can be written as,

$$-( \quad )$$

Differentiating with respect to ,

$$-( \quad )$$

$$\quad$$

In order to reach the maximum efficiency operation condition, the minimum loss condition is achieved by differentiating with respect to and then set it to zero as,  $—$  . Thus, the optimal value of is obtained as,

$$—$$

$$\frac{\quad}{\quad}$$

The steady-state value of core loss component of d-axis current can be calculated from as the follows:

$$\underline{\quad ( \quad )}$$

$$\quad$$

$$\quad$$

$$\quad$$

$$\quad$$

( )

---

The steady-state value of core loss component of q-axis current can be calculated from as follows:

---

— — —

— —

— — — ( — — )

— — — ( — — )

— — — —

( )

---

Differentiating \_\_\_\_\_ with respect to \_\_\_\_\_ ,  
 \_\_\_\_\_ ( \_\_\_\_\_ ) \_\_\_\_\_  
 \_\_\_\_\_

\_\_\_\_\_

\_\_\_\_\_

Differentiating \_\_\_\_\_ with respect to \_\_\_\_\_ ,  
 \_\_\_\_\_ \_\_\_\_\_ \_\_\_\_\_ \_\_\_\_\_  
 \_\_\_\_\_

\_\_\_\_\_

\_\_\_\_\_

Since \_\_\_\_\_ , \_\_\_\_\_ are oriented orthogonally,  
 \_\_\_\_\_

Substituting the values of \_\_\_\_\_, \_\_\_\_\_, \_\_\_\_\_ into \_\_\_\_\_ , the optimal value of \_\_\_\_\_ as follows,

$$\frac{\partial \text{_____}}{\partial \text{_____}} = \text{_____}$$

$$\frac{\partial \text{_____}}{\partial \text{_____}} = \text{_____}$$

$$\frac{\partial \text{_____}}{\partial \text{_____}} = \text{_____}$$

Using (3.10), (3.19) and the relation \_\_\_\_\_ , the command value of \_\_\_\_\_ can be obtained as,

---

Substituting the command values of  $\omega^*$  and  $i^*$  into the following equation to acquire the final flux reference value for DTFC scheme can be calculated as,

where,  $\lambda$  is the magnetic flux linkage,  $\omega$  is the electrical speed. The motor model parameters are shown in Appendix A.

Efficiency Calculation:

Motor electrical power loss,

$$P_{loss} = \frac{3}{2} R_s i^2$$

Total power consumed by motor,

$$P_{total} = P_{mech} + P_{loss}$$

Motor electrical efficiency is given by,

### 3.3 Simulation Results

The performance of the proposed LMA based DTFC scheme for PMSM drive is tested in simulation at different operating conditions using MATLAB/SimuLink software. Sample results are presented below.

Fig. 3.3 shows the starting responses of the proposed LMA based DTFC scheme for IPMSM drive at rated conditions. It is clearly seen from Figs 3.3(a) and 3.3(b) that the speed can follow the command speed quickly and smoothly without any overshoot/undershoot while it can maintain high efficiency in steady-state. The corresponding current responses are shown in Figs. 3.3(c) and 3.3(d). The balanced operation is verified by steady state 3-phase currents shown in

Fig. 3.3(d). Fig. 3.4 shows the response of the proposed LMA based DTFC scheme for IPMSM drive at a speed of  $\omega_r$  / for different load conditions. It is clearly seen that the efficiency drops at light load ( $\frac{1}{3}$  of the rated load) condition. It is the usual case as the mechanical losses are almost constant at any load condition. Fig. 3.5 shows the response of the proposed LMA based DTFC scheme for IPMSM drive at low speed of  $\frac{\omega_r}{10}$  / for different load conditions. It is found that the proposed drive can maintain high efficiency even at low speed condition. Therefore, it is found from Figs. 3.5~3.7 that the proposed LMA based DTFC scheme can maintain high efficiency as well as high dynamic performance at different speed and load conditions.

Fig. 3.6(a) shows the responses of the proposed drive for step changes in command speeds from  $\frac{\omega_r}{10}$  / to  $\frac{\omega_r}{5}$  / in a step of  $\frac{\omega_r}{10}$  / . It is found that the motor can follow the command speed smoothly while the LMA based flux observer can maintain high efficiency ( $\geq 86\%$ ) over a wide speed range. Fig. 3.6(b) shows the estimated flux which is decreasing with the increase in speed. This is due to the fact that the stator current increases and hence, the d-axis demagnetizing current  $i_{d1}$  increases with the increase in speed. The increase in  $i_{d1}$  in negative direction can be seen in Fig. 3.6(c). The q-axis current is almost constant as the load is constant. Thus, the stator air-gap flux decreases with the increase in speed. Fig. 3.7 shows the motor speed and efficiency responses for step changes in command speed at full load with conventional constant flux based DTFC control. If the flux command value is kept constant at high value, the motor is not able to follow the high command speed due to the non optimal value. It can be seen from Fig. 3.7(a) that the motor was able to follow only up to around  $\frac{\omega_r}{5}$  / but the efficiency was almost same as the proposed LMA based flux observer. If the command speed is more than  $\frac{\omega_r}{5}$  / the motor became unstable and came to stop. If the flux is kept constant at low value, the motor can follow the either way of command speed but the efficiency is lower than that of proposed controller, which can be seen from Fig. 3.7(b)

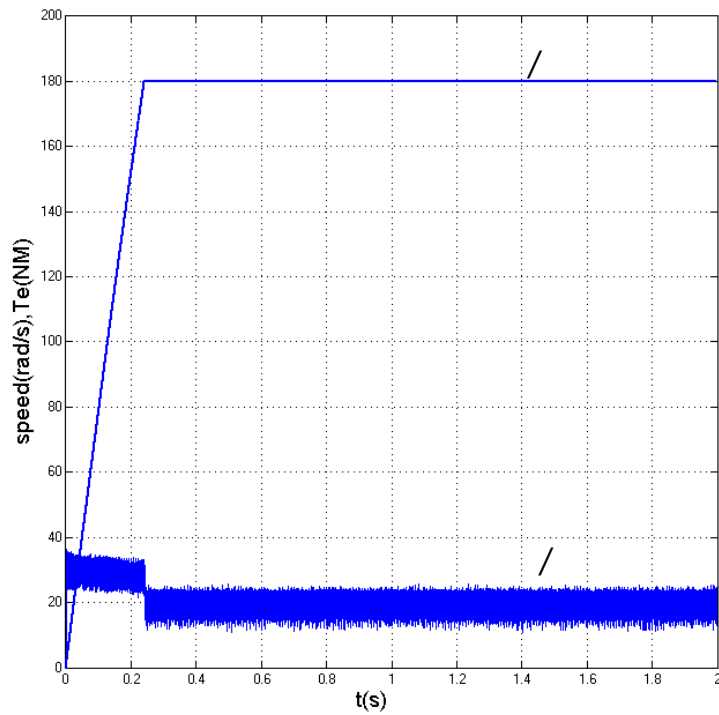
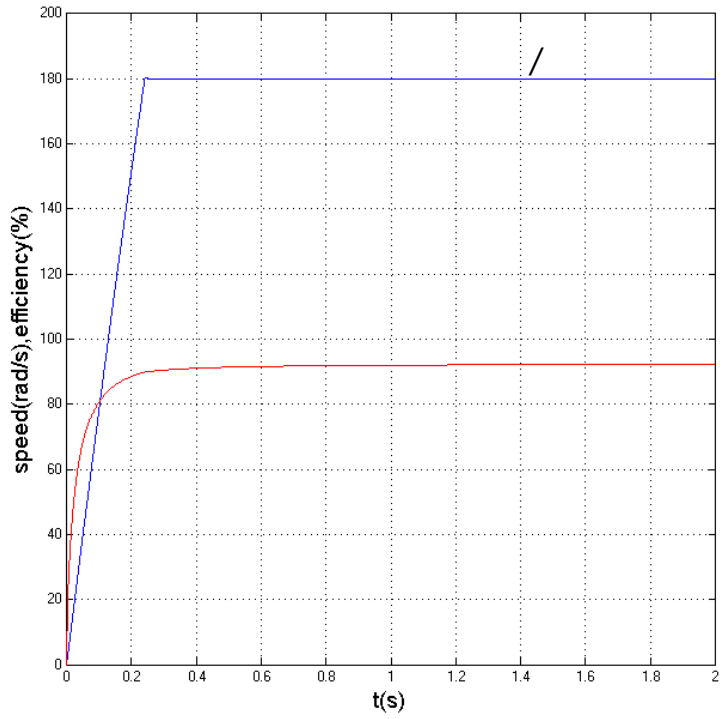


Fig. 3.3: Simulated starting responses of the proposed LMA based DTFC scheme for IPMSM drive at rated load ( ) and rated speed ( / ) conditions: (a) speed & efficiency, (b) speed and torque.

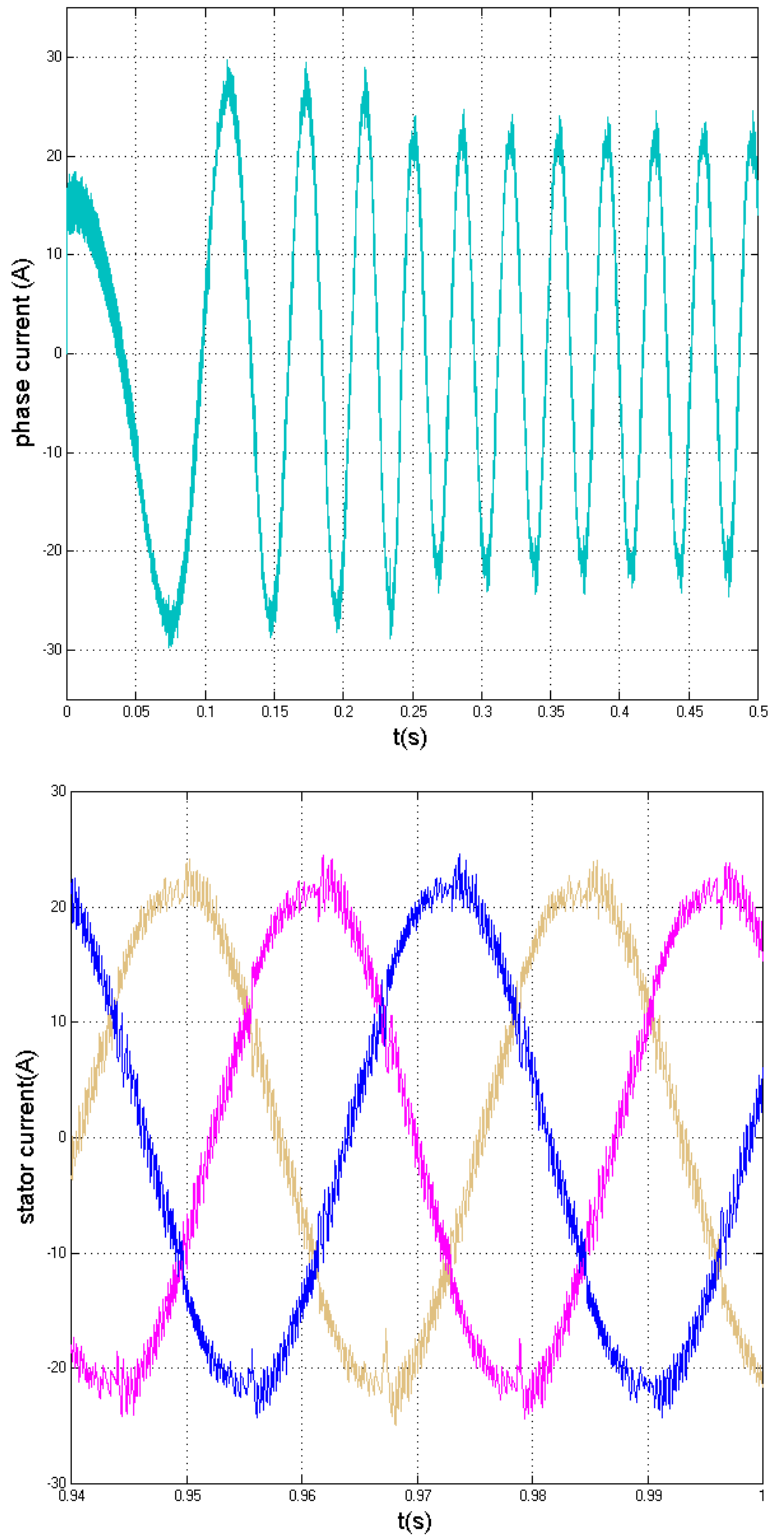


Fig. 3.3: Simulated current responses of the proposed LMA based DTFC scheme for IPMSM drive at rated load ( ) and rated speed ( / ) conditions: (c) single phase current (d) 3-phase stator current.

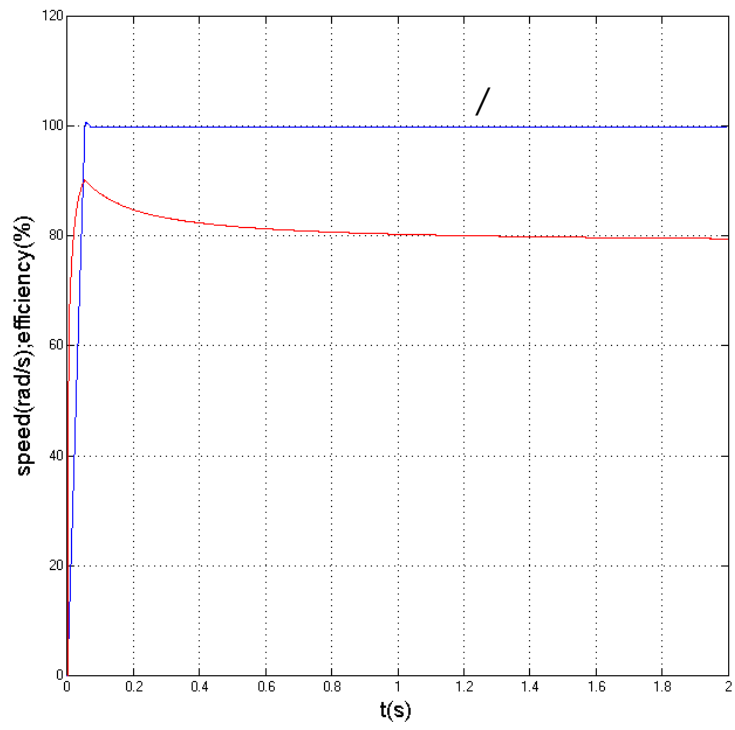
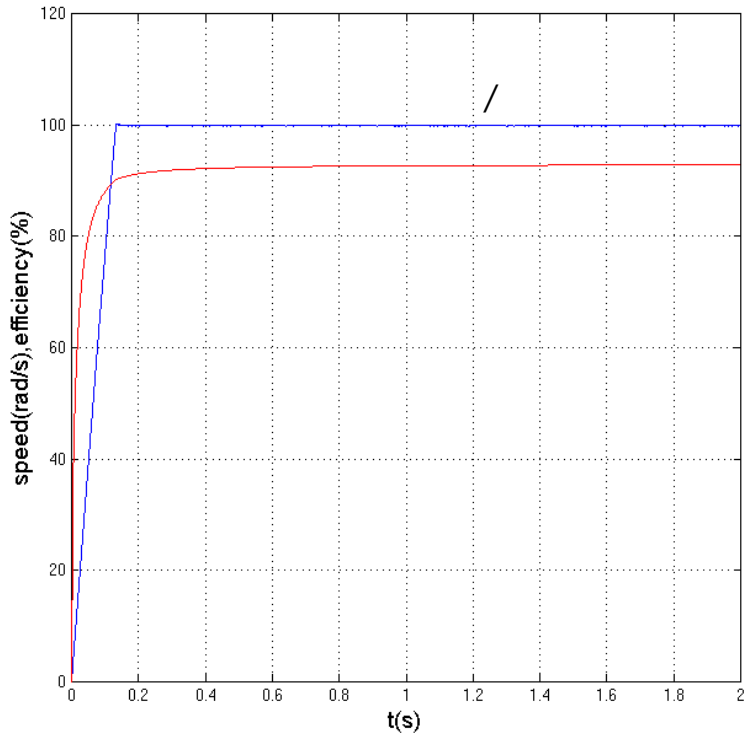


Fig. 3.4: Responses of the proposed LMA based DTFC scheme for IPMSM drive at a speed of  $\omega$  for different load conditions: (a)  $\omega$ , (b)  $\omega$ .

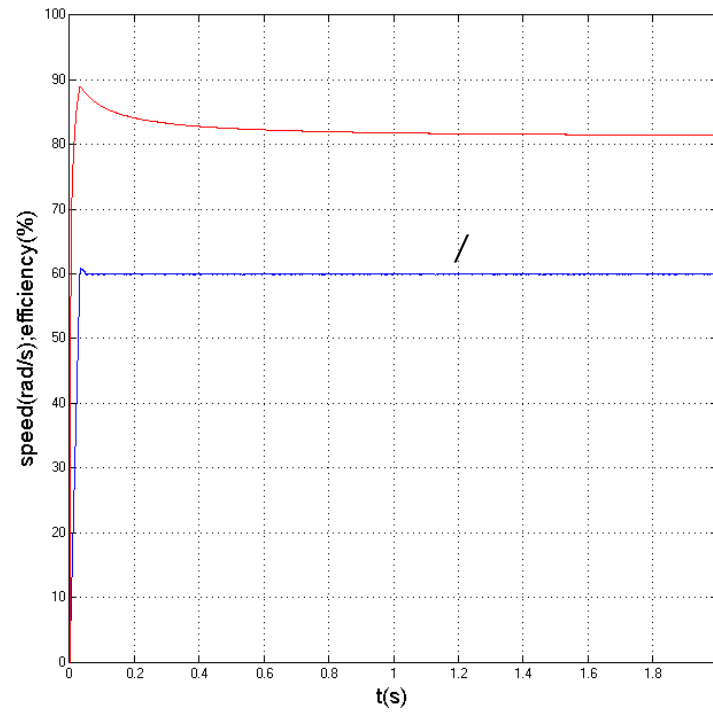
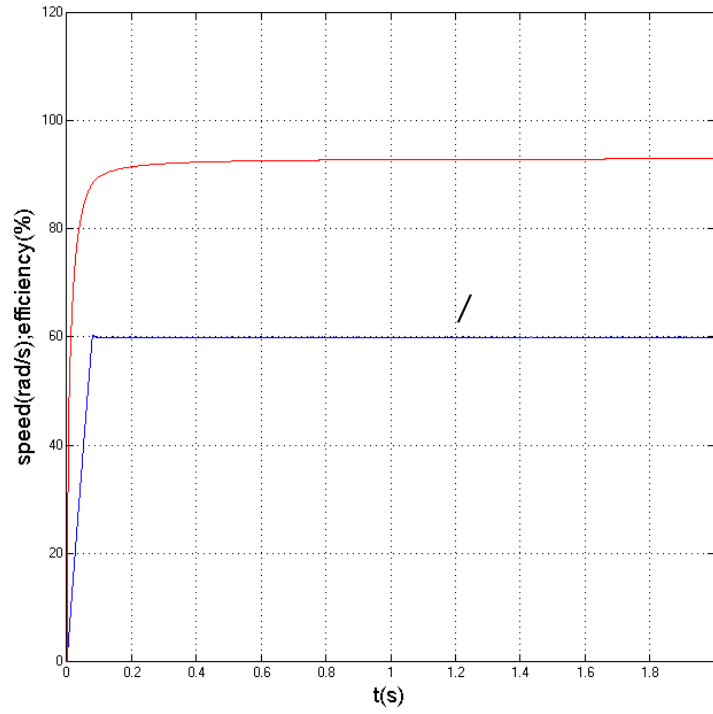


Fig. 3.5: Responses of the proposed LMA based DTFC scheme for IPMSM drive at low speed of  $\omega_r$  : (a)  $\omega_r = 60$  rad/s, (b)  $\omega_r = 88$  rad/s.

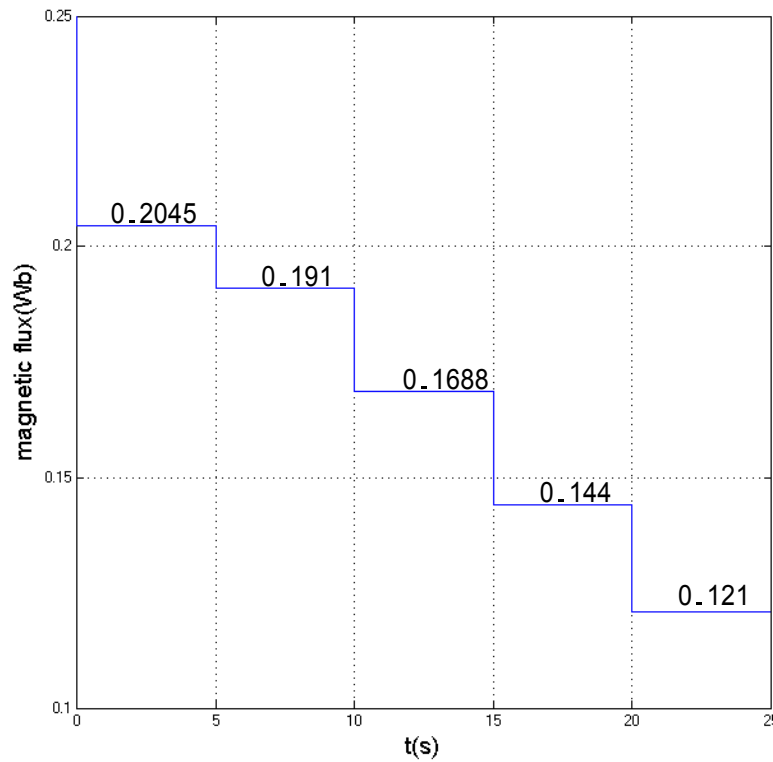
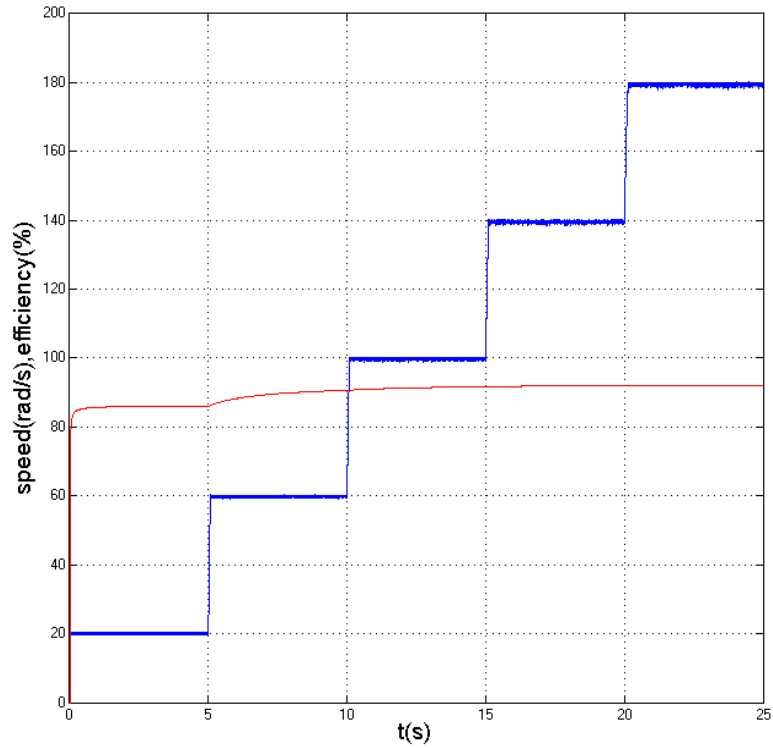


Fig. 3.6: Responses of the proposed LMA based DTFC scheme for IPMSM drive for step changes in command speeds from 20 / 180 at full load: (a) speed & efficiency, (b) estimated flux.

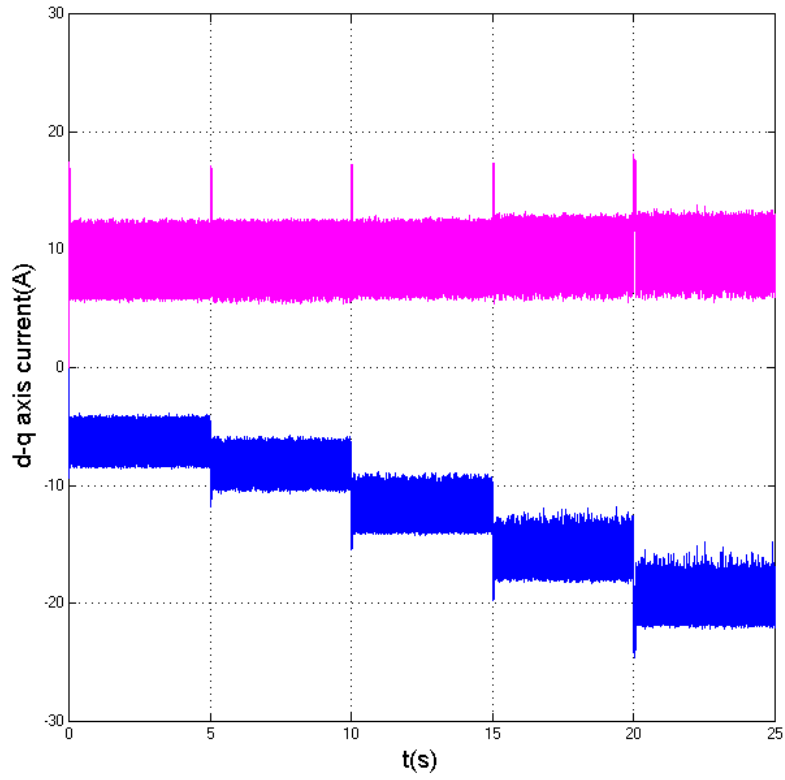


Fig. 3.6: Responses of the proposed LMA based DTFC scheme for IPMSM drive for step changes in command speeds from  $\omega^* = 1000$  /  $\omega^* = 1500$  /  $\omega^* = 2000$  /  $\omega^* = 2500$  at full load: (c) current

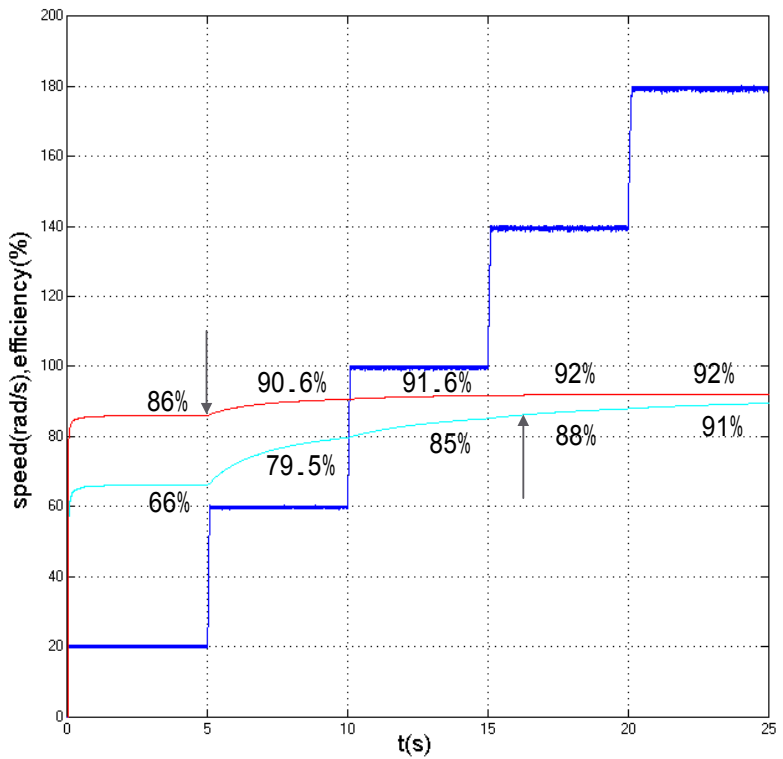
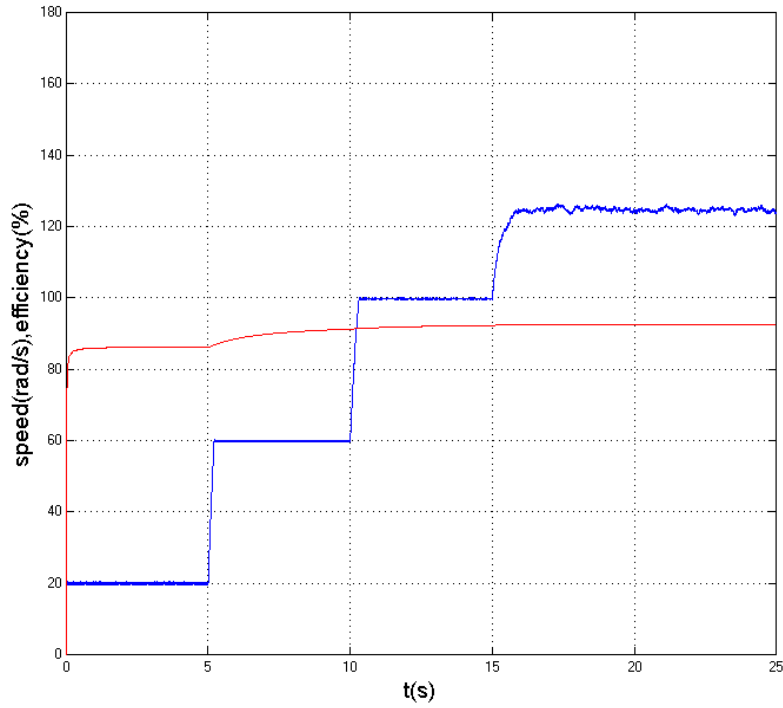


Fig. 3.7: Motor speed and efficiency responses for step changes in command speed at full load with: (a) constant high flux command value, (b) constant low flux command value.

Fig. 3.8 shows the comparative motor efficiency of the proposed LMA based flux observer with the conventional constant flux based DTFC scheme for step changes in load while the motor is running at a speed of  $\omega_r$  /  $\omega_b$ . The simulation result proved that both proposed flux observer and conventional constant low flux based DTFC scheme have good efficiency and speed response. Moreover, with constant high flux motor can follow only low speed. Therefore, the motor was tested at relative low speed  $\omega_r$  /  $\omega_b$  condition for the sake of comparing the efficiency of the proposed flux observers with constant low and high flux based DTFC scheme. It is clearly seen from this figure that the proposed LMA based DTFC scheme can always maintain higher efficiency as compared to the conventional constant flux based DTFC control of IPMSM drive. The comparative efficiency of the proposed LMA based flux observer with constant flux based DTFC scheme is summarized in Table 3.1. It is obvious that the efficiency of constant command flux value is lower than the efficiency of adjustable flux observer. The efficiency difference reaches the maximum value at  $\omega_r$  /  $\omega_b$  which is over 20 percent and it decrease as the speed increase. At rated conditions ( $\omega_r$  /  $\omega_b$  ,  $T_r$  /  $T_b$ ), the efficiencies are same for the proposed and constant high flux based IPMSM drive. These results prove that the proposed flux observer minimizes the electrical loss and hence reaches the maximum efficiency at any operating condition. On the other hand, the constant low command flux value only let the motor work at all speed region but the electrical loss will increase significantly at motor low speed operation region.

Therefore, it is found from simulation results that the proposed LMA based flux observer for DTFC scheme can achieve both high efficiency and high dynamic performance at different load and speed conditions.

Table 3.1: comparative efficiency at different speed and load condition.

/				
/				
/				
/				

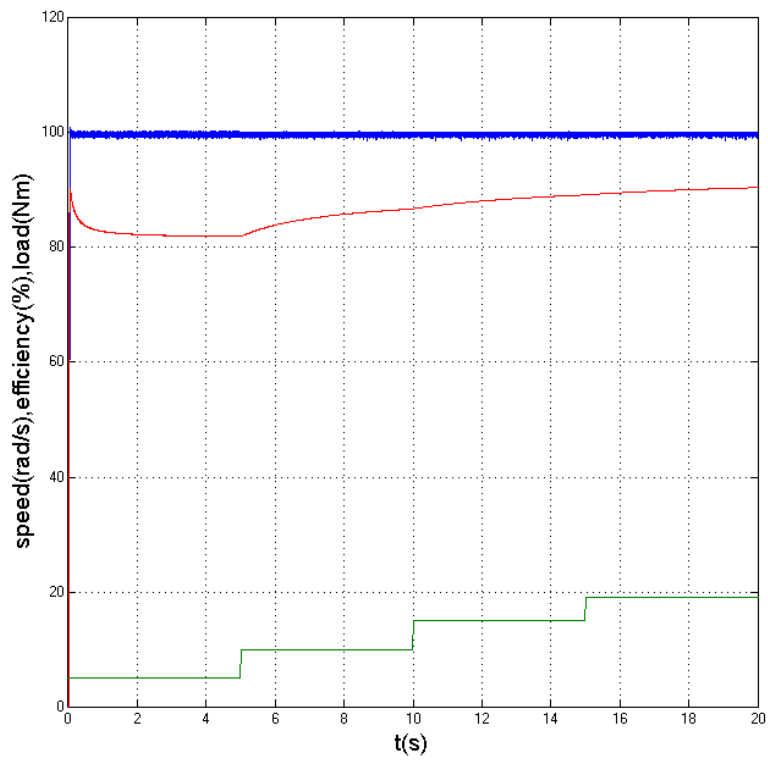
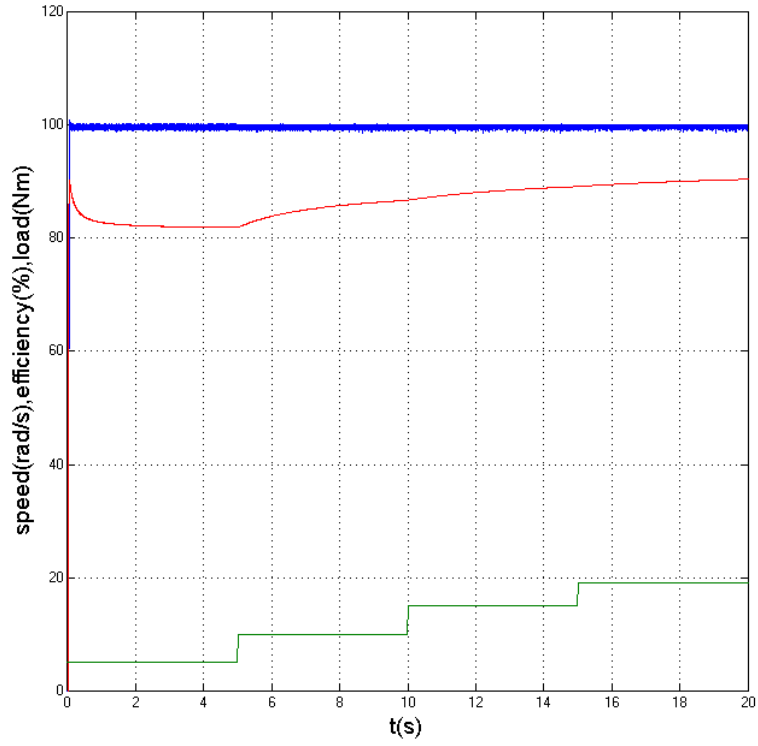


Fig. 3.8: Motor efficiency for step changes in load at a speed of 100 rad/s : (c) constant high flux based DTFC scheme.

### 3.4 Comparison of DTFC and Vector Control Techniques for IPMSM Drive with Loss Minimization Approach

Over the years, the vector control (VC) technique has been used for high performance motor drives as it decouples the torque and flux controls of ac motor.

Thus the ac motor behaves like a separately excited dc motor while maintaining its advantages over dc motors [68-70]. Recently, researchers paid some attention to the application of DTFC scheme for motor drives due to its advantages over conventional VC scheme such as, it doesn't need any coordinate transformation, pulse width modulation (PWM) and current regulators [71-75]. The PWM modulator stage takes almost 10 times longer processing time than the DTFC to respond to the actual change [76]. The DTFC uses flux and torque as primary control variables which are directly obtained from the motor itself. Thus, the DTFC is simpler and much faster to respond as compared to the conventional VC [71-75]. Therefore, in this chapter a performance comparison between DTFC and VC techniques for IPMSM drives in the context of loss minimization and dynamic responses is provided. Simulation models of the PMSM drives with both DTFC and VC techniques along with LMC are built using MATLAB/SimuLink software.

Fig. 3.9 shows the loss minimization based vector control of PMSM drive. The torque observer generates the command torque which is the input to the LMC block. The LMC generates the d-q axis command current. Then the three phase command currents ( ) are generated using the inverse Park's and Clark's transformation as,

$$\begin{bmatrix} i_a \\ i_b \\ i_c \end{bmatrix} = \begin{pmatrix} \cos & -\sin \\ \sin & \cos \\ 1 & 1 & 1 \end{pmatrix} \begin{bmatrix} i_d \\ i_q \end{bmatrix}$$

These command currents are then compared with the corresponding actual currents and the current errors are processed through the current controllers which generates the pulse width modulated (PWM) logic signals for the inverter switches.



really high as compared to that of DTFC scheme. Therefore, the VC scheme will create more thermal stress on the motor.

Fig. 3.12 shows the comparative speed and efficiency response for step changes in command speed. It is found that the DTFC can maintain higher efficiency than that of VC scheme at all speed conditions. Fig. 3.13 shows the speed and efficiency responses of both DTFC and VC schemes. The load is increased from \_\_\_\_\_ to \_\_\_\_\_ of rated load at \_\_\_\_\_ while the motor is running at \_\_\_\_\_. It is seen that the efficiency is low at light load condition while it is increasing at rated load condition but the DTFC always maintain higher efficiency than that of VC.

Further investigation was done to see why the vector control consumes more power from source than that of DTFC. Fig. 3.14(a) and 3.14(b) show the selected voltage vectors and corresponding torques during sector-2 \_\_\_\_\_ operation for DTFC and VC, respectively. There are total six active sectors for the air-gap flux, as a sample sector 2 is selected to show the difference in selection of voltage vectors between DTFC and VC. From Fig. 3.14(a), it can be seen that only voltage vectors 6, 4, 3 are applied at steady state condition. Whereas, with vector control not only \_\_\_\_\_, \_\_\_\_\_, \_\_\_\_\_, but also \_\_\_\_\_, \_\_\_\_\_, \_\_\_\_\_ are applied showed as the Fig. 3.14(b). That means all voltage vectors applied in each sector operation. These voltage vectors and different sequence of application cause higher phase current and more energy loss for the VC scheme. On the other hand, the DTFC exhibits higher peak-to-peak torque ripple than that of VC scheme as only three voltage vectors are active in any sector.

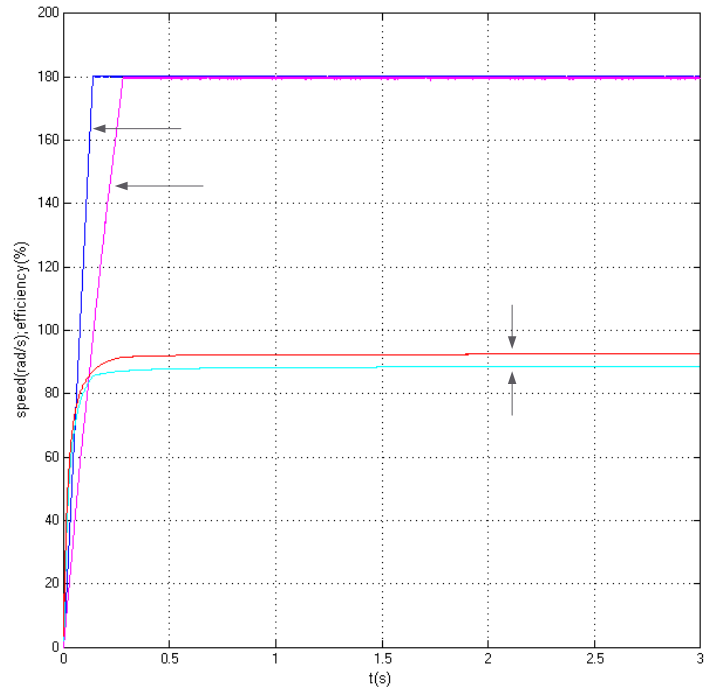


Fig. 3.10: Comparison of speed & efficiency responses for DTFC and VC based IPMSM drive at rated load and rated speed.

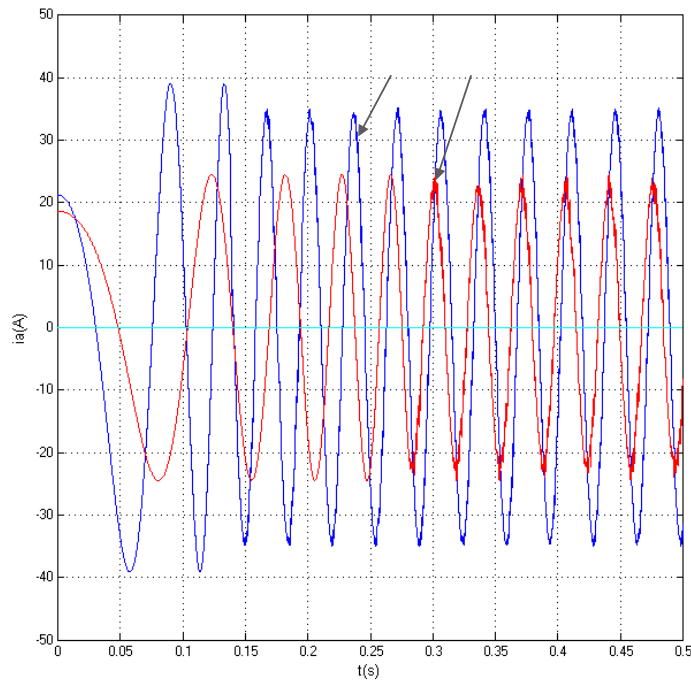


Fig. 3.11: Stator 'a' phase current comparison between DTFC and VC schemes.

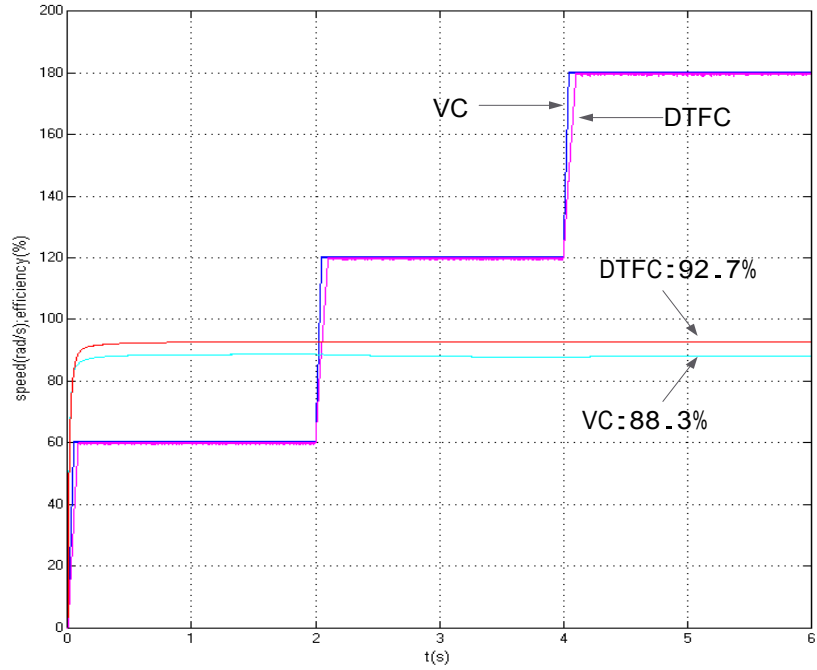


Fig. 3.12: Speed and efficiency responses of PMSM drives using DTFC and VC schemes for step changes in command speed.

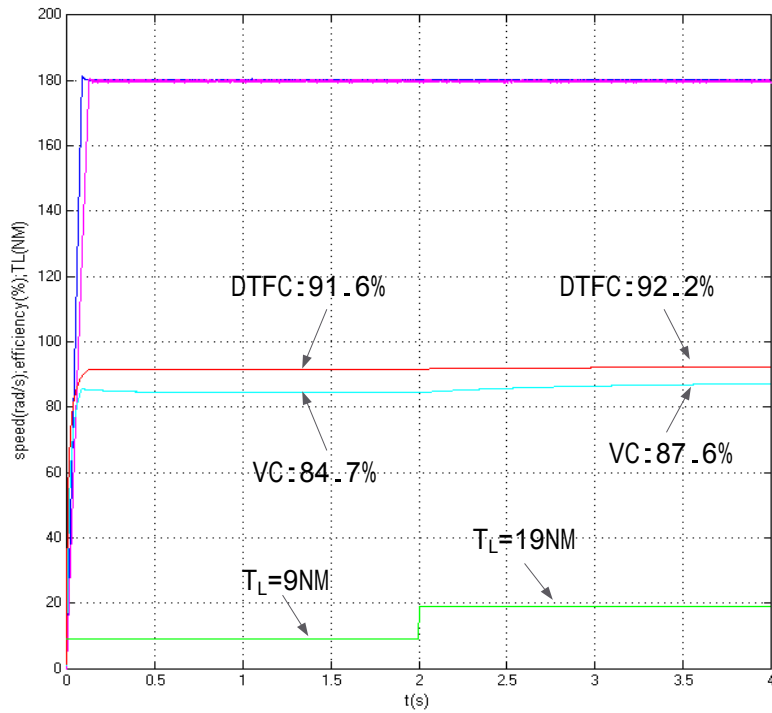


Fig. 3.13: Speed and efficiency responses of PMSM drives using DTFC and VC schemes for step changes in load.

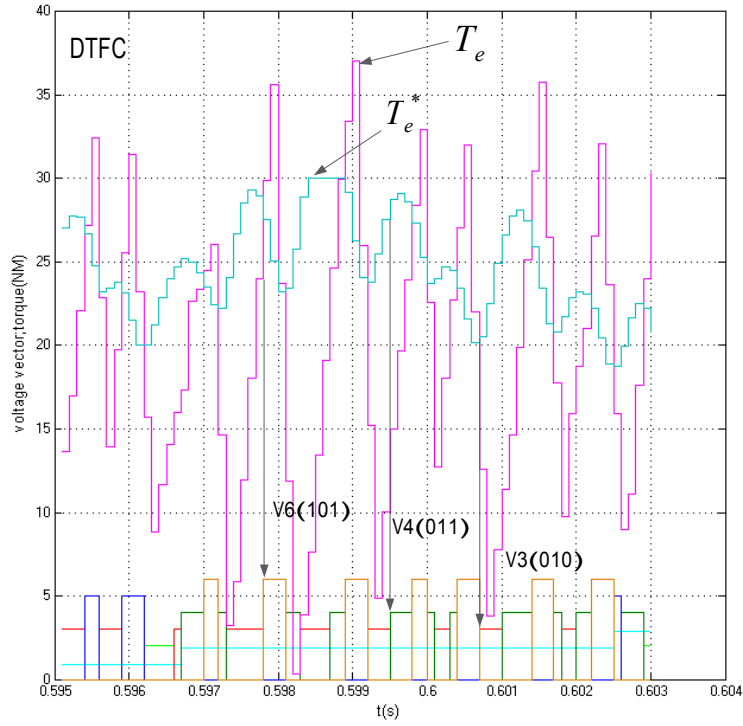


Fig. 3.14(a): Voltage vectors of DTFC during sector 2 ( $30^{\circ}\sim 90^{\circ}$ ).

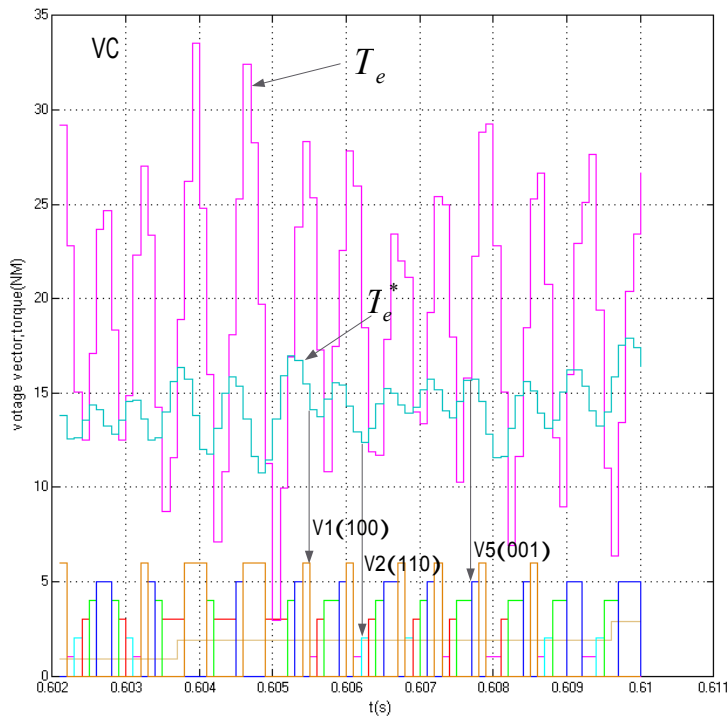


Fig. 3.14(b): Selected voltage vectors of VC during sector-2 ( $30^{\circ}\sim 90^{\circ}$ ).

## 3.5 Conclusion

In this Chapter first, the performance of the proposed LMA based flux observer for DTFC based IPMSM drive has been investigated extensively at different speed and load conditions. It is found that the proposed flux observer can work better than that of conventional constant flux based DTFC scheme. Then, a performance comparison between DTFC and VC techniques for IPMSM drive has been presented in this chapter. The particular emphasize was given in the loss minimization and dynamic response of both control techniques. The same LMC based LMA is utilized with both DTFC and VC based IPMSM drives to optimize the efficiency of the IPMSM drive. The performances of the IPMSM drive incorporating the LMC based DTFC and VC techniques were investigated in simulation at different operating conditions. It is found from the results that the LMA based DTFC provides better efficiency than that of LMA based VC technique. On the other hand, the VC technique provides better dynamic response than that of DTFC based PMSM drive. Thus, the DTFC scheme could be a better choice over vector control scheme for high performance and highly efficient motor drive applications.

## Chapter 4

# Experiment Verification of the Proposed DTFC Based IPMSM Drive

### 4.1 Introduction

The direct torque and flux control and vector control of IPMSM with LMC based controller are successfully implemented in real-time using DSP controller board DS 1104 on a laboratory 5 hp motor. The detailed real-time implementation is described in this chapter.

### 4.2 Hardware Implementation of the Drive

The block diagram of hardware schematic of VSI fed IPMSM drive is shown in Fig. 4.1. The DSP board DS1104 board is installed in an Intel PC with uninterrupted communication through dual port memory to implement the control scheme in real-time. The DS1104 board is mainly based on a Texas Instrument MPC8240 64-bit floating point digital signal processor. The block diagram of the DSP board is shown in Fig. 4.2. The DS1104 board uses a PowerPC type PPC603e processor which operates at the clock of 250 MHz with 32 KB cache. This board has a 32 MB of SDRAM global memory and 8 MB of flash memory. The DSP is supplemented by a set of on-board peripherals used in digital control systems including analog to digital (A/D), digital to analog (D/A) converters and digital incremental encoder interfaces. This board is also equipped with a TI TMS320F240 16-bit micro controller DSP that acts as a slave processor and provides the necessary digital I/O ports configuration and powerful timer functions such as input capture, output capture and PWM generation. In this thesis, the slave processor is used for only digital I/O subsystem configuration. Rotor position is sensed by an optical incremental encoder mounted at the rotor shaft and is fed back to the DSP board through the encoder interface. The encoder used in this work generates 1024 pulses per revolution. By using a built-in 4-fold pulse multiplication the output of the encoder is increased to  $4 \times 1024$  pulses per revolution in order to get a better resolution. So the resolution of the encoder is . These

pulses are fed to the one of two digital incremental encoder interface channels of the board. A 24-bit position counter is used to count the encoder pulses and is called by a calling function in the software. The counter is reset in each revolution by the index pulse generated from the encoder. The motor speed is computed from the measured rotor position angles using discrete difference equation ( — ————). The actual motor currents are measured by the Hall-effect sensors, which have current range of 0 ~ ±200A and a frequency range of 0~250 KHz. The current signals are fed back to DSP board through A/D channels. The output current signal of these sensors is converted to a voltage across the resistor connected between the output terminal of the sensor and ground. One can scale the output voltage by selecting the value of the resistors. These resistors can be within the range 0~100Ω. As the output voltages due to these current sensors are low, interface circuit is used to amplify the output of the sensor. The interface circuit

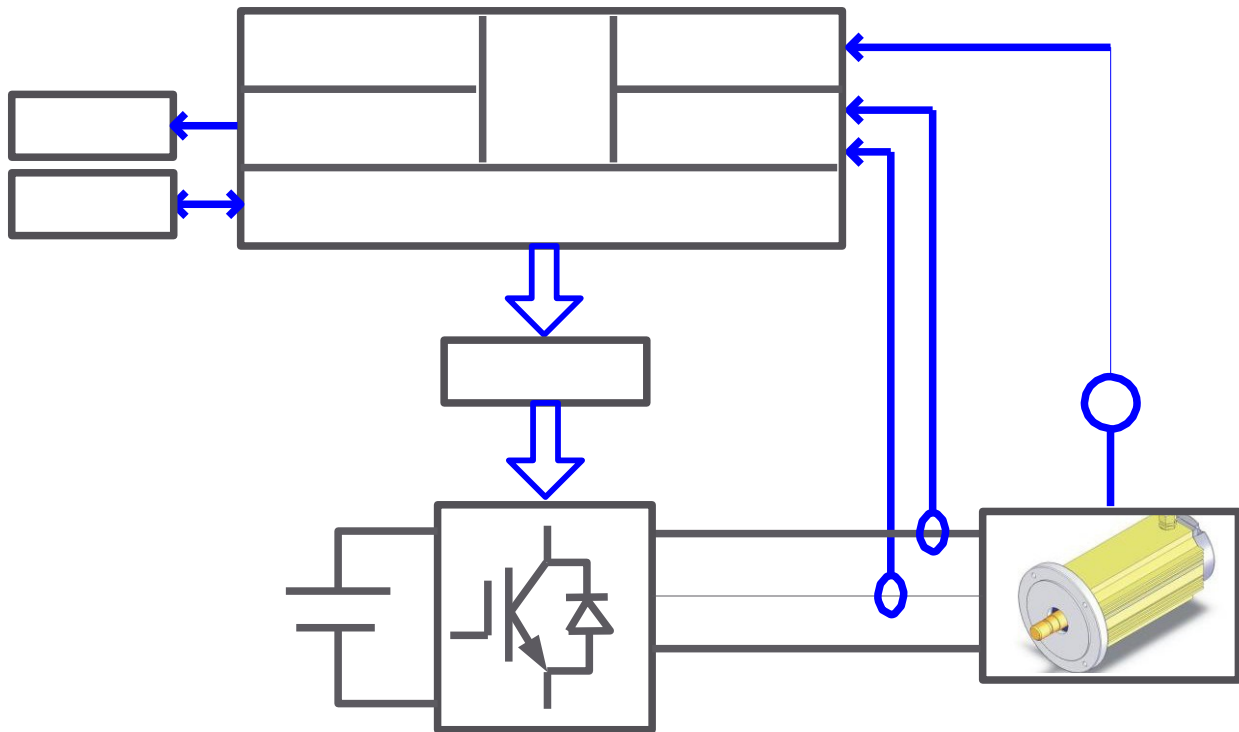


Fig. 4.1: Block diagram of hardware schematic of VSI fed IPMSM drive.

consists of a gate drive circuit as shown in Appendix D. As the motor neutral is not grounded, only two phases current are measured and the third phase current is calculated using Kirchoff's Current Law in software.

The command voltages are generated from the proposed controller and compared with the triangular carrier wave. This generates the logic signals which act as firing pulses for the inverter switches. Thus, these six logic signals are the outputs of the DSP board and fed to the base drive circuit of the IGBT inverter power module. The outputs of the digital I/O subsystem of the DS 1104 are six pulses with a magnitude of 5 V. This voltage level is not sufficient for the gate drive of IGBTs. Therefore, the voltage level is shifted from +5 V to +15V through the base drive circuit with the chip SN7407N as shown in Appendix D. At the same time it also provides isolation between low power and high power circuits.

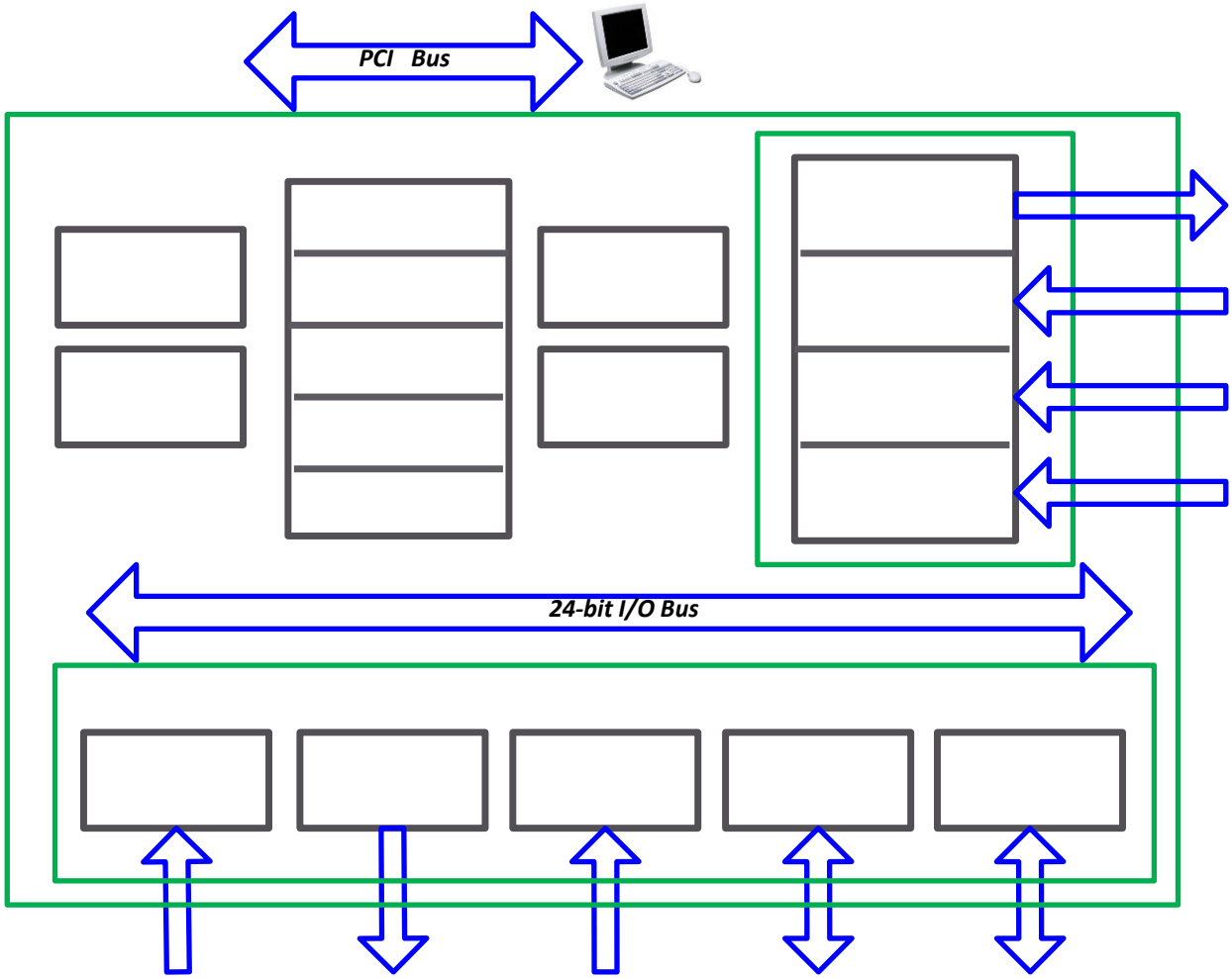


Fig. 4.2: Block diagram of DS1104 board.

## 4.3 Hardware Setup

The hardware setup for the real-time implementation of IPMSM drive is shown in Fig.4.3. The test IPMSM is labeled as 'M'. The rotor position of the test motor is measured by an optical incremental encoder which is labeled as 'E'. The encoder is directly connected to the rotor shaft. The motor is coupled with a DC machine (G) which works as a generator to act as loading machine to the motor. Some resistors (L) are connected to the output voltage terminals of the DC machine as load. The actual motor currents are measured by Hall-effect current transducers. Interface circuit (I) is located between the Hall-effect sensor and the A/D channel of DSP board. These transducers are labeled as 'CS'. These current sensors (CS) have a linear response over wide range of frequencies (up to 250 kHz). Another gate drive circuit is used to increase the power level of the firing pulses so that these are sufficient to drive the inverter insulated gate bipolar transistor (IGBT) switches. The gate drive circuit also provides isolation between low power control and the high power supply circuits. The gate drive circuit is labeled as 'D'. The power circuits consist of a 3-phase variable ac autotransformer (A), power supply (PS), rectifier and IGBT inverter (V). The DC bus voltage of the voltage source inverter (VSI) is obtained by rectifying ac voltage and filtered by a large capacitor ( $\approx 1000$  uF). The ac voltage is supplied by the power supply through autotransformer. The rectifier enclosed within 3-phase (6 pulses) IGBT inverter is labeled as 'V'. This inverter has active security feature against short circuit, under voltage of power supply as well as built in thermal protection, which prohibits destructive heat sink temperatures. The variable ac power of the rectifier is supplied by autotransformer (A). The personal computer, in which the DSP board DS1104 is installed, is labeled as 'PC'. A digital storage oscilloscope is used to capture the desired analog signal coming out through D/A port of the DSP board. The oscilloscope is labeled as 'O'. The complete drive has been implemented through both hardware and software which are discussed below.



Fig. 4.3: Experimental setup of the proposed DTFC based IPMSM drive.

## 4.4 Software Implementation of the Drive

In order to implement the control algorithm, a real-time SimuLink model is developed according to the complete drive system as shown in Appendix B. Then the model is downloaded to the DSP board using the Control Desk software [77]. The dSPACE DS1104 board is a self-contained system, not an embedded system. This means the board installed in the lab computer through a PCI slot has its own entity and the host PC does none of the processing for a system implemented on the board. As a result, the board requires that software to be created and downloaded to the board for the system to function.

The 'ControlDesk' software is used to download software to the DSP board, start and stop the function of the DS1104 as well as create a layout for interfacing with global variables in dSPACE programs. The sampling frequency used in DTFC is set to be 4 kHz and in VC is set to be 10kHz. If the sampling frequency that is higher than it can be, the 'overrun error' occurs, which indicates too much computational burden for the processor.

The flow chart of the software for real-time implementation is shown in Fig. 4.4. After initializing all the required variables, the timer interrupt routine is set up to read the values of the currents and rotor position angle every  $100 \mu\text{s}$ . The motor currents obtained through analog to digital converter (ADC) channels 1 and 2 are multiplied by the gain 18.814 and 16.6667, respectively in order to obtain the actual current values in software. These constants depend on the hall-effect sensors specifications, the resistors used at the output node of these sensors and the resistors used in the interface circuit. After these digitalized currents in  $abc$  coordinates are converted into rotating reference frame of  $d-q$  axis coordinates.

The rotor position angle is measured by encoder and can be calculated in radian by the equation of  $\theta = \frac{2\pi n}{n_p}$ , where  $n$  is the number of pulses counted in the counter. Once the rotor position angle is calculated, the rotor speed is computed from the measured rotor position angles using numerical backward differentiation. Based on the calculated speed, the speed error between actual and reference speed is calculated. Using the speed error and load torque, command currents are calculated according to the proposed LMA technique explained in Chapter-3. Based on the output of torque and flux hysteresis comparators and sector numbers, the DTFC scheme selects the PWM signals to control switches. All off-to-on transitions of the PWM pulses are delayed by the dead time of 0.5 milliseconds in order to prevent the shorting of the dc bus voltage to ground. These pulses are sent to the inverter gate drive through a digital I/O subsystem of the board.

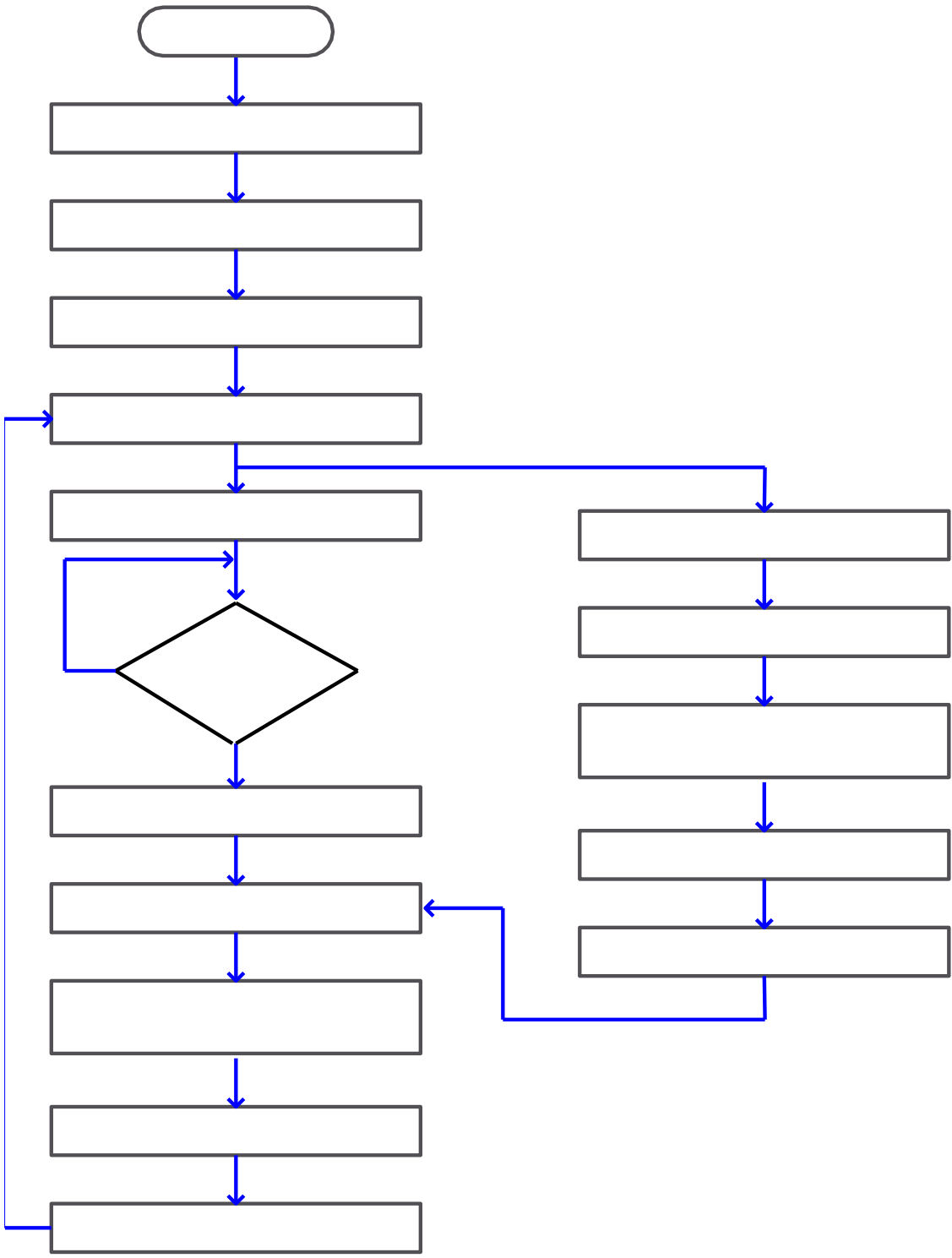


Fig. 4.4: Flow chart of the software for real-time implementation of the proposed LMA based DTFC scheme of IPMSM drive.

## 4.5 Experimental Results

Real time implementation is done to verify the design of the proposed LMA based DTFC scheme for IPMSM drive under different operating conditions. Real time implementation is also carried out for comparison of the DTFC with VC. Fig. 4.5 shows the starting speed, efficiency and torque responses of the proposed DTFC based PMSM drive. It is found from Fig. 4.5(a) that the proposed LMA based DTFC can follow the command speed smoothly without any overshoot/undershoot while maintaining high efficiency. The torque ripple was found reasonable, which can be seen from Fig. 4.5(b). The transient current and steady-state 3-phase current responses are shown in Fig. 4.6. The balance operation of the motor is verified by steady-state 3-phase currents shown in Fig. 4.6(b). Fig. 4.10 shows the speed response of the proposed LMA based DTFC scheme for a step change in command speed from 40rad/s to 70 rad/s. It is found that the motor can follow the command speed smoothly.

The experimental speed and efficiency responses of the IPMSM drive with LMC based DTFC and VC schemes are shown in Fig. 4.7. The motor was tested at relatively light load (25% of rated load) as the efficiency decreases at light load conditions. It is found that the DTFC maintains around 2.3% higher efficiency than that of VC. Although the efficiency improvement in DTFC is not same as simulation but it shows higher efficiency even in real-time. The settling time of VC is found less but not that significant. However, the DTFC exhibits higher peak-to-peak torque ripple than that of VC scheme, which can be seen from the phase current responses in Fig. 4.7 and torque responses in Fig. 4.8. It is also seen from Fig. 4.7 that the VC takes more input current than that of DTFC, which cause the difference in efficiency.

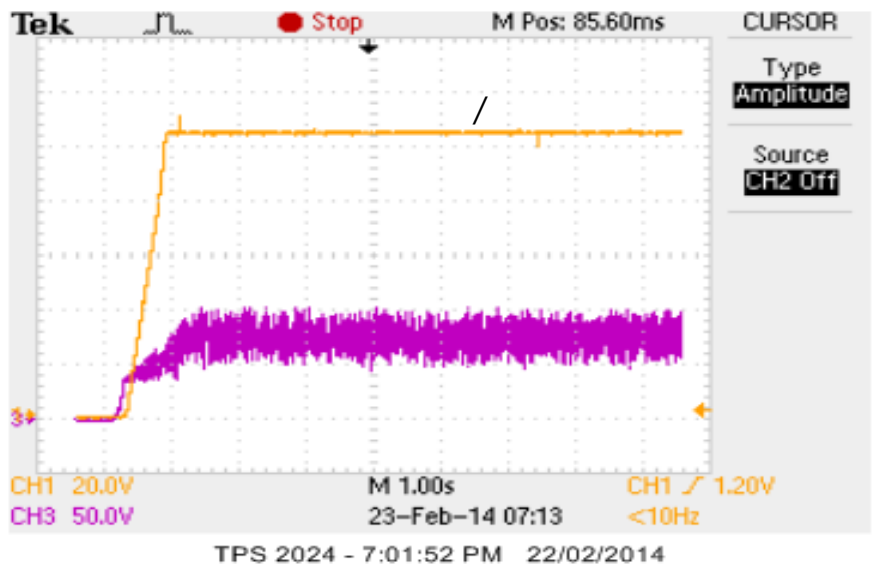
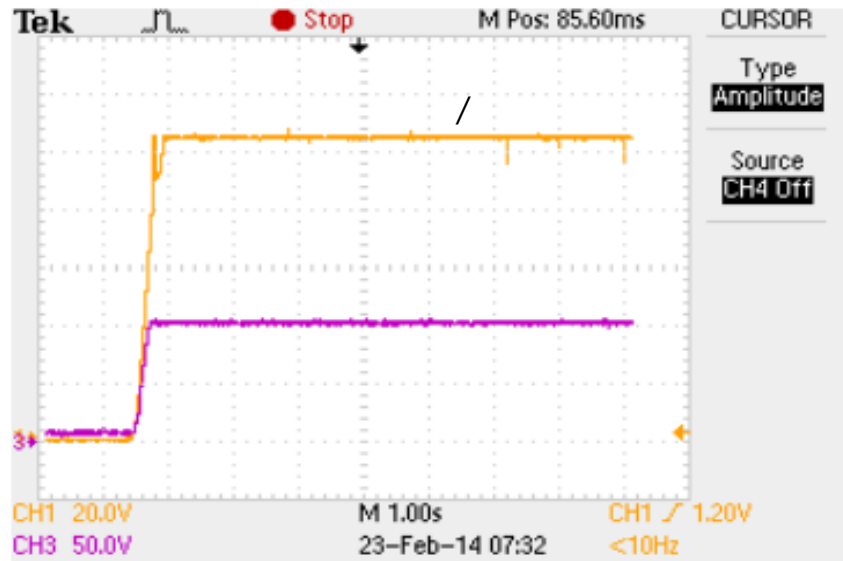
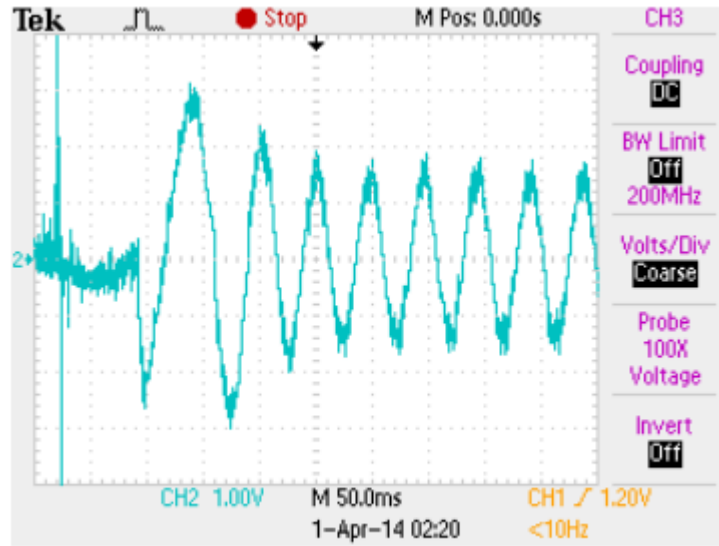
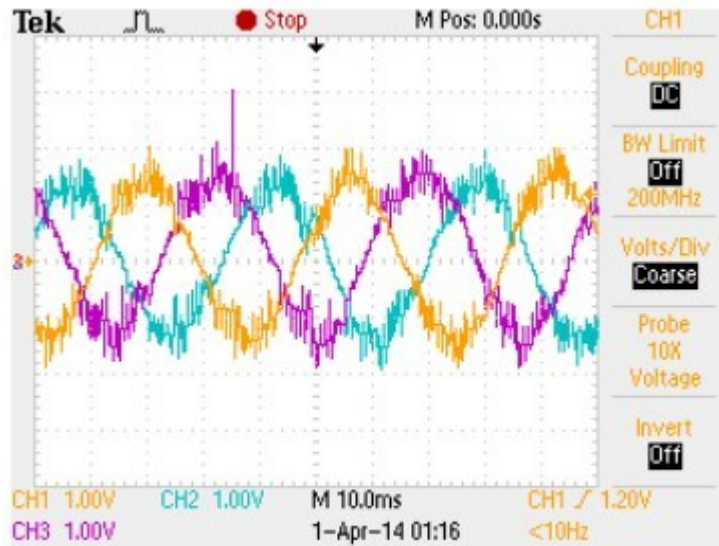


Fig. 4.5: Experimental starting responses of the proposed LMA based DTFC scheme for IPMSM drive at a speed of / and load of : (a) speed & efficiency, (b) speed and torque.



TPS 2024 - 3:09:41 PM 31/03/2014



TPS 2024 - 2:05:33 PM 31/03/2014

Fig. 4.6: Experimental current response of the proposed LMA based DTFC scheme for IPMSM drive: (a) 'a' phase currents, (b) 3-phase currents.

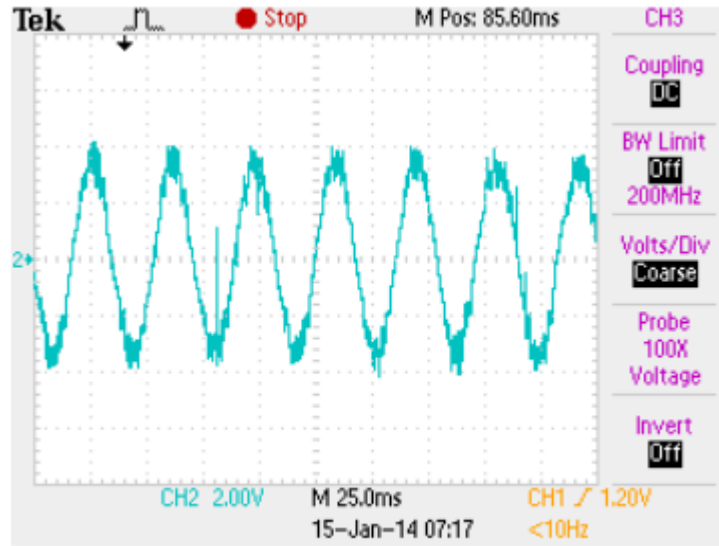


TPS 2024 - 7:21:21 PM 12/01/2014

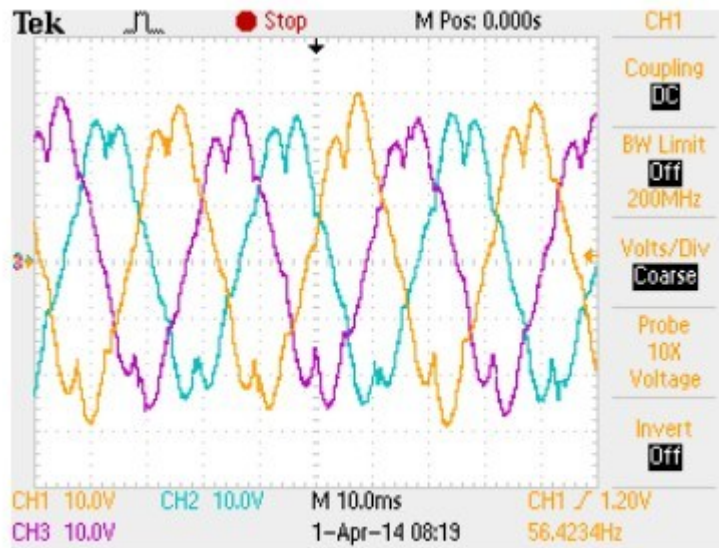


TPS 2024 - 5:51:16 PM 12/01/2014

Fig. 4.7: Experimental speed and efficiency responses of IPMSM drive at rated speed and 25% of rated load condition: (a) DTFC, (b) VC .

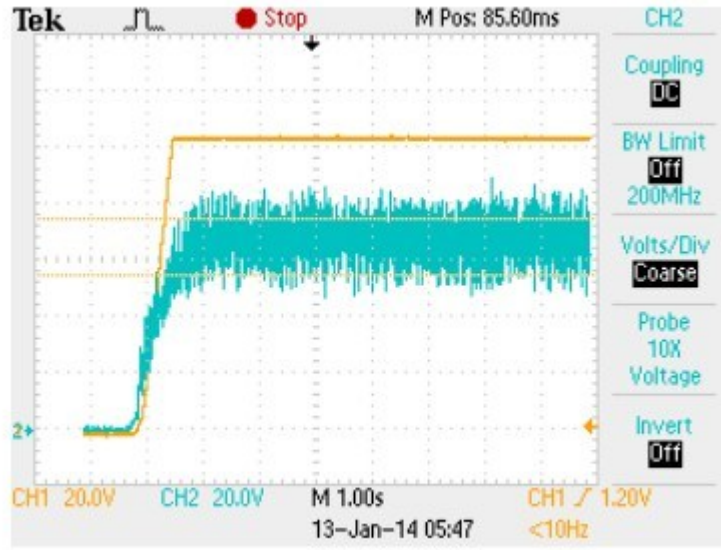


TPS 2024 - 7:04:26 PM 14/01/2014

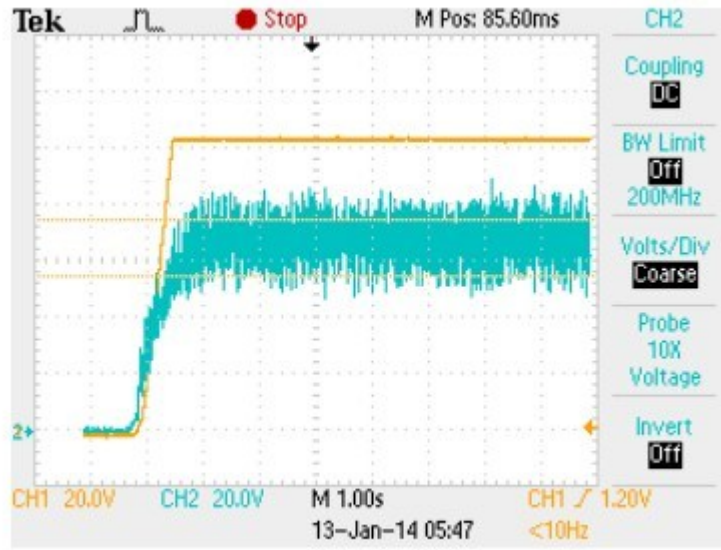


TPS 2024 - 9:08:19 PM 31/03/2014

Fig. 4.8: Experimental steady-state current responses of IPMSM drive at rated speed and 25% of rated load condition: (a) DTFC—‘a’ phase, (b) VC—‘3-phase’.



TPS 2024 - 5:34:28 PM 12/01/2014



TPS 2024 - 5:34:28 PM 12/01/2014

Fig. 4.9: Experimental speed and torque responses of IPMSM drive at rated load condition: (a) DTFC, (b) VC .

and 25% of

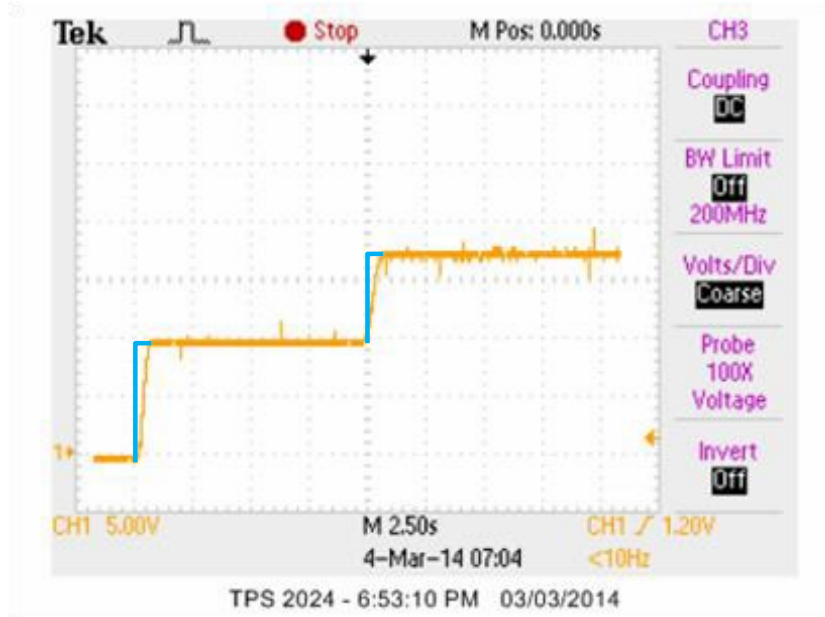


Fig. 4.10: Experimental speed response of the proposed LMA based DTFC scheme for PMSM drive for a step increase in command speed from / / at 25% rated load.

## 4.6 Conclusion

A novel adaptive flux observer based direct torque and flux control of PMSM drive has been presented in this Chapter. An LMA for IPMSM drive is developed to estimate the air-gap flux so that the motor operates at minimum loss condition while taking the general advantages of DTFC scheme over conventional vector control scheme. The proposed DTFC based PMSM drive incorporating the LMA based flux observer was experimentally implemented using the DSP board DS1104 for a prototype 5 hp motor. The performance of the proposed LMA based DTFC control of PMSM drive is tested in experiment at different operating conditions. It was found that the proposed LMA based DTFC control scheme can maintain both high efficiency and high dynamic performance.

# Chapter 5

## Conclusion

A novel loss minimization algorithm based flux observer for DTFC based IPMSM drive has been developed in this thesis. A simulink model of the proposed LMA based DTFC scheme for IPMSM drive has been developed using MATLAB-Simulink software. The proposed LMA based DTFC scheme for IPMSM drive has also been implemented in real-time using DSP board DS1104 for a laboratory 5 hp motor. A performance comparison between DTFC and vector control techniques for IPMSM drive has been presented. The simulation and experimental results verify the effectiveness of the proposed drive to maintain both high efficiency and high dynamic performance at different operating conditions.

### 5.1 Achievements of the Thesis

Major achievement of the thesis can be summarized as follows:

- A state-of-the-art literature search on the DTFC based IPMSM drive has been done.
- A loss model based controller has been developed to minimize the electrical losses developed to minimize the electrical losses of the motor.
- The LMA has been incorporated with the DTFC for online estimation of the reference flux.
- The proposed DTFC based IPMSM drive has been experimentally implemented using DSP based DS1104.

- The effectiveness of the proposed LMA based flux observer for DTFC based IPMSM drive has been verified in both simulation and experiment at different operating conditions such as sudden change in load, step change in command speed, etc.

## **5.2 Future scope of this work**

Although the complete direct torque and vector control scheme of IPMSM incorporating the proposed flux controller was successfully implemented in real-time using DSP controller board DS 1104 on a laboratory 5 hp motor, the torque ripple is still an issue. The controlled algorithms should be developed and integrated with proposed LMA based DTFC scheme so that the torque ripple is at the minimum level. Again, the look-up table of the DTFC causes some kind of time delay, so an optimized algorithm should be developed to replace the look-up table in DTFC drive system. Again, the intelligent algorithms based LMA may be developed and incorporated with the DTFC to estimate the reference flux so that the algorithms will be independent of motor parameters.

# Reference

- [1] M. A. Rahman and P. Zhou, "Analysis of brushless permanent magnet synchronous motors", IEEE Transactions on Industrial Electronics, vol.43 , no.2 , 2011 , April 199, pp. 256-267.
- [2] R.M. Crowder, *Electric Drives and Their Controls*, Clarendon Press, 1995.
- [3] R.H. Park, "Two-reaction theory of synchronous machines generalized method of analysis part-I", Trans. of the American Institute of Electrical Engineers, vol.48, no.3, 1929, pp.716-727.
- [4] P.C. Sen, "Electric motor drives and control-past, present, and future" , IEEE Transactions on Industrial Electronics, vol. 37 , no. 6, 1990 , pp. 562 - 575.
- [5] A. Abbondanti, "Methods of flux control in induction motors driven by variable frequency, variable voltage supplies", in conf. Rec. Int. Semiconductor Power Converter, 1977.
- [6] B.K. Bose, *Modern Power Electronics and AC Drives*, Upper Saddle River, NJ: Prentice Hall, 2002.
- [7] S.J. Chapman, *Electric Machinery Fundamentals*, New York, NY: McGraw-Hill, 1999.
- [8] E.C. Lister and M.R. Golding, *Electric Circuits and Machines*, McGraw-Hill Ryerson Limited, 1987.
- [9] M. N. Uddin, "Intelligent Control of an Interior Permanent Magnet Synchronous Motor", PhD. Thesis, Memorial University of Newfoundland , St. John's, 2000.
- [10] G.R. Slemon, *Electric Machines and Drives*, Addison-Wesley Publications, 1992.
- [11] W. Leonhard , "Field-orientation for controlling AC machines-principle and application", Third International Conference on Power Electronics and Variable-Speed Drives, 1988 , pp. 277 – 282.
- [12] M. Depenbrock, "Direct self-control (DSC) of inverter-fed induction machine", IEEE Trans. Power Electron., vol. 3, no. 4, 1988, pp. 420-429.
- [13] I. Takahashi and T. Noguchi, "A new quick-response and high-efficiency control strategy of an induction motor" IEEE Trans. Ind. Appl., vol. IA-22, no. 5, 1986, pp. 820-827.
- [14] M. Preindl, S. Bolognani , "Model Predictive Direct Torque Control With Finite Control Set for PMSM Drive Systems, Part 2: Field Weakening Operation", IEEE Transactions, on Industrial Informatics, vol. 9 no. 2, 2013 , pp. 648 – 657.

- [15] J. Faiz, S.H.M. Zonoozi, "A novel technique for estimation and control of stator flux of a salient-pole PMSM in DTC method based on MTPF", *IEEE Transactions on Industrial Electronics*, vol. 50 no. 2, 2003 , pp. 262 – 271.
- [16] S. Bolognani, L. Peretti, M. Zigliotto, "Online MTPA Control Strategy for DTC Synchronous Reluctance Motor Drives", *IEEE Transactions on Power Electronics*, vol. 26 , no. 1, 2011, pp.20 – 28.
- [17] Y. Inoue, S. Morimoto, M. Sanada, "Comparative Study of PMSM Drive Systems Based on Current Control and Direct Torque Control in Flux-Weakening Control Region", *IEEE Transactions on Industry Applications*, vol. 48 , no. 6, 2012 , pp. 2382 - 2389.
- [18] Y. Yan , J.G. Zhu, Y.G. Guo, "Initial rotor position estimation and sensorless direct torque control of surface-mounted permanent magnet synchronous motors considering saturation saliency", *IET Transactions on Electric Power Applications*, vol. 2 , no. 1, 2008 , pp. 42 – 48.
- [19] K. Jun-Koo, S. Seung-Ki, "New direct torque control of induction motor for minimum torque ripple and constant switching frequency", *IEEE Transactions on Industry Applications*, vol. 35 ,no. 5, 1999 , pp. 1076 - 1082.
- [20] G. Foo , M.F. Rahman, "Direct torque and flux control of an IPM synchronous motor drive using a backstepping approach", *IET on Electric Power Applications*, vol. 3 , no. 5, 2009 , pp. 413 – 421.
- [21] L. K. Beum, S. J. Ho, I. Choy, Y. Ji-Yoon, "Torque ripple reduction in DTC of induction motor driven by three-level inverter with low switching frequency", *IEEE Transactions on Power Electronics*, vol. 17 , no. 2, 2002 , pp. 255 – 264.
- [22] Z. Yongchang, Z. Jianguo, "Direct Torque Control of Permanent Magnet Synchronous Motor With Reduced Torque Ripple and Commutation Frequency", *IEEE Transactions on Power Electronics*, vol. 26 , no. 1, 2011 , pp. 235 – 248.
- [23] Z. Yongchang, Z. Jianguo, "A Novel Duty Cycle Control Strategy to Reduce Both Torque and Flux Ripples for DTC of Permanent Magnet Synchronous Motor Drives With Switching Frequency Reduction", *IEEE Transactions on Power Electronics*, vol. 26 , no. 10 , 2011 , pp. 3055 – 3067.
- [24] L. Yong, Z.Z. Qiang, D. Howe, "Instantaneous Torque Estimation in Sensorless Direct Torque Controlled Brushless DC Motors", *IEEE Transactions on Industry Applications*, vol. 42 , Issue: 5, 2006 , pp. 1275 – 1283.

- [25] L. Yaohua, D. Gerling, "Voltage vector selection strategy for the interior PMSM DTC system", Proceedings of the 2011-14th European Conference on Power Electronics and Applications (EPE 2011), 2011, pp. 1 - 9.
- [26] J. Mengjia, S. Cenwei, Q. Jianqi, L. Ruiguang, "Stator flux estimation for direct torque controlled surface mounted permanent magnet synchronous motor drives over wide speed region", Proceedings of the Eighth International Conference on Electrical Machines and Systems 2005, vol. 1, 2005 , pp. 350 - 354.
- [27] A. Khoobroo, B. Fahimi, "Magnetic Flux Estimation in a Permanent Magnet Synchronous Machine Using Field Reconstruction Method", IEEE Transactions on Energy Conversion, vol. 26 , no. 3, 2011 , pp. 757 – 765.
- [28] N.R.N. Idris, A.H.M. Yatim, "An improved stator flux estimation in steady-state operation for direct torque control of induction machines", IEEE Transactions on Industry Applications, vol. 38 , Issue: 1, 2002 , pp. 110 – 116.
- [29] Z. Hao, X. Xi, L. Yongdong, "Torque Ripple Reduction of the Torque Predictive Control Scheme for Permanent-Magnet Synchronous Motors", IEEE Transactions on Industrial Electronics, vol. 59 , no. 2, 2012 , pp. 871 – 877
- [30] H. Ziane, J.M. Retif, T. Rekioua, "Fixed-switching-frequency DTC control for PM synchronous machine with minimum torque ripples", Canadian Journal on Electrical and Computer Engineering, vol. 33 , no. 3/4, 2008 , pp. 183 – 189.
- [31] Z. Chunmei, L. Heping, C. Shujin, W. Fangjun, "Application of neural networks for permanent magnet synchronous motor direct torque control", Journal on Systems Engineering and Electronics, vol. 19 , no. 3, 2008 , pp. 555 – 561 .
- [32] L. Zhong, M. F. Rahman, W. Y.Hu, K.W. Lim, M. A. Rahman, "A direct torque controller for permanent magnet synchronous motor drives", IEEE Transactions on Energy Conversion, vol.14, no.3, 1999, pp. 637 – 642.
- [33] M. N. Uddin, and M. Hafeez, "FLC Based DTC Scheme to Improve the Dynamic Performance of an IM Drive", IEEE Trans. on Industry Applications, vol. 48, no.2, March/April 2012, pp. 823 – 831.
- [34] L. Tang, L. Zhong, M. F. Rahman, Y. Hu , "A novel direct torque controlled interior permanent magnet synchronous machine drive with low ripple in flux and torque and fixed

- switching frequency”, IEEE Transactions on Power Electronics, vol. 19, no. 2, 2004, pp. 346 – 354.
- [35] M. Hafeez, M. N. Uddin, N. A. Rahim and H. W. Ping, “Self-Tuned NFC and Adaptive Torque Hysteresis based DTC Scheme for IM Drive”, IEEE Trans. on Industry Applications, vol. 50, no.2, March/April 2014, pp. 1410 - 1420.
- [36] L. Tang, L. Zhong, M. F. Rahman, Y. Hu, “A novel direct torque control for interior permanent-magnet synchronous machine drive with low ripple in torque and flux-a speed-sensorless approach”, IEEE Transactions on Industry Applications, vol. 39, no. 6, 2003, pp.1748 - 1756.
- [37] L. Kyo-Beum, S. Joong-Ho, I. Choy, Y. Ji-Yoon, “Torque ripple reduction in DTC of induction motor driven by three-level inverter with low switching frequency”, IEEE Transactions on Power Electronics, vol. 17 , no. 2, 2002 , pp. 255 – 264.
- [38] I.G. Bird, D. Zelaya, H. Parra, “Fuzzy logic torque ripple reduction for DTC based AC drives”, Electronics Letters, vol. 33, no. 17, 1997, pp. 1501 – 1502.
- [39] L. Romeral, A. Arias, E. Aldabas, M.G. Jayne, “Novel direct torque control (DTC) scheme with fuzzy adaptive torque-ripple reduction”, IEEE Transactions on Industrial Electronics , vol. 50, no.3,2003, pp. 487 – 492.
- [40] L. Yong, Z.Q. Zhu, D. Howe, “Direct torque control of brushless DC drives with reduced torque ripple”, IEEE Transactions on Industry Applications, vol. 41 , no. 2, 2005 , pp. 599 - 608.
- [41] L. Yong, Z.Q. Zhu, D. Howe, “Commutation-Torque-Ripple Minimization in Direct-Torque-Controlled PM Brushless DC Drives”, IEEE Transactions on Industry Applications, vol. 43 , no. 4, 2007, pp.1012 – 1021.
- [42] Y.A.-R.I. Mohamed, “Design and Implementation of a Robust Current-Control Scheme for a PMSM Vector Drive With a Simple Adaptive Disturbance Observer”, IEEE Transactions on Industrial Electronics, vol. 54 , no. 4, 2007 , pp. 1981 – 1988.
- [43] K. J. Sheok, S. S. Ki, “New approach for high-performance PMSM drives without rotational position sensors”, IEEE Trans. on Power Electronics, vol.12 , no. 5, 1997 , pp. 904 - 911.
- [44] B. Singh, D. Goyal, “Improved DSVM-DTC Based Current Sensorless Permanent Magnet Synchronous Motor Drive”, 7th Int. Conf. on Power Electronics and Drive Systems, 2007, pp. 1354 – 1360.

- [45] K. Chikh, M. Khafallah, A. Saad, D. Yousfi, H. Chaikhy, A novel fixed-switching-frequency DTC for PMSM drive with low torque and flux ripple based on Sinusoidal Pulse With Modulation and predictive controller”Int. Conf. on Multimedia Computing and Systems (ICMCS), 2012, pp. 1069-1075.
- [46] M. NasirUddin and M. I. Chy, “On-Line Parameter Estimation Based Speed Control of PM AC Motor Drive in Flux Weakening Region”, IEEE Trans. on Ind. Applications, vol. 44, no. 5, Sept./Oct. 2008, pp. 1486-1494.
- [47] M. A.Rahman, M.Vilathgamuwa, M. N.Uddin, and K. J. Tseng, “Nonlinear Control of Interior Permanent Magnet Synchronous Motor”, IEEE Transactions on Industry Applications, Vol. 30, No. 2, March/April 2003, pp. 408-416.
- [48] B. Patel, “Development and Implementation of High Performance and High Efficiency Interior Permanent Magnet Synchronous Motor Drive”, M.Sc., Thesis, Lakehead University, 2013.
- [49] G.C.D. Sousa, B.K. Bose, J.G. Cleland, “Fuzzy logic based on-line efficiency optimization control of an indirect vector-controlled induction motor drive”, IEEE Transactions on Industrial Electronics, vol. 42 , no. 2, 1995 , pp. 192 – 198.
- [50] Z. Qing, A. Zhongliang, T. Lijian, W. Yanzhong, T. Renyan, Y. Shenbo,“Study and design of large capacity high efficiency permanent magnet synchronous motor”, Proceedings of the Fifth International Conference on Electrical Machines and Systems, 2001. ICEMS 2001., vol.2 , pp. 888 - 890 .
- [51] M. N. Uddin, R. S. Rebeiro and S. H. Lee, “Online Efficiency Optimization of an IPMSM Drive Incorporating Loss Minimization Algorithm and an FLC as Speed Controller”, in IEEE-ISIE, 2009, pp. 1263-1268.
- [52] R.S.Colby, D.W.Novotny,“An efficiency-optimizing permanent-magnet synchronous motor drive”, IEEE Transactions on Industry Applications, vol. 24 , no. 3, 1988 , pp. 462 – 469.
- [53] C. Mademlis, I. Kioskeridis, N. Margaris, “Optimal efficiency control strategy for interior permanent-magnet synchronous motor drives”, IEEE Transactions on Energy Conversion, vol. 19 , no. 4, 2004 , pp. 715 – 723.
- [54] I. Kioskeridis and N. Margaris, “Loss Minimization in Scalar-Controlled Induction Motor Drives with Search Controllers”, IEEE Trans. Power Electron., vol. 11, no. 2, pp. 213-220, Mar. 1996.

- [55] M.N.Uddin, S.W. Nam, “New Online Loss-Minimization-Based Control of an Induction Motor Drive”, IEEE Transactions on Power Electronics, vol. 23 , Issue: 2 , 2008 , pp. 926 – 933.
- [56] S. Morimoto, Y. Tong, Y. Takeda, T. Hirasa, “Loss minimization control of permanent magnet synchronous motor drives”, IEEE Transactions on Industrial Electronics, vol. 41 , no. 5, 1994 , pp. 511 – 517.
- [57] S. Vaez-Zadeh, M. Khayamy, “Efficiency-optimizing direct torque control of interior permanent magnet synchronous machines with fastest start up”, Machines and Drives 2008. PEMD 2008. 4th IET Conference on Power Electronics, 2008 , pp. 218 – 224.
- [58] S. Vaez, V.I. John, M.A. Rahman, “An on-line loss minimization controller for interior permanent magnet motor drives”, IEEE Transactions on Energy Conversion, vol. 14 , no. 4, 1999 , pp. 1435 – 1440.
- [59] S. Vaez-Zadeh, M. Zamanifar, J. Soltani, “Nonlinear Efficiency Optimization Control of IPM Synchronous Motor Drives with Online Parameter Estimation”, Power Electronics Specialists Conference, PESC '06 . 37th IEEE, 2006 , pp. 1 - 6 .
- [60] M.A. Khan, M.N. Uddin, M. A. Rahman, “A new loss minimization control of interior permanent magnet motor drives operating with a wavelet based speed controller”, Industry Applications Society Annual Meeting (IAS), 2011 IEEE, 2011 , pp. 1 - 8.
- [61] Y. Kaiping, G. Hong, S. Zedong, W. Zhiyong, “Efficiency optimization control of Permanent Magnet Synchronous Motor for Electric Propulsion System”, 2013 International Conference on Electrical Machines and Systems (ICEMS), 2013 , pp. 56 – 61.
- [62] C. Cavallaro, A. Tommaso, R. Miceli, A. Raciti, G. R. Galluzzo, and M. Trapanese, “Efficiency Enhancement of Permanent-Magnet Synchronous Motor Drives by Online Loss Minimization Approaches”, IEEE Trans. Ind. Electron., vol. 51, no. 4, pp. 1153-1160, Aug. 2005.
- [63] L. Fang, B. H. Lee, H. J. Kim and J. P. Hong, “Study on High Efficiency Characteristics of Interior Permanent Magnet Synchronous Motor With Different Magnet Material”, in Inter. Conf. IEEE-ICEMS, 2009, pp. 1-4.
- [64] C. Y. Young, L. H. Joon, C. S. Yeon, H. K. Pyo and L. Ju, “A Study on Improvement Efficiency of Surfaced Permanent Magnet Spherical Motor”, in Inter. Conf. IEEE-ICEMS, 2011, pp. 1-4.

- [65] M. N. Uddin, and R. S. Rebeiro, "Online Efficiency Optimization of a Fuzzy Logic Controller Based IPMSM Drive", *IEEE Trans. on Ind. Appl.*, March/April 2011, pp. 1043-1050.
- [66] M. Cao, J. Egashira and K. Kaneko, "High Efficiency Control of IPMSM for Electric Motorcycles", in *Inter. Conf. IEEE-IPEMC*, 2009, pp. 1893-1897.
- [67] B. K. Bose, N. R. Patel and K. Rajashekara, "A Neuro-Fuzzy-Based On-line Efficiency Optimization Control of a Stator Flux-Oriented Direct Vector Controlled Induction Motor Drive", *IEEE Trans. Ind. Electron.*, Apr. 1997vol. 44, no. 2, pp. 270-273.
- [68] S. Chi, Z. Zhang, and L. Xu, "Sliding-Mode Sensorless Control of Direct-Drive PM Synchronous Motors for Washing Machine Applications" *IEEE Trans. on Ind. Applications*, vol. 45, no.2, March/April 2009, pp. 582-590.
- [69] M. N. Uddin and M. I. Chy, "A Novel Fuzzy Logic Controller Based Torque and Flux Controls of IPM Synchronous Motor", *IEEE Trans. on Ind. Applications*, vol. 46, no.3, May/June 2010, pp. 1220-1229.
- [70] M.N. Uddin, and M.M.I. Chy, "Online parameter-estimation-based speed control of PM AC motor drive in flux-weakening region," *IEEE Trans. Industry Appl.*, vol. 44, Sept./Oct. 2008, pp. 1486-1494.
- [71] M.N. Uddin, and M. Hafeez, "FLC Based DTC Scheme to Improve the Dynamic Performance of an IM Drive", *IEEE Trans. on Industry Applications*, vol. 48, no.2, March/April 2012, pp. 823 – 831.
- [72] Y. Liu, Z. Q. Zhu, and D. Howe, "Commutation-Torque-Ripple Minimization in Direct-Torque-Controlled PM Brushless DC Drives", *IEEE Trans. on Industry Applications*, vol. 43, no.4, July/Aug. 2007, pp. 1012-1021.
- [73] J. Faiz, and S. H. M. Zonoozi, "A Novel Technique for Estimation and Control of Stator Flux of a Salient-Pole PMSM in DTC Method Based on MTPF", *IEEE Trans. on Ind. electronics*, vol. 50, no. 2, April 2003, pp. 262-271.
- [74] S. Sayeef, G. Foo, and M. F. Rahman, "Rotor Position and Speed Estimation of a Variable Structure Direct-Torque-Controlled IPM Synchronous Motor Drive at Very Low Speeds Including Standstill", *IEEE Trans. on Ind. Electronics*, vol. 57, no. 11, Nov. 2010, pp. 7716-3723.

- [75] G. D. Andreescu, C. I. Pitic, F. Blaabjerg, and I. Boldea, "Combined Flux Observer With Signal Injection Enhancement for Wide Speed Range Sensorless Direct Torque Control of IPMSM Drives" IEEE Trans. on Energy Conversion, vol. 23, no. 2, June 2008, pp.393-402.
- [76] M. N. Uddin, and R. S. Rebeiro, "Online Efficiency Optimization of a Fuzzy Logic Controller Based IPMSM Drive", IEEE Trans. on Industry Applications, March/April 2011, pp. 1043-1050.
- [77] dSPACE, "Digital Signal Processing and Control Engineering", Implementation Guide, Paderborn, Germany, 2003.

## **Appendix A: IPMSM Parameters**

Number of phases:

Number of poles:

d-axis inductance:

q-axis inductance:

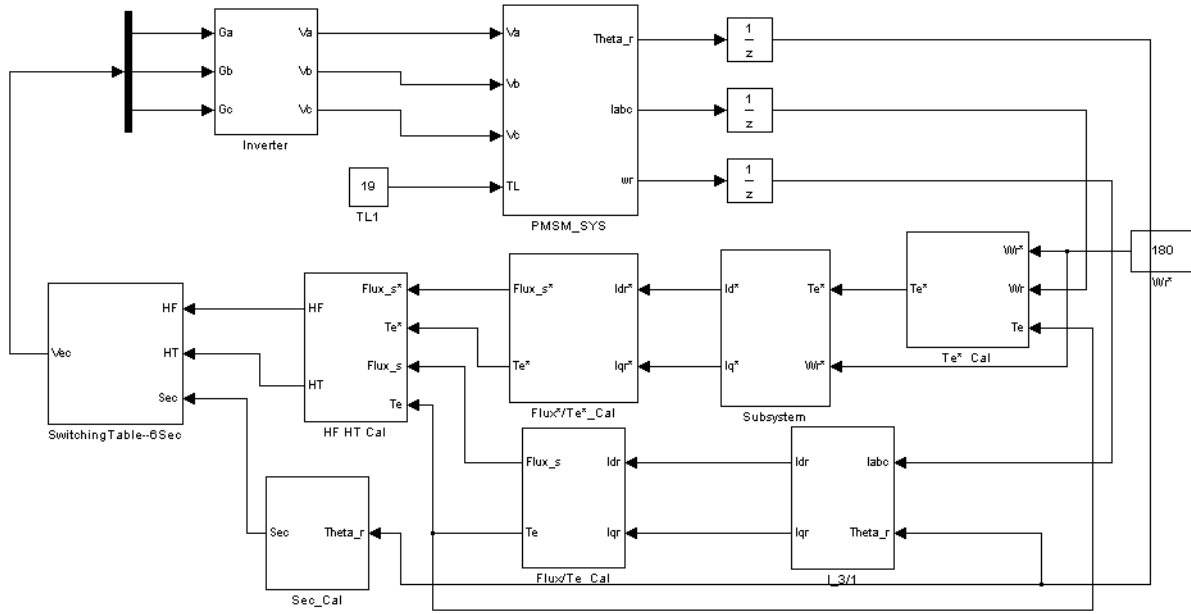
Stator resistance per phase:

Inertia constant:

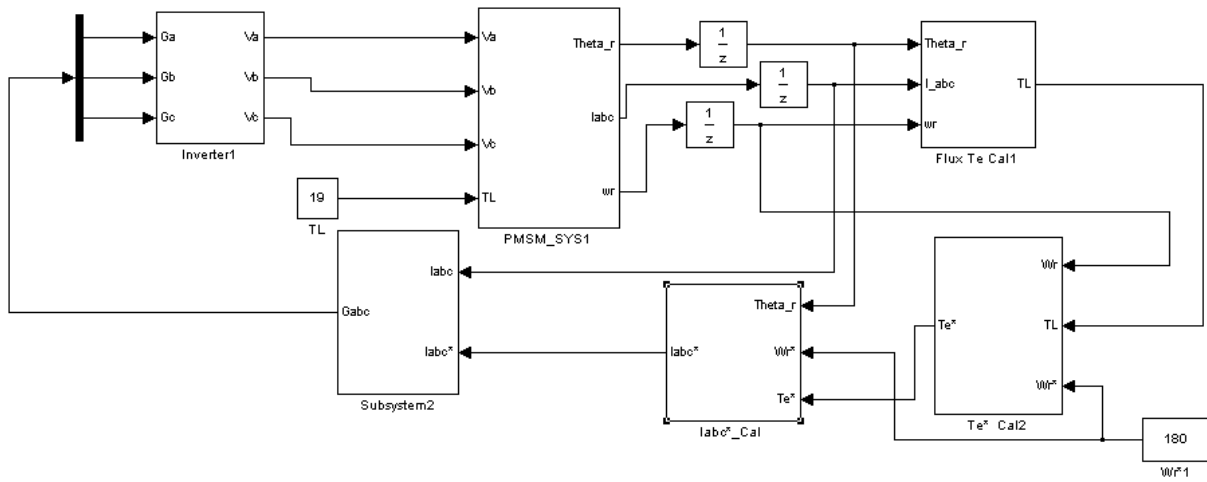
Rotor damping constant:

Permanent magnet flux linkage:

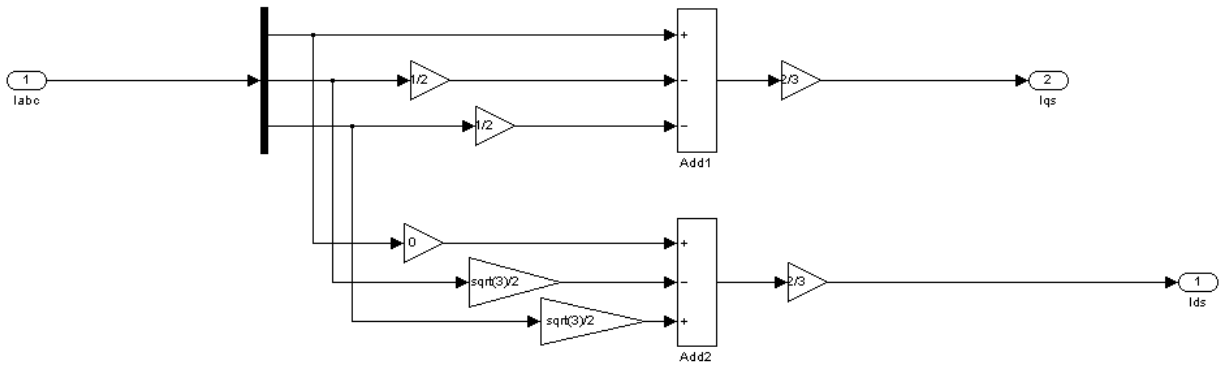
# Appendix B: Subsystem for MatLab/SimuLink Model



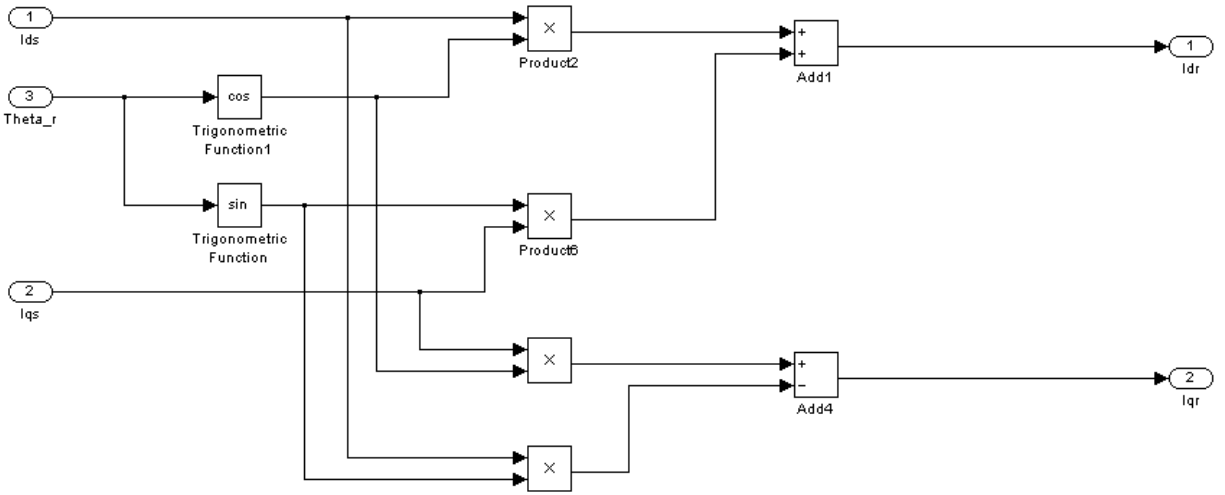
Appendix B.1: DTC simulation system



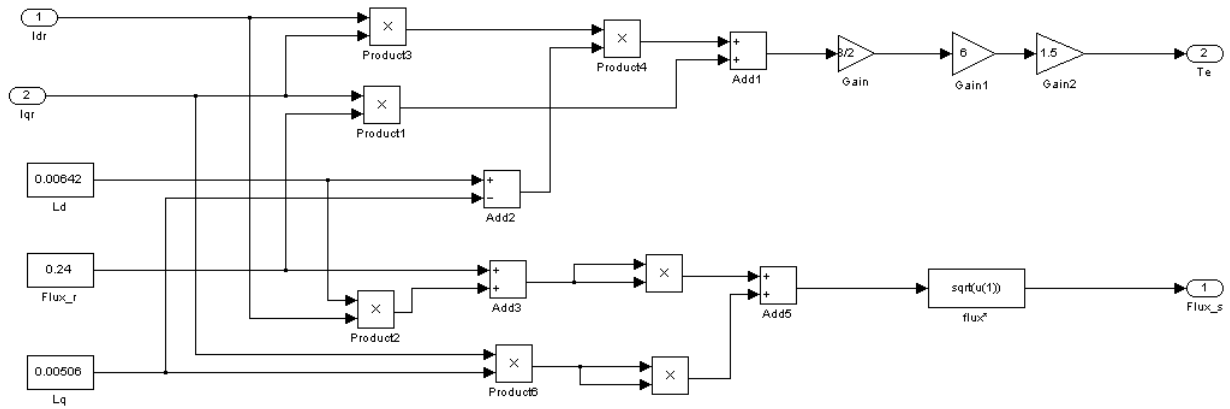
Appendix B.2: VC simulation system



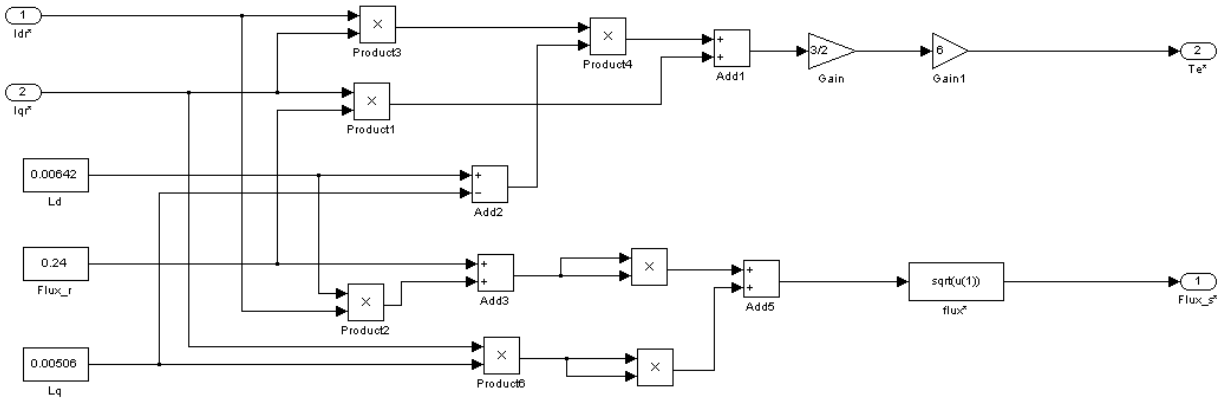
Appendix B.3: Subsystem of “converting to and ”



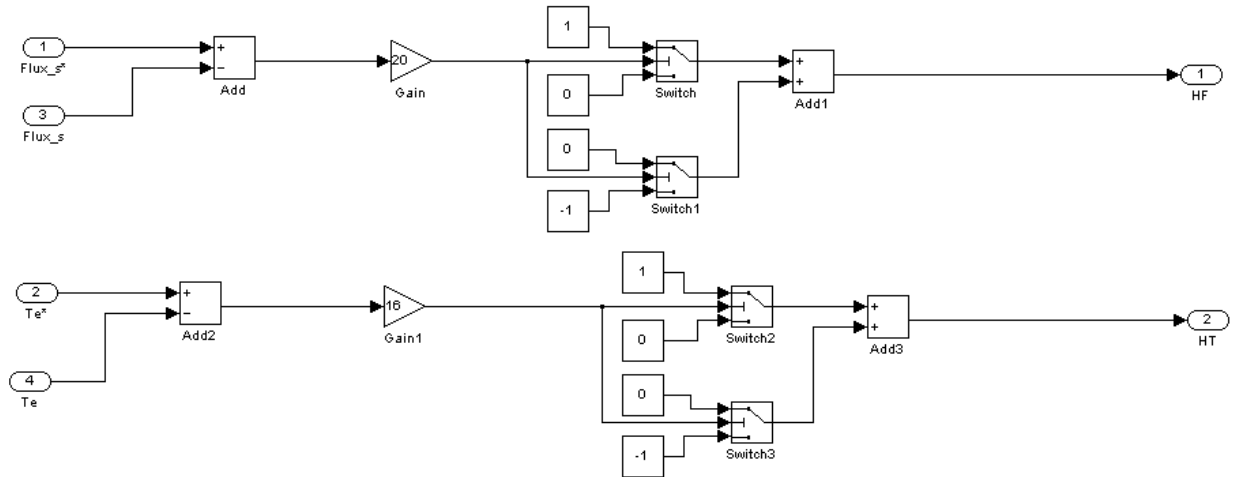
Appendix B.4: Subsystem of “converting to and ”



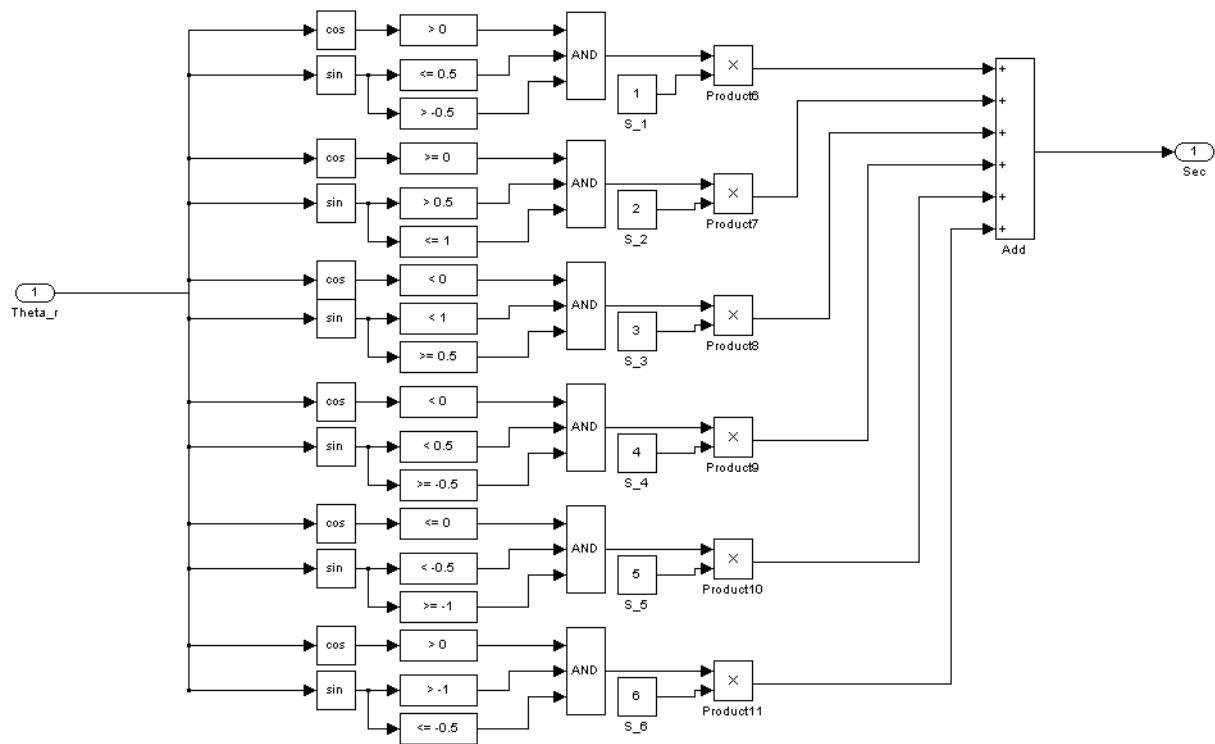
Appendix B.5: Subsystem of “converting  $I_{dr}$  and  $I_{qr}$  to  $T_e$  and  $\text{Flux}_s$ ”



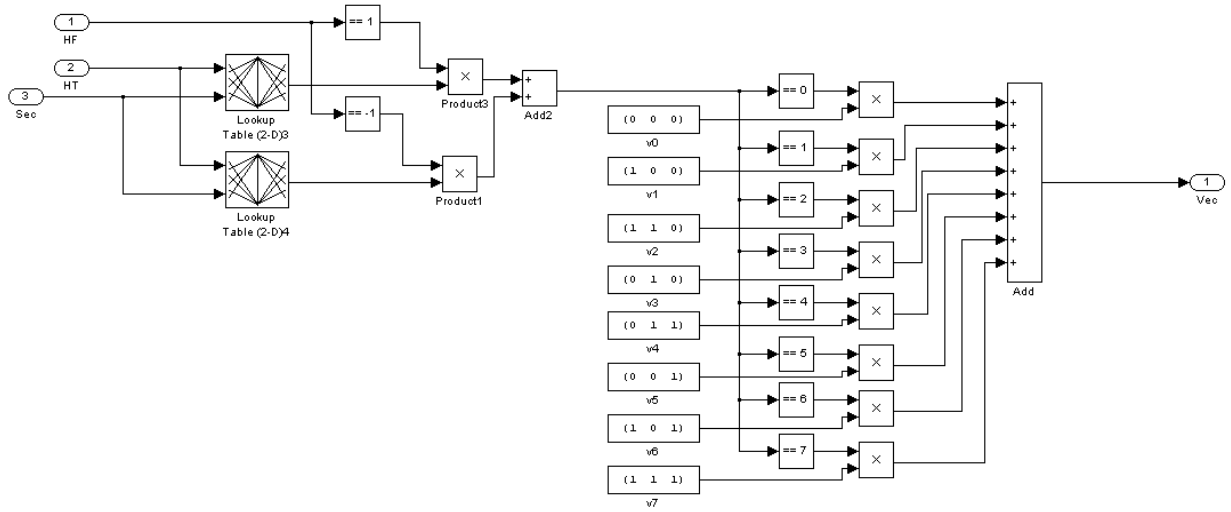
Appendix B.6: Subsystem of “converting  $I_{dr}$  and  $I_{qr}$  to  $T_e$  and  $\text{Flux}_s$ ”



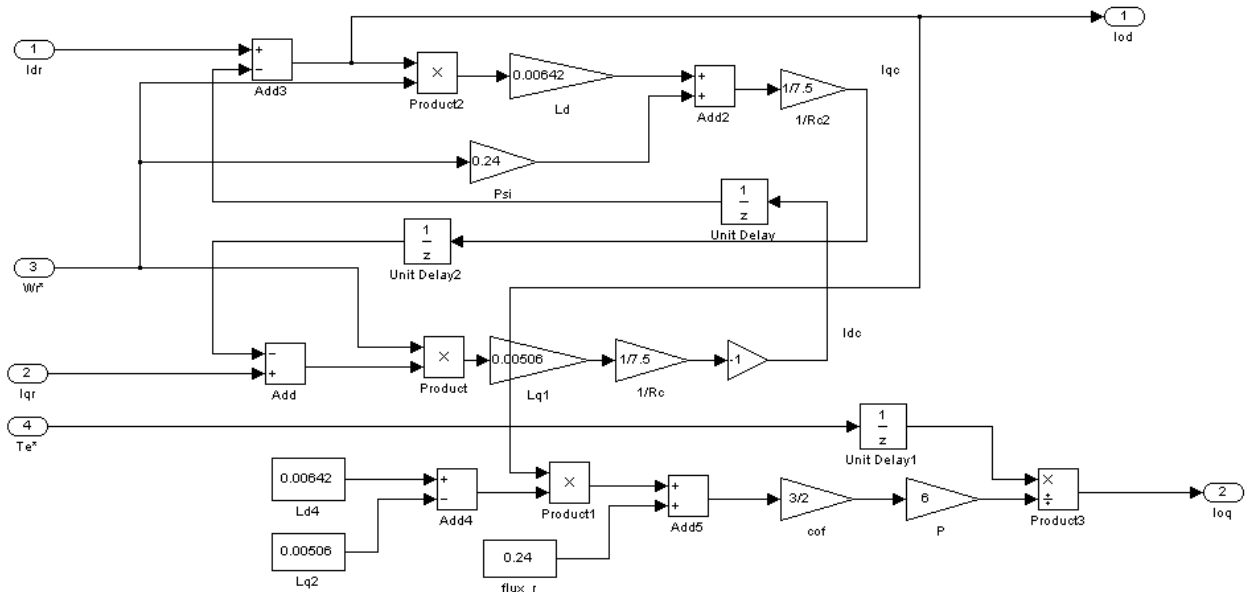
Appendix B.7:Subsystem of “flux and torque band”



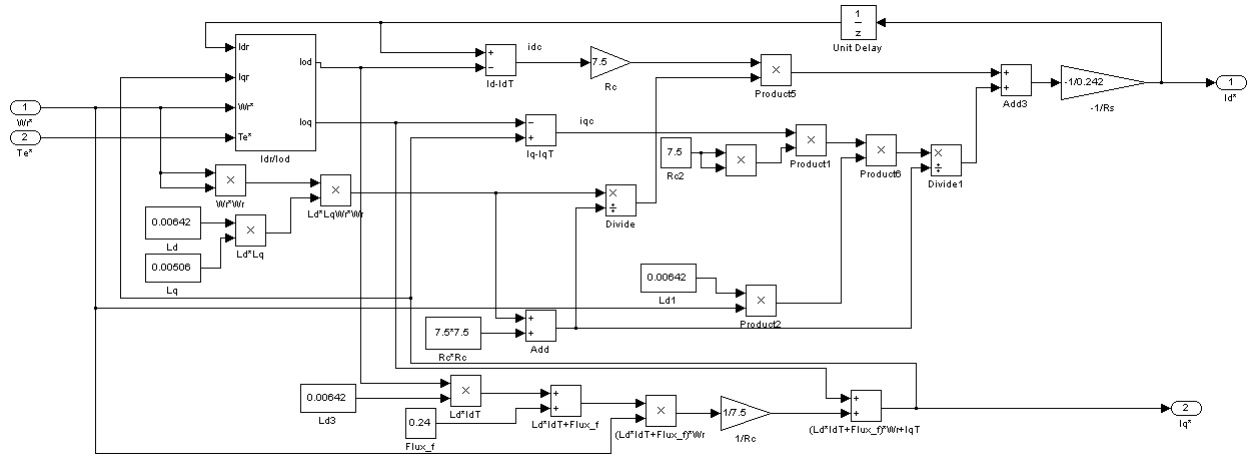
Appendix B.8:Subsystem of “angle to sector number”



Appendix B.9: Subsystem of “lookup-table to voltage vectors”

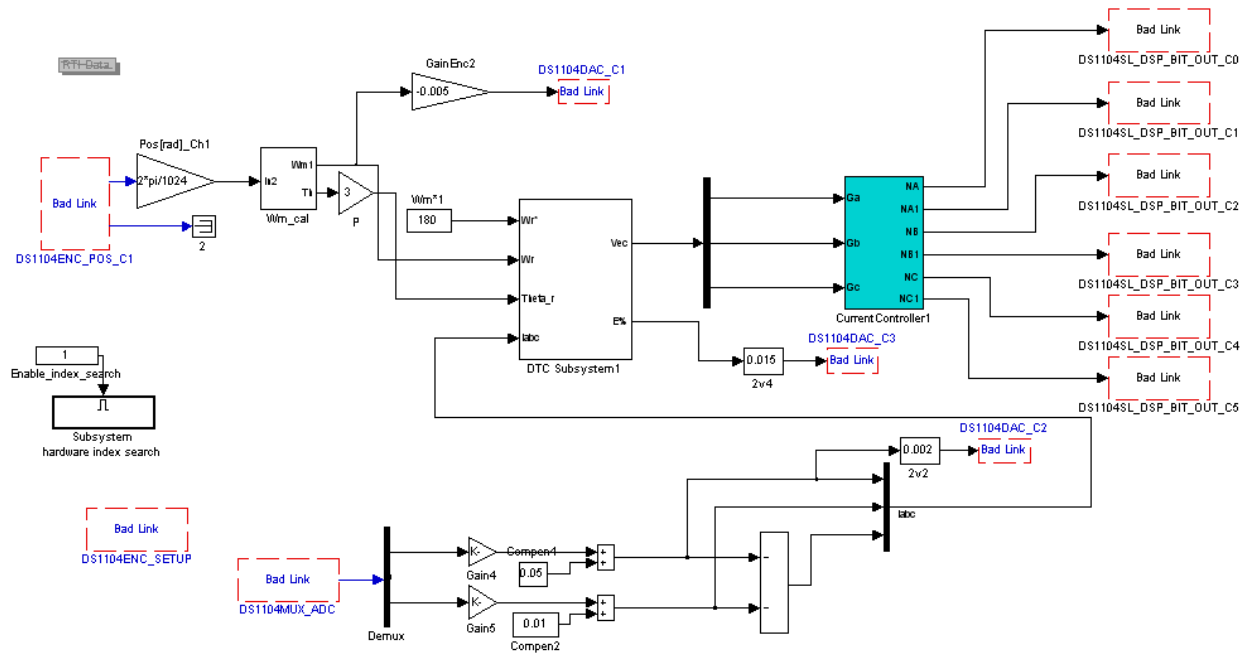


Appendix B.10: Subsystem of “converting to ”

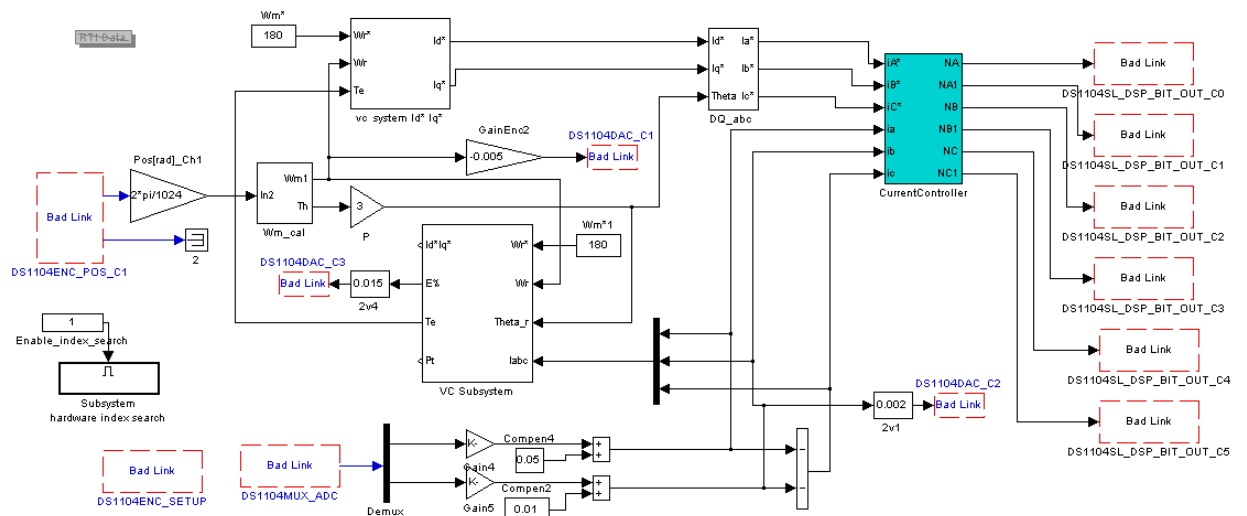


Appendix B.11:Subsystem of “LMA based flux observer”

# Appendix C: Real-time Implementation for DTFC/VC

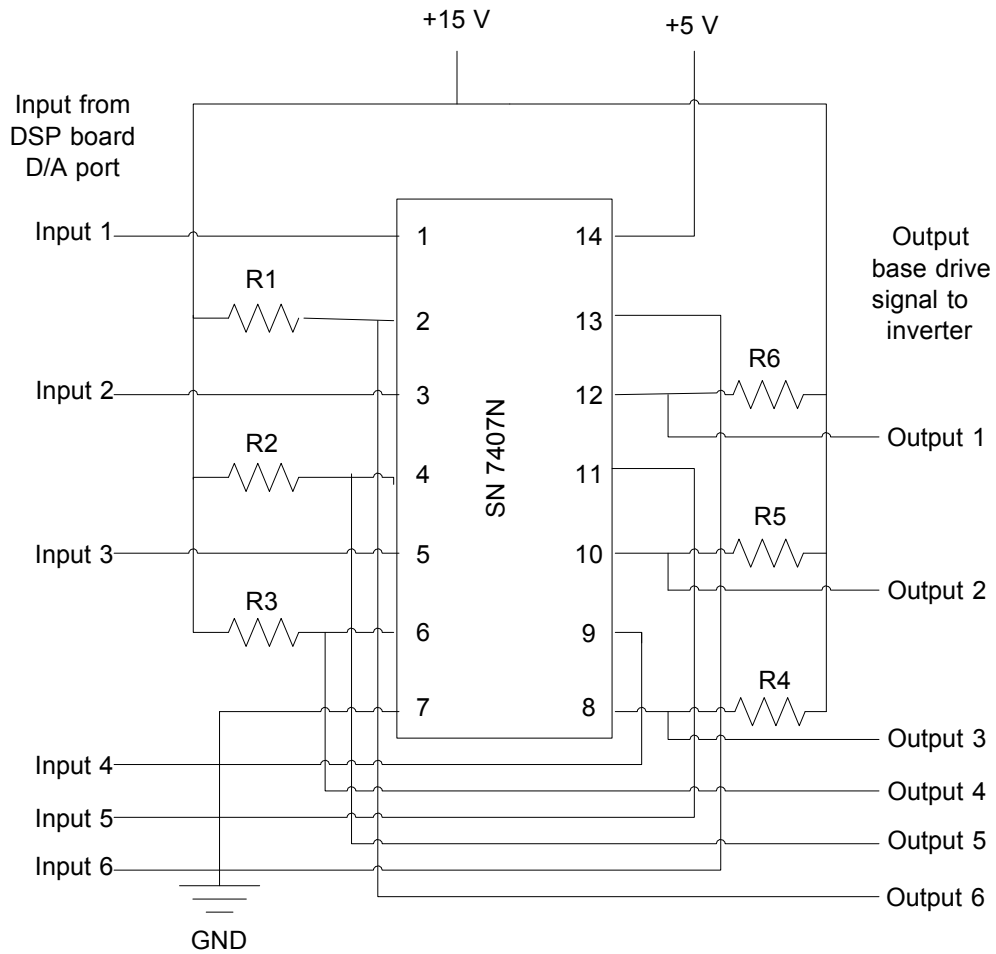


## Appendix C.1: Implementation of IPMSM System(DTFC)

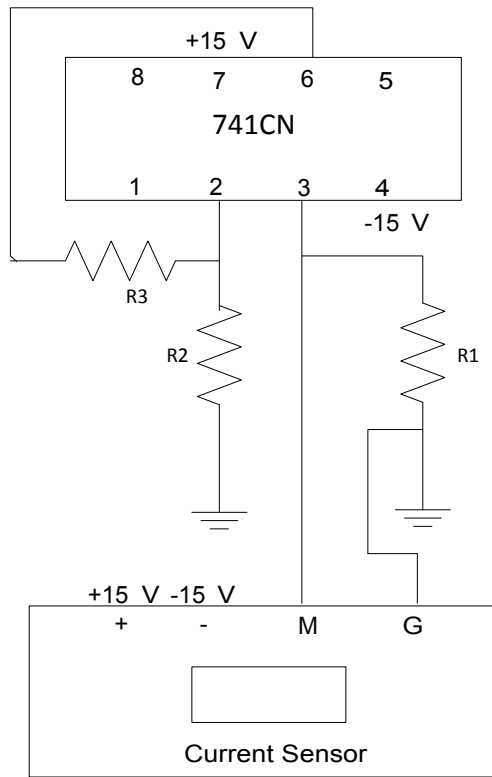


## Appendix C.2: Implementation of IPMSM System(VC)

# Appendix D: Drive and Interface Circuit



Appendix D.1: Base drive circuit for the inverter

Appendix D.2: Interface circuit for the current sensor